ON-MACHINE MEASUREMENT OF WORKPIECE FORM ERRORS IN ULTRAPRECISION MACHINING

ON-MACHINE MEASUREMENT OF WORKPIECE FORM ERRORS IN ULTRAPRECISION MACHINING

By

Fiona Gomersall

A Thesis

Submitted to the School of Graduate Studies

in Partial Fulfilment of the Requirements

for the Degree

Master of Applied Science

McMaster University

MASTER OF APPLIED SCIENCE (2016) McMaster University

(Mechanical Engineering) Hamilton, Ontario

TITLE: ON-MACHINE MEASUREMENT OF WORKPIECE FORM ERRORS IN ULTRAPRECISION MACHINING

AUTHOR: Fiona Gomersall (McMaster University, Canada)

SUPERVISOR: Dr. Stephen Veldhuis

Department of Mechanical Engineering

McMaster University

NUMBER OF PAGES: XVII, 144

Abstract

Ultraprecision single point diamond turning is required to produce parts with sub-nanometer surface roughness and sub-micrometer surface profiles tolerances. These parts have applications in the optics industry, where tight form accuracy is required while achieving high surface finish quality. Generally, parts can be polished to achieve the desired finish, but then the form accuracy can easily be lost in the process rendering the part unusable.

Currently, most mid to low spatial frequency surface finish errors are inspected offline. This is done by physically removing the workpiece from the machining fixture and mounting the part in a laser interferometer. This action introduces errors in itself through minute differences in the support conditions of the over constrained part on a machine as compared to the mounting conditions used for part measurement. Once removed, the fixture induced stresses and the part's internal residual stresses relax and change the shape of the generally thin parts machined in these applications. Thereby, the offline inspection provides an erroneous description of the performance of the machine.

This research explores the use of a single, high resolution, capacitance sensor to quickly and qualitatively measure the low to mid spatial frequencies on the workpiece surface, while it is mounted in a fixture on a standard ultraprecision single point diamond turning machine after a standard facing operation. Following initial testing, a strong qualitative correlation exists between the surface profiling on a standard offline system and this online measuring system. Despite environmental effects and the effects of the machine on the measurement system, the capacitive system with some modifications and

awareness of its measurement method is a viable option for measuring mid to low spatial frequencies on a workpiece surface mounted on an ultraprecision machine with a resolution of 1nm with an error band of ±5nm with a 20kHz bandwidth.

Acknowledgements

I am truly thankful to my advisor, Dr. Veldhuis for giving me the opportunity to come up with unique, interesting solutions to an array of problems encountered along the way to achieving the end results and goals of this research. Whether it was coming up with the many functions of the sensor fixture, finding a way to achieve the end results of the various programs, or finding a way to fixture a part on the milling machine in an unheated garage in the middle of a polar vortex, I am quite thankful for being given the opportunity to apply my ideas to solve innumerable problems that arose during this project.

I am also thankful for the time and resources that were found before and after my second son was born. And that I was able to complete this project, despite sacrifices on the part of my family. I really enjoyed and am thankful for being able to work through the challenges of this project.

Table of Contents

List of Figures

List of Tables

List of all Abbreviations and Symbols

A:	capacitance sensor's operational face, m^2
Al:	Aluminum
BeCu:	Beryllium Copper
C:	capacitance in Farads
CCD:	charge coupled device
CCW:	counter-clockwise
CMM:	co-ordinate measuring machine
CW:	clockwise
Cu:	Copper
D:	diameter of capacitance electrode, m
d:	distance between the plates in meters
DAQ:	data acquisition
Dia.:	diameter, mm
Δe:	change in surface waviness of workpiece, m
ε_0:	electric constant, or vacuum permittivity, $F.m^{-2}$
ε_r:	electrical permittivity of the material between the plates, $F.m^{-2}$
EVSI:	enhanced vertical scanning interferometry
F:	Farad
$f_{ex:}$:	frequency of magnetic field in Hertz
FEA:	finite element analysis
FFT:	Fast Fourier transform
He:	Helium
Hz:	hertz
ICS:	capacitance sensor interface, or probe driver

in.:	inches
K:	Kelvin
L:	length of plate side when considering parallel plates for capacitance, m
LVDT:	linear variable differential transducer
m:	meter
min:	minute
mm:	millimeter
N/A:	not available
Ne:	Neon
NI:	National Instruments
nm:	nanometer
no.:	number
PSI:	phase shifting interferometry
PCD:	poly-crystal diamond
Pub.:	published
Ra:	arithmetic average of the roughness profile
rms:	root mean square
rpm:	revolutions per minute
RSA:	Rapidly Solidified Aluminum
S:	samples
s:	seconds
SNR:	signal to noise ratio
SPDT:	single point diamond turning
Std. Dev.:	standard deviation
SWLI:	scanning white light interferometry
UP:	ultraprecision

UP-SPDT:	ultraprecision single point diamond turning
V:	volts
VDC:	voltage direct current, or constant in volts
VSI:	vertical scanning interferometry
μm:	micrometer
λ:	wavelength
º:	degrees
δ:	depth of penetration in meters
ρ:	material conductivity constant in S/m
Ø:	abbe error angle from Figure 9
φ:	tilt of capacitance sensor face to reference plane, or target in rads
σ:	one standard deviation from mean, median, or mode in normal curve
#:	number

Declaration of Academic Achievement

The main contribution of this research is the development and validation of a capacitance sensor system for on-line measurement of mid- to low spatial frequency workpiece errors in ultraprecision machining. My research involved developing fixtures, integrating the sensor into the machine, calibrating it for this application, and demonstrating its ability to measure form errors on an optical grade part.

Chapter 1. Introduction

Ultraprecision machining

Background

The process under consideration: a multi-axis freeform ultraprecision single point diamond machine capable of producing optical grade functional surfaces on a wide range of materials.

Research generally focuses on improving the process to enhance the manufacturability of the end product, ultimately allowing designers to expand optics design limits creatively and produce a new line of products that enhance, and/or change the current product environment for high end optics' applications.

UP-SPDT Industry

Ultraprecision single point diamond turning (UP-SPDT) is a machine tool process that plays an integral part in the progression and advancement of high end photonics applications.

Photonics is everything that is procured from the fundamentals of light and optics and engenders a large field within science and engineering. Photonics has been established due to the unique characteristics of the photon when compared against electrons in electronics: a photon moves at the speed of light, has a high capability for focusing, and photon streams can carry multiple unique lines of communications without interference and do not suffer from "electrical interference" as electrons due [1].

The process under discussion to some extent produces products for all of the industrial segments shown in Figure 1. Influence wise, the market segments that are predicted to undergo substantial growth: optical components and systems to a large extent and the photovoltaic segment to a smaller extent will be affected by the research achievements made in the underlying UP-SPDT process that is further described in later portions of this thesis. The underlying research performed on the freeform UP-SPDT machining system is primarily in the bigger picture of improving the functionality of photonics applications that rely heavily on tight form accuracy and surface finish of the component. The main segments that make-up the photonics industry are shown in Figure 1.

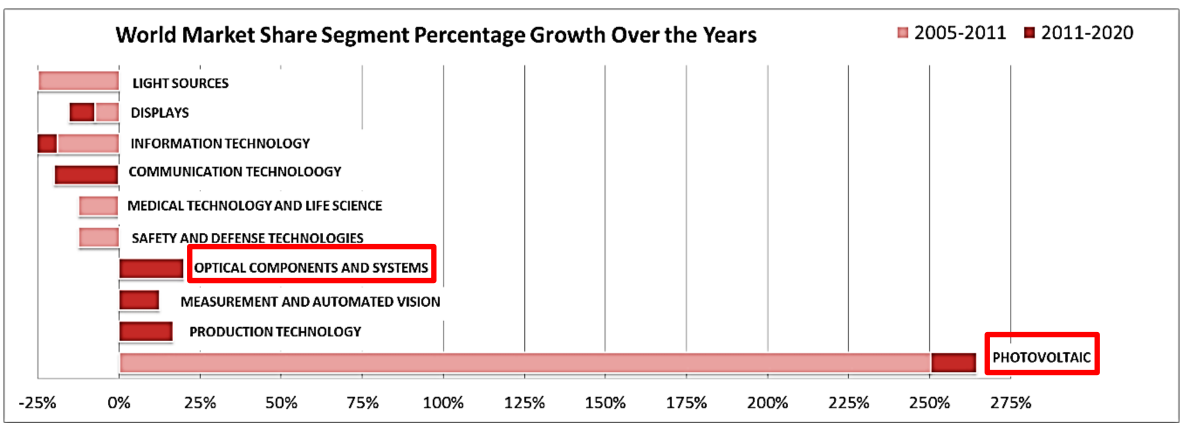

Figure 1: Photonics world market segment growth in the past (2005-2011) and into the future (2011-2020). [2]

While according to Figure 1, most market segments will see a negative growth, the optical systems and components segment will see substantial growth, where there was no growth previously in this segment. This segment consists largely of products produced using UP-SPDT freeform machining technology. These products consist of reflective and refractive components that are seen in headlights, or as part of a satellite system, or the compact optics in mobile phone cameras produced using UP-SPDT moulds [1].

Defining Surface Finish: Product Requirements and Equipment Capability

The optical components segment of the photonics industry will see the most growth as seen in Figure 1. Optical components can range from simple planar surfaces four inches in diameter as in this study to complex freeform components with micron size features organized in an array across a miniature optical part or a macro mirror like that used in the Hubble Telescope. Typically, to achieve the required functionality of the optical component, such terms as form error and surface finish are qualitatively defined by the machine. However, more accurately, in optical terms, the spectrum of light the optical component is intended for and the qualities of the transmission expected with the optical component would be more accurately defined in relation to the spatial frequency range. Figure 2 encapsulates the spatial domains in relationship to the workpiece, as will be presented in this thesis. This thesis will only deal with the realm of low to mid spatial frequencies shown in Figure 2 and does not consider high spatial frequency surface finish defects.

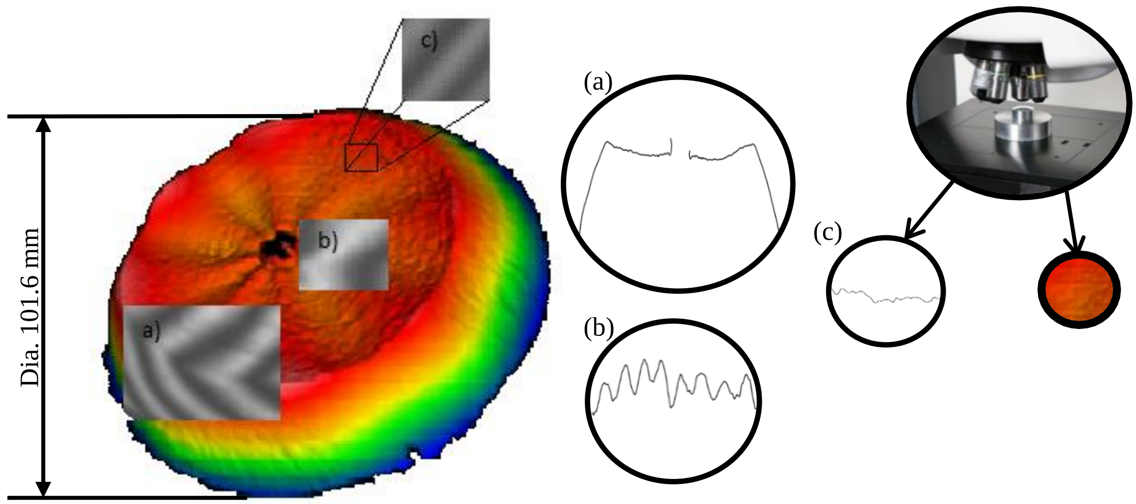

Figure 2: (a) Low, (b) mid, (c) high spatial frequencies constituting the figure/form, waviness, and surface roughness sub-groups of surface finish respectfully. (a) and (b) are the spatial frequencies as seen through an He-Ne laser interferometer and (c) is seen through a white light interferometer.

Waviness and form error typically encompasses the low to mid spatial frequencies. Here these results are defined by improper part or machine set-up, an issue with the machine's process parameter selection, or an issue with the machining process such as unforeseen low frequency vibrations interacting with the machine's dynamics, or otherwise spatial frequencies that are usually independent of the tool condition, or the workpiece material on the machine. High spatial frequencies in this study capture surface roughness. The sensor system under consideration is not able to spatially resolve high spatial frequencies and thus surface roughness is outside of the scope of this research.

With the expected increase in demand for optical components in the near future, one way to increase volume is through decreasing production time. The focus of this study is to increase throughput for optical components, or the moulds used to produce moulded optical components. Optical components machined on an ultraprecision machine have surface finish requirements that fall within the spatial frequencies of interest to this study.

Ultraprecision Single Point Diamond Turning Machining System

There are many different types of ultraprecision single point diamond turning machines. The one under consideration is a multi-axis freeform ultraprecision single point diamond turning machine capable of producing simple flat optics to complex spherical and aspherical optical grade functional surfaces. The machine under consideration can have numerous configurations and is generally placed in a carefully controlled environment with temperature fluctuations and external vibration minimized. The objective of this section is to give an overview of the machining system as viewed from its current state within a laboratory environment. This section will provide an understanding of the research conditions under which the data has been collected.

The machining system can be broken into seven main sections of influence acting on the finished product: the lab environment, the metrology system, the machine environment, the machine system including fixturing, the cutting tool system, and the workpiece system. A pictorial of the machining system and the areas of influence are shown in Figure 3. For clarification, note that in Figure 3, the machine environment is the environment within the barrier or enclosure surrounding the machine.

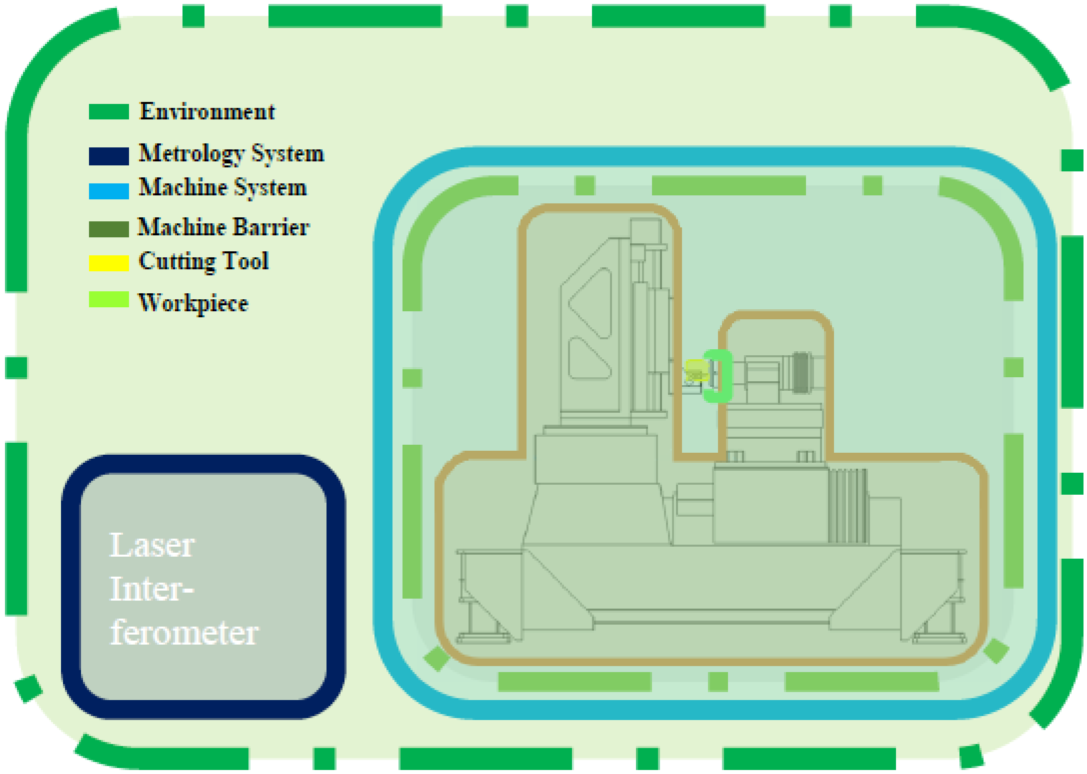

Figure 3: Main systems comprising work envelope for UP Freeform Machine production.

The Tooling and the Workpiece

The tool and the workpiece are generally accepted variants in the production system. The stiffness and the dynamics of the machine have been set based on the machine design and component selection. The configurations of the machine are determined by the operations to be performed, which influence the effective stiffness and resulting dynamics of the system. Given the profile and surface finish expectations, one assumes that the machine, tool and workpiece dynamically change over time.

New tools and materials are also being introduced all the time to the machining process. The tool setup and the workpiece setup may vary, but recommended setup procedures are provided by the machine manufacturer for optimum performance. In a production environment, picking the tool and the material comes down to a decision that is a combination of cost and functionality and this is never more clearly seen then when it comes to considering the advantages and drawbacks of single point diamond turning given the nanometer expectations of the process and the slow feed rates typically used to realize the nm surface finishes.

The tool is a single crystal of diamond sharpened to a 30-50 nm edge radius which is a critical aspect of achieving a surface finish of a few nanometers (nm) and surface form of less than a micrometer (μm) given a stiff tool- workpiece machining loop. Several characteristics of diamond give this material the ability to attain these finishes. Diamond is one of the hardest materials on earth, is an excellent conductor of heat, and can be lapped and polished through empirical means to a very sharp cutting edge radius [3]. However, single crystal natural diamond has drawbacks. A commonly known detriment of single crystal diamond is its cost in comparison to other tool materials and its affinity to diffuse into ferrous materials under the high temperatures and loads associated with machining.

Ferrous materials such as steel, tool steel, and some stainless steels degenerate the sharp cutting edge of the tool quite rapidly when compared with other non-ferrous materials like aluminum and copper. The reason for this rapid degeneration is the movement of carbon atoms from the diamond tool into the material being cut. Under high temperature and relatively high load, one carbon atom per five atoms of iron workpiece material passed over can be lost from the diamond tool when cutting ferrous material [4]. In addition to iron, other materials with an unpaired d-shell electron such as titanium have been shown to wear diamond tools quite rapidly [5].

The wear rate and type of wear is quite significantly different, between aluminum and its alloys, where they have zero unpaired d-shell electrons and 1215 steel, where iron is present and has four unpaired d-shell electrons. These characteristics aside, these materials have similar hardness and would typically be machined under similar conditions using traditional tooling, but when using a single point diamond tool (SPDT) on an ultraprecision machine [6] performance is substantially different with tool life lasting a very short time for 1215 steel as compared to an Aluminum alloy. In the test performed in [6], typical mechanical wear mechanisms such as abrasion and adhesion wear are typically observed on SPDT, but the wear rate during the SPDT process is substantially different for 1215 steel. The tool used to cut the 1215 Steel shows more wear on the rake face of the tool compared with the flank face, where most of the wear is seen with SPDT of Aluminum.

The differences in the wear location between 1215 Steel and Aluminum can be attributed in part to the higher wear rates that are seen with high carbon steels compared to low carbon steels. The removal of carbon was seen to intensify with the increase in temperature when machining high carbon steel. In general, the highest temperature seen on the tool in SPDT is on the rake face, therefore chemical, or dissolution wear is clearly the main wear mechanism with the wear from machining steel showing more significantly on the rake face of the tool as opposed to the flank face [6].

Taking these well-known issues into consideration, in today's production environment, common mould materials used by SPDT are BeCu materials coated with electroless nickel and Al 6061.

Apart from limited material for manufacturing moulds due to rapid tool failure from carbon dissolution, there are other considerations to take into account when setting up and using SPDT. Diamond is highly anisotropic. Diamond is strongest along the (110) crystallographic orientation. Incorrect crystallographic orientation of the diamond on the tool shank increases tool wear by a factor of eight [7]. Furthermore, the point of contact as the tool moves across the workpiece will not remain the same when machining a curved surface, so subtle changes in diamond properties naturally occurs in the process and can lead to unacceptable surface finish and form errors. Additionally, the radius of a tool will have errors which will transfer onto the part as the contact point between the tool and workpiece changes and the material being machined, in this paper, Aluminum has directional strength properties that will change the forces associated with cutting and thus influence form errors. Since the precision of the final workpiece usually requires sub-micrometer surface finish form, these factors need to be taken into account.

Research has provided limited ways around chemical wear and abrasive wear. New materials such as Rapidly Solidified Aluminum (RSA), now in commercial use, lessens mechanical tool wear and allows a more precision surface to emerge. RSA is a melt spun aluminum that is frozen or quickly solidified to attain a consistent fine microstructure with few inclusions. The inclusions seen with regularly processed Aluminum are the main factor in abrasive tool wear and result in parts being scrapped due to surface defects.

This section provided an overview of the tool and the workpiece from a microscopic perspective and not as entities with defined attachment to the frame of the machine. In sections further along in this thesis, a discussion will progress about the tool and the workpiece with regards to how they fit within the framework of the machine, such as how they are fixed to the machine and set-up to create a dynamically stable machining process that is in-line with the machine's design and ultimately optimizes the product outcome.

The Machine

The tests are conducted on a custom built 2001 Precitech 700 Freeform machine. The control system was designed to be able to precisely move the z-axis of the machine with a resolution of 2nm. The y-axis and the x-axis of the machines can move with a resolution of 8.6nm. Additional details on the machine's specifications can be found in Table 1.

Table 1: Machine Axis Specifications

Axis/Specification	**Travel**	**Max. Speed**	**Position Resolution**
Y	150 mm	500 mm/min	8.6 nm
X	350 mm	500 mm/min	8.6 nm
Z	250 mm	500 mm/min	2 nm
B	360^0	N/A	0.001^0
Spindle	360^0	*5000 rpm	N/A

*20 rpm is the minimum speed for the spindle with minimal workpiece load and no cutting.

The current set-up is capable of providing four-axis of motion: three linear motions and one spindle rotation. The spindle assembly sits on the b-axis and the tool can be positioned with respect to the workpiece using the x-axis and y-axis. This setup provides the most amount of control over positioning of the tool with respect to the spindle face.

This is an ultraprecision machining center and the criteria for this type of machining system is outlined in the remainder of this section. This section will demonstrate those characteristics by outlining how this type of machine is different from precision machines.

A precision turning machine is more commonly used to finish a range of mid to high volume production products primarily for the automotive and aviation industries, whereas the ultraprecision machine's focus is the topographical features of a component or essentially a surface finishing tool, where the surface profile of the component is important, while achieving the desired mirror grade surface finish.

As far as machine dynamics are concerned in this application, in order to make a clear distinction between the present ultraprecision machine and a precision machine, this section will compare a twenty plus year old ultraprecision machine center with the present, more modern machine center, which will show a progression in the machine tool system dynamics that moves away from the broader functionality of the precision machine and moves towards a clearly distinguishable machine tool focused on finishing optical and other photonics component surfaces.

Firstly, the machine tool system can be broken into a simple set of sub-systems: the machine base, the slide axes, the spindle, and the enclosure, where the emphasis is on the characteristics that give the machine tool the ability to achieve sub-micrometer form and sub-nanometer surface roughness, and can offer areas of further improvement, or challenges to production.

The main function of the base of the machine is the attachment of the axes sub-assemblies to the same surface. The base must remain kinematically and dynamically stable when the machine is and is not in operation. To meet this criteria, the base consists of the following attributes: vibration isolators to isolate the machine from floor vibrations, a rigid, thermally stable mass to directly affix the sub-assemblies to, and an arrangement, whereby the table supports (defined as the isolators between the ground and the machine) create the working envelope for a dynamically stable moving center of mass, and finally a leveling system that levels the machine that is located between the ground floor and the isolators.

This base of the UP-SPDT from twenty years ago to the more recent decade has had some significant modifications that improved the performance of those characteristics outlined in the previous paragraph. The previous design had passive air isolators that are akin to a set of bellows arranged in an optimal kinematic three-position arrangement with a single larger diameter isolator located beneath the heavier sub-assembly (spindle axis) and two smaller diameter isolators beneath the perpendicular axis that moves the tool. The isolators are separated from the floor by the enclosure frame of the machine. The isolators rest on the enclosure frame and a simple set of leveling feet exist between the frame and the ground. The passive isolators are separated from the table top by a plate, which is bolted to the tabletop. The table top to which the axes assemblies are attached has been designed using seasonally aged cast iron (thermally stable) material with a hollowed out grid designed for rigidity, dynamic stability, and weight considerations. The more recent five-axis machine has active pneumatic isolators located at four locations between the frame of the machine and the machining base table that forms a rectangular plane, in which the axes of the machine move. A leveling system is between the floor of the machine and the frame upon which rests the active pneumatic isolators. The machine table is made from a granite composite, so the table is thermally stable.

The more recent design better isolates the machine from ground vibrations, is more thermally stable, and has more flexibility in terms of manufacturability. The active pneumatic isolators unlike the passive isolators can control vertical and horizontal vibrations, not just vertical vibrations. A study conducted on floor vibrations within a production environment has shown that horizontal vibrations are more common than vertical vibrations; thereby have more of an effect on the quality of the completed part [8].

Granite composite over cast iron improves performance based on the added mass density and thermal capacity. The composite is also easier to manipulate into a functional shape as it can be cast.

Attached to the base are the linear axes. The older machine consists of two completely separate linear axes with the spindle attached to one of the linear axes. The more recent machine has three linear axes with a rotary axis mounted on the z-axis, currently where the spindle resides. The cutter is mounted on the x- and y-axes, where the y-axis is mounted on the x-axis. The newer machine has a kinematic chain of motions that can lead to more kinematic error, then the older machine, if not controlled.

The functional focus of the sub-system, the linear axes, is achieving ultraprecision motion and repeatability to within sub micrometers. The design should minimize resulting kinematic error by minimizing the work envelope, minimizing the number of components, or connections, and minimizing the distance between actuation and sensing of motion and the point where the actual cutting takes place in addition to minimizing machine distortion resulting from vibration and fluctuations in temperature.

In the past, older machines used laser interferometers for position sensing, while newer machines use high resolution laser encoders with the lines etched onto thermally inert glass mounted to the sides of the carriages. Glass scales have proved themselves to be more robust to temperature fluctuations. The laser encoders have sinusoidal interpretation for even higher resolution between etched lines. Both machines also have a thin layer of pressurized oil between the slide rails and the carriage. The difference between the machine models is seen in the design of the oil film system and the slide actuation system.

The previous machine carriages and slides had a thin recirculating film of oil between the carriage slide rails and the carriage rail mounts. The rail mounts enclose the rail on three sides of the rail: the top, one side of the bottom, and the adjacent side. As well, the carriage assembly is moved using a kinematically coupled ball screw that is isolated from the carriage through a thin film of oil and the ball screw is attached at the mass center of the carriage and actuated by a motor.

The more recent machine carriages and slides have a thin recirculating oil film with rail mounts enclosing four sides of the rail. The carriage is no longer driven by a ball screw with a rotating motor, but is driven by a linear motor system mounted along the center line of the carriage. This difference in design lends to a reduction in kinematic error and more repeatability in motion. As well, the slide’s oil film is equally pressurized from all sides leading to less variation in motion as the carriage moves. One drawback of the linear motor system is it generates a high amount of heat and generally requires a water cooling system. Since the machine used in this research does not have a dedicated cooling system for the motor more care needs to be placed on stabilizing the thermal profile of the machine before making a final finishing pass.

Overall, an ultraprecision machine is designed with a focus on minimizing the effects of vibration and fluctuations in temperature on the workpiece and being able to move in sub-micron increments. All in order to create sub-micrometer surface profiles and nanometric surface finishes with light cuts.

Metrology Equipment: Laser Interferometer

The form error measurements that were used as the base against which to compare the on-machine sensor readings were taken using the GPI XPHR Zygo Corporation Fizeau laser interferometer. Some of the more important specifications of this laboratory equipment are provided in Table 2.

Table 2: Research Lab Laser Interferometer GPI XPHR Specifications [9]

Characteristics	Specifications
GPI Laser System	Analog Camera Pixels (max. no. measurements): 640x480
	Fringe Resolution (1X): 180 fringes
	System Quality: λ/20 Plano testing (< 7 fringes)
	Test Duration: > 0.25seconds
	Wavelength, λ: 632.8 nm
	Coherence Length: >100m
	Beam Aperture Size: 4in
Test Part Characteristics	Reflectivity 0.1-99% based on GPI transmission element
	Material: glass, super-finished metals, ceramics, plastics
	Part Fixture: 3-point clamp
Operating Environment	Temperature Range: 15-30 degrees Celsius
	Rate of Temperature Change: < 1.0 degree Celsius per 15 minutes
	Humidity: 5-95% relative noncondensing
	Vibration Isolation: 1-120 Hz
	Remove Air Turbulence and uneven air density

Additionally, taking the information provided by Table 2, the spatial resolution of the laser interferometer is 0.04 mm^2 given the camera pixels in a square configuration and a maximum workpiece diameter of 101.6 mm and a 1X magnification. The spatial resolution is approximately ten times better than the sensor used, where the spatial resolution is 0.3 mm^2.

Beyond the specifications listed in Table 2, an understanding of how the measurement is taken and the environment of the measurement system is important for differentiating this system from the on-machine system.

When measuring a planar surface element as done within this research, the test piece is placed within a spring loaded three-point perimeter clamp, shown in Figure 4.

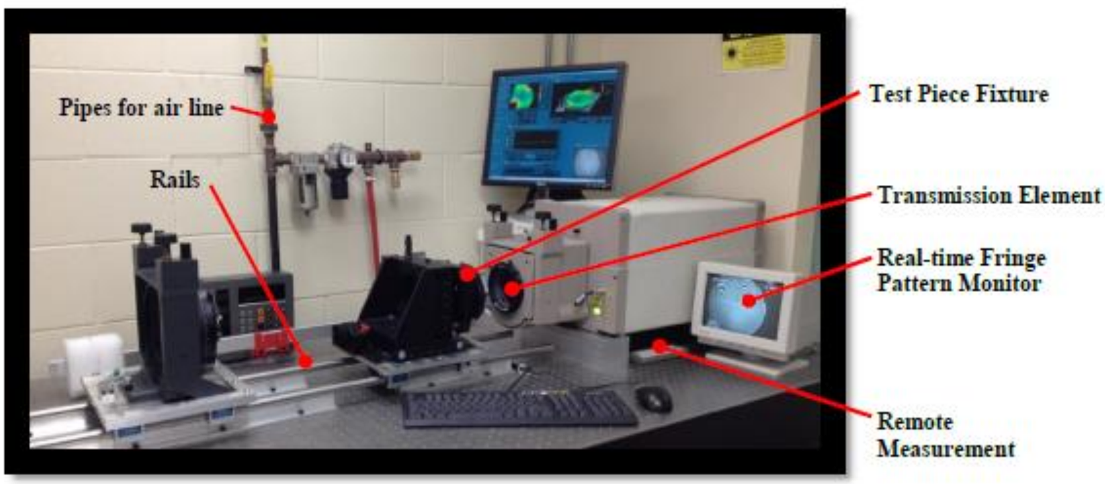

Figure 4: Laboratory GPI XPHR Laser Interferometer set-up

The measuring beam and the reference beam are aligned, the fringe pattern adjusted based on the operating procedure, and the surface finish measurement of the entire workpiece (if less than 4 inches) is taken by pushing a button on the remote control that initiates the measurement process and activates the high-resolution digital camera. The accuracy of the measurement is limited by the manual set-up, and the operating environment.

The horizontal set-up and the operating environment present some interesting challenges to achieving a good measurement from the workpiece. From Table 2, the manual clearly outlines the optimum operating environment conditions. If the operating conditions are not met, then when taking the measurements, the fringe pattern on the monitor will not be stable and will drift or disappear and re-appear. Using the current set-up, the real-time fringe pattern can be seen to drift over a two-minute time frame. Thus the measurement itself is taken internally, very quickly to ensure reasonable repeatability.

The fringe pattern drift is usually the result of fluctuations in temperature and humidity within the vicinity of the test piece and/or air movement around the equipment. These changes in air density within the space between the element being measured and the transmission element, changes the laser light's wavelength, which impacts the measurement as laser interferometry compares the laser light from two paths to measure distance.

The drift occurs across the face of the fringe pattern. Fluctuations in temperature across the surface would be most likely shown as localized fluctuations of the fringe pattern. This is not the case, so the drift may be from air currents passing through that area. However, the fringe pattern is attained through manual visual experience and adjustment. The fringe pattern should be maximized across the area being measured, but there can be slight variations in the measurement depending on the person taking the measurement, so a slight shift in the fringe pattern may not be noticeable.

Other aspects of the operating environment and the set-up to be aware of that may cause issues, are as follows. Vibration, however subtle can cause the fringe pattern to disappear usually resulting in the software notifying the operator to retake the measurement, but the operator should still be aware that subtle vibrations will disturb the measurement process. The pipes for the air leading to the vibration isolation table slightly touch the tabletop and as a precaution everything should be isolated from the table where ever possible. As well, when taking a measurement, the remote is used to initiate the measurement, not the keyboard. The slight motion of pressing the keys will result in an erroneous measurement.

Another problem with this measurement system is that the fixture holding the workpiece is a three-point, spring clamp gripping the cylindrical planar surface in place. Depending on the material being measured and the length of the cylinder, the points of contact can deform the surface at the point of contact. One should be able to see this artifact in the measurement by rotating the part and taking another measurement. The laser interferometer, while useful has drawbacks and limitations like any measurement system.

With this in mind, the capacitive based sensor system outlined in this thesis was developed to address the drawbacks associated with removing the part from the machine to do an offline measurement of the workpiece form errors. Drawbacks to offline measurement are the errors that may result from transferring the workpiece from the machine environment to the lab environment. As discussed earlier and as happens in this environment, using two different types of fixtures can ultimately lead to a false assessment of the machine's performance making it difficult to take corrective action in the production environment.

Process Environment Influence on Measurement and Machining

The ultraprecision machine and metrology resides in an environmentally controlled room. The temperature of the room is controlled at approximately 20 degrees Celsius at all times. The machine has two additional physical barriers isolating the machine from the environment in the room. The inner barrier contains the machining fluids used during cutting and sits on a large isolated granite slab for vibration isolation. The outer barrier provides another layer of thermal protection and blocks sound coming from inside the room. An air conditioning unit attached to the outer barrier is required for very high precision machining involving long machining cycles.

The air conditioning fan for the room is immediately in front and above the ultraprecision machine operator door. With the machine doors open, the temperature inside the machine and in the vicinity of the machine tools are the same as the room temperature. The temperature within the machining envelope with the doors open does not fluctuate by more than one degree Celsius over an hour.

The rate of fluctuation in temperature and humidity can affect the readings of an ultraprecision measuring device. Fluctuation in air density between the workpiece surface and the measuring device can result in inaccurate fluctuations in measurements taken. Table 3 provides an idea of how much material expands and contracts with a change in temperature, which is quite significant when measuring at the micrometer and nanometer level.

Table 3: Common Ultraprecision Materials and their Heat Expansion Coefficients [10]

Material	Coefficient of Linear Thermal Expansion *10^{-6} m/(m.K)*
Aluminum	12.3
Diamond	0.66
Steel	6.7
High Molecular Weight Polyethylene	60

Humidity also has an adverse effect on electronic equipment. Air that is too dry will cause static discharge or air with a high content of moisture will cause moisture to appear on the equipment. Either way, the humidity in this context will affect the performance of the electronic equipment. For optimum operation of the metrology equipment, the relative humidity should be kept to within the metrology manufacturer guidelines.

Machining Production Process

Figure 5 provides a generic idea of the process involved to complete an optical component using single point diamond turning on an ultraprecision lathe within a production environment.

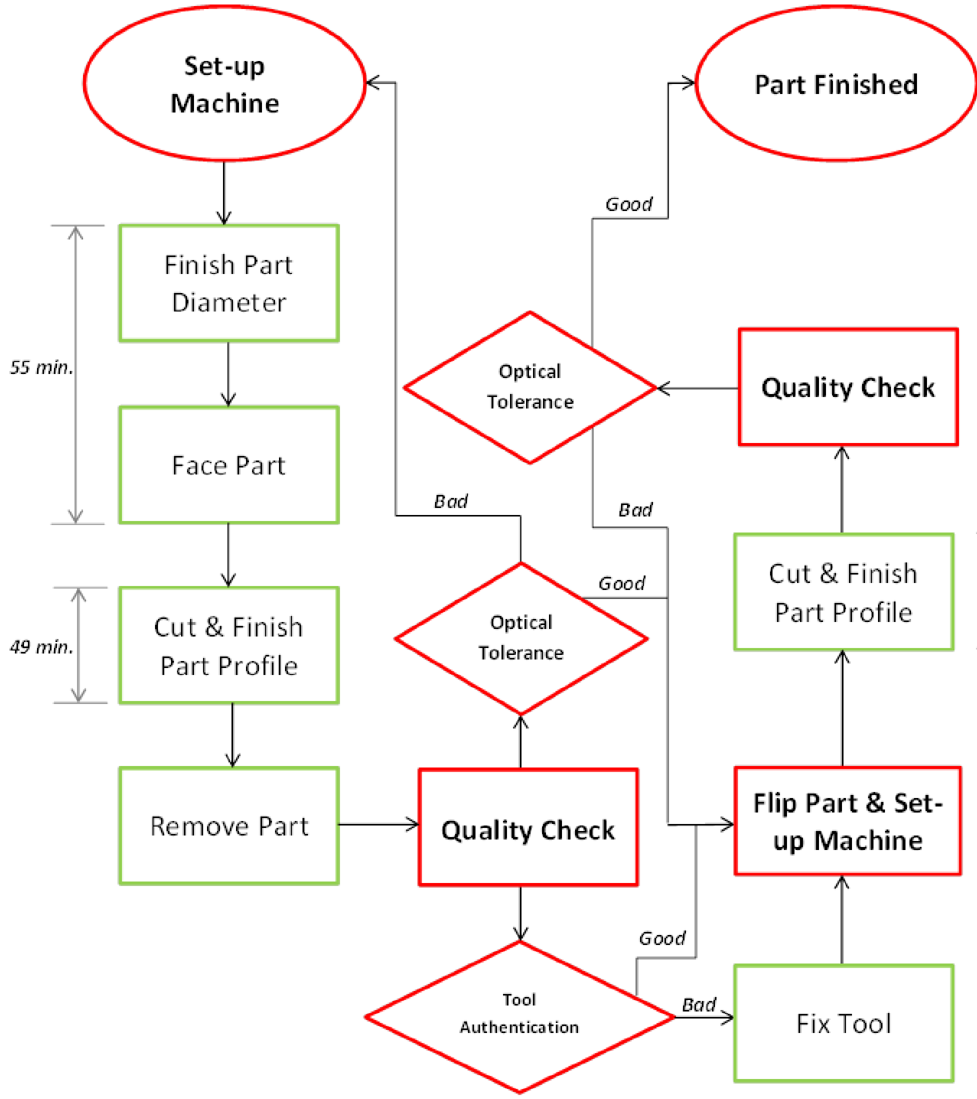

Figure 5: Process flow diagram for an aspheric glass lens manufactured on an UP-SPDT machine [11].

The cutting time is approximately two hours for this rotationally symmetric aspheric glass lens mould that will be used in a high production volume press.

This time frame does not include set-ups or quality checks, which may vary in duration and quantity depending on operator expertise, environment, machine performance, etc.

Machine Set-up

Assuming the machine is functioning within acceptable parameters the two main parts requiring detailed set-up are the workpiece and the tooling. The workpiece starts by being turned on a conventional lathe. The initial round can be centered to within 25 µm on a standard lathe. Provided one side is not to be finished a transfer dowel hole can be used to facilitate the transfer and setup of the part on the ultraprecision machine.

The faces of the workpiece should be machined to a surface finish on par with the face of the surface finish on the spindle face of the ultraprecision machine. This reduces the finish machining cutting time on the ultraprecision machine by ensuring proper support of the workpiece on the vacuum chuck face and minimum stock removal on the machined side of the part. The ultraprecision machine is designed to only make relatively light depths of cut on the order of 1-10 micrometers and as such if the workpiece fixture face is not cleaned prior to finishing the functional surface, then form errors may appear related to the fixture support surface mismatch, however slight.

Once the surface of the spindle has been inspected, the back side of the part is vacuum chucked to the spindle face. The operator then mechanically centers the part to within 2 µm using a dial indicator (this assumes that the part is axis symmetric). This is done to ensure concentricity and optimal spindle performance as described by the machine manufacturer. The spindle is then run at the cutting speed and balance is checked using an algorithm on the machine accessed through the operator interface, or using an externally mounted accelerometer. The operator first rough machines the surface using a carbide or a poly crystal diamond tool, then the surface is finished using a single crystal diamond tool. Once the first side is finished, this side is flipped and placed against the spindle face with the dowel hole being used as a rough centering tool. The high resolution electronic indicator with a 0.1 μm/volt over a 20 volt range electronic indicator is then used to center the workpiece on the spindle once again to minimize imbalance, then the part is machined along the side of the workpiece to obtain better dynamic centering of the workpiece. Then the workpiece surface is finished to an optical finish same as the first side. Prior to finishing this workpiece, or maybe using this workpiece if sufficient material is available for multiple passes, a test workpiece is used to establish the tool center with respect to the center of the spindle, or the x-axis and y-axis co-ordinate points are established to diminish the error of missing the center. Missing the center of the tool results in ogive error. Ogive error is the material left at the center of a face turned workpiece. The shape of the ogive depends on the lateral position of the tool with respect to the center of the part. If the tool is perfectly aligned with the center axis, but falls short of cutting the part to the part's center, then the shape will be a perfect ogive shape similar to an arched dome. The asymmetry of the dome shape will be effected by the lateral offset and can be quantified through interferometry. The error can only be corrected to within the 2 μm concentricity established with the electronic indicator. Once this error is reduced, the surface of the workpiece can be machined to the required surface finish. As shown in Figure 5, achieving the required surface finish will require removing the workpiece and measuring the surface finish using a Zygo white light interferometer, after first measuring the workpiece using a Zygo laser interferometer to ensure that the machine is running properly by not generating a noticeable vibration pattern or form error. Removing and setting up the workpiece back on the machine may occur many times depending on the experience with machining this component.

Importance of On-Machine Monitoring

Even with a high level of machine operator expertise, ultraprecision single point diamond turning can still lead to a high number of set-ups depending on machine performance and experience manufacturing a specific product. With an optical component, both sides of the component require finishing, so the finished component will go through at least two set-ups. Each set-up results in variation to the machine dynamics and adds a certain amount of unpredictability to the end result. Typically, in a conventional lathe, a workpiece is placed in a chuck and can be centered to within 25 micrometers. For an ultraprecision single point diamond turning lathe running at a high spindle speed, the workpiece for good dynamic balance and machine performance must be centered on the workpiece spindle to within two micrometers. If such a small amount of error can lead to poor machine performance, then logically other geometric factors related to the workpiece and machine geometry can affect the machine performance following a set-up.

Furthermore, from Figure 5, there are multiple points at which the component will need to be removed and then reset-up on the machine. This is done when finishing the other side of the part, or to improve the finished quality of the part following a quality check. When cutting a planar surface, the workpiece is rough machined until material is removed uniformly across the entire surface of the workpiece. At this point the cutting plane and the spindle plane are parallel and each subsequent cut thereafter should be removing material at an equal depth across the entire workpiece. If the workpiece must be removed for inspection, then an orientation relationship between the spindle face and the workpiece must be established, otherwise the workpiece will essentially be re-finished from the starting point whenever the workpiece is removed from the machine and placed back on the machine for further machining. As well, selecting machining parameters such as feed and speed to consistently achieve the required surface finish is often times required to meet the final desired quality.

The ability to not detect a host of errors without removing the workpiece from the machine, or likewise not being able to maintain part orientation with respect to the spindle makes producing these components in sizable batches time prohibitive and establishing consistent high quality parts complex. These are two issues that lead to high manufacturing costs. Given these factors and the advantages outlined in Table 4, one can easily see the overwhelming benefits of on-machine quality checks of the workpiece surface finish requirements.

Table 4: On-machine versus off-machine measurement

Advantages:	Disadvantages:
Operational time reduction Decreases machine downtime	May Increase machine downtime
Same environment for error measurement	Does not detect deformation from fixture
Maintain part orientation	Does not eliminate off-line quality checks
Improving repeatability by reducing error	General Environment: thermal error, cleanliness, vibration
Ability to measure and correct error without introducing further error.	Lab Environment, in addition to above: humidity, temperature, and spindle does not lock and has no position control.

The disadvantages are highly dependent on the measurement system design and how the sensor technology is implemented. A well designed system can eliminate many of the disadvantages and the deformation from the fixture must be corrected whether on-machine or off-machine measurements are used.

Chapter 2. Literature Review

On-machine surface finish monitoring can improve machine performance and lay the foundation for implementing other production efficiencies. Numerous issues must be addressed to achieve on-machine surface finish and form requirements. The foremost of those being: cost, spatial constraints, measurement cycle time, precision repeatability, use of non-destructive testing, and robustness to variation in the environment. Most nanometric measuring sensor systems available in the market can be eliminated for use in the application based on cost and the spatial constraints associated with the machine's workspace. Beyond this criteria, precision and the environment are issues, where all current sensor technology that is relatively low cost and fits within the current spatial requirements of the machine have similar drawbacks and advantages, when trying to meet the requirements and the goal of the application, in this case, measuring the sub-micrometer, mid to low level spatial frequencies comprising the surface finish of a flat single point diamond turned aluminum workpiece.

On-Machine Surface Finish Monitoring: Current and Previous Research

Sensors for Monitoring On-Machine Surface Finish

Many systems involving a variety of different sensors have been investigated and applied to on-machine metrology applications. In Figure 6, a diagram outlines some of the difficulties in finding a sensor that fulfills the measurement requirements.

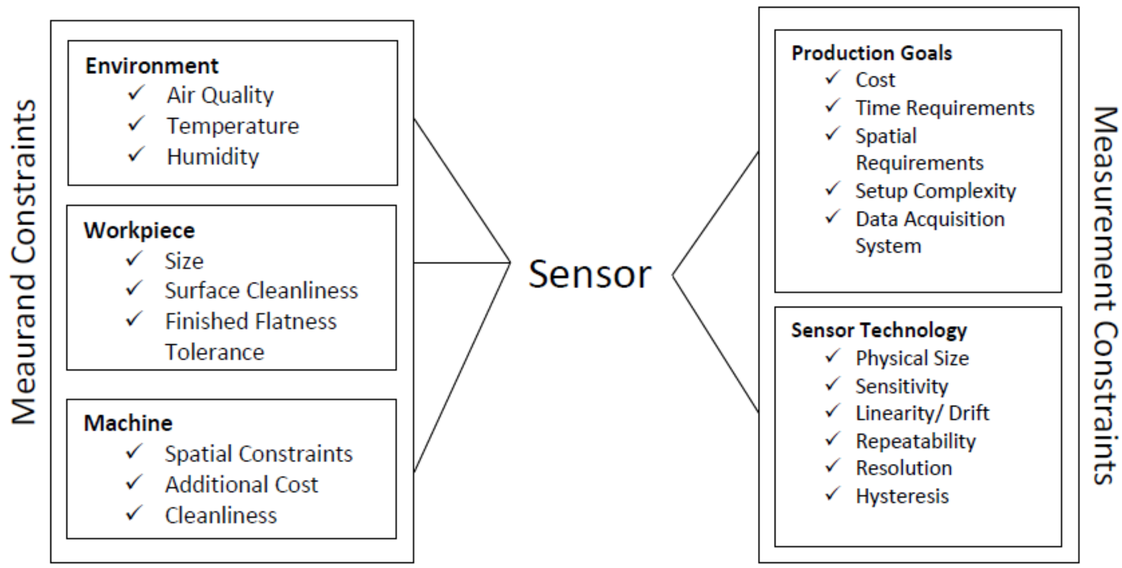

Figure 6: Non-application Specific, Various On-Machine Sensor Constraints

In the case of ultraprecision surface metrology, the sensor technology must have a high resolution and repeatability and yet meet standard production environment constraints: the sensor must be built into an application system while being inexpensive, simple to setup, and not significantly increase production cycle time.

There exist a few non-contact sensors and contact sensors that can meet some of the measurement criteria outlined in Figure 6 with more or less a similar amount of advantages and disadvantages, when placed within an off-line, sensor specific designed environment.

Figure 7 provides an overview of those sensors that meet nanometer level resolution with their advantages and disadvantages.

A.

Sensor Type	Advantages	Drawbacks
Capacitance	• Noncontact • Commercially available • Vertical Resolution • Small physical size • Simple system • Cycle Time	• Vertical Range • Environmentally Sensitive
Optical Sensor (Fiber optic Interferometry)	• Vertical Resolution • Probe on machine is physically small • Cycle Time • Spatial Resolution	• Still in Research Phase • Environmentally Sensitive • Complex system
Tactile Probes (LVDT and piezoresistive)	• Vertical Resolution • Simple system • Small physical size	• Contact, surface damage if scanning • Cycle time • Wear • Sensitivity to noise

B.

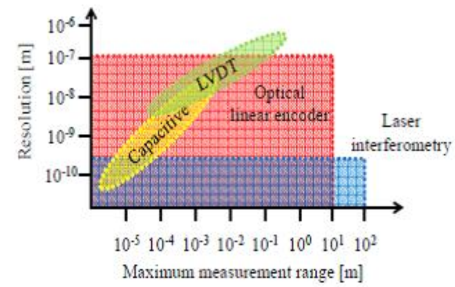

Figure 7: Sensor comparison chart of sensors viable for nanometrology surface finish measurements. a) highlights of advantages and disadvantages and b) resolution and range for high resolution sensors [12].

For on-machine measurement done on a machine designed primarily for creating ultraprecision surface finishes, these same sensors, given the same measurement quality requirements tend to fail when placed against the measurand constraints. The measurand requirements tend to make the measurement requirements prohibitive in terms of cost and production.

Sensors that are competitively viable for on-machine nanometrology for measuring surface finish are reviewed in the following sections with regards to their current application and main disadvantages when used as a single, standalone sensor.

Optical Sensors

In the field of measuring surface finish, topography, and geometrical features commercially; interferometry offers nanometric, vertical resolution over a long range of depth offline. Commercially available offline isolated systems may practice one of three viable methods: scanning white light interferometry, or vertical scanning interferometry (SWLI or VSI), phase shifting interferometry (PSI), and enhanced vertical scanning interferometry (EVSI). EVSI incorporates the better qualities of PSI and VSI [13]. PSI is capable of providing a resolution of less than 0.1 nm in less than one second. The drawbacks of this method is that the surface must have high reflectivity, where the incident light cannot resolve steps greater than a quarter of the wavelength of incident light. In most cases, the rms surface finish measurement must be less than 30nm and steps on the component must be less than 140nm. VSI, in comparison, can obtain a vertical resolution of 3nm, can measure rough and steep surfaces with variations up to 10 mm and complete these measurements at 5 to 80 µm per second depending on the microscopic lens used [14]. These forms of interferometry are a part of isolated and highly controlled surface measurements systems that cannot be incorporated into manufacturing environments without vastly modifying and increasing the spatial layout of the production system and incorporating in some cases a cost-prohibitive or incurring a substantial cost to ensure accurate, repeatable results seen with offline systems. A significant complicating factor is the requirement to use mist lubricant when machining which can end up on the optics making it impossible to make reliable measurements.

Fiber optic interferometry can achieve high frequency, nanometer resolution displacement measurements. Within the field of optics, fiber optic probes using interferometry offers the best means for online surface finish metrology measurements. The optical probe for displacement measurement can be compact and relatively low cost. The system for manipulating the optical beam and restructuring the captured data is offline and separate and may be isolated from the machine. The Attocube FPS3010 is an example of a compact fiber optic sensor that is used in industry with the ability for sub-nanometer resolution. The sensor has been applied in research, where the environment is cryogenic, or in a vacuum. Recent research delves into using commercially available optical sensors for nanometric displacement measurements. The dimensions of a few of these optical sensors can be found in [15]. While optical sensor technology exists that can provide nanometeric resolution at a high frequency, the current manufacturing applications do not require scanning the entire surface required of surface form measurements, and their implementation is for taking quality check measurements, where the results must fall within a certain predefined range.

Light based interferometry

There are various interferometric techniques that can be used for online measurements. A common one is to superimpose light from two paths: one from a reference surface and the other from the measurement path. The two signal method can overcome some environmental effects like air quality variation. A recent research study has incorporated a two signal method to overcome vibration and air turbulence. The study uses a reference mirror with a piezoelectric sensor on the mirror to use the data from the reference to remove unwanted signal data from the surface measurements. The system, in addition to a reference signal has a CCD camera and lens to relate the measurement taken to known positions on the surface. The measurement takes under 2s and can achieve nanometric accuracy. The drawback with this setup as seen with other previous and recent online measurement systems is the complexity and associated system cost [16]. The sensor in and of oneself will achieve nanometric accuracy at high frequency within a compact space and low cost. However, the system with the cabling for the sensor, reference mirrors, CCD cameras, etc., create a complex, costly and bulky system for this application. This is only a marginal view of the problems associated with calibrating and setting up an optical sensor topography measurement system. Light is sensitive to air turbulence, temperature gradients, humidity and vibration that also lends to the system complexity.

With Aluminum, the primary material machined in this study and with the UP-SPDT industry, the homogeneous nature of the material comes into play. Changes in the refractive index across the surface of an inhomogeneous material can lead to altering the optical path length of the reflected beam. This change in path length does not have to do with the topography of the surface and leads to measurement errors [17]. Pure aluminum is inhomogeneous and often times contains microvoids, which are opened up and can be seen on the surface of the machined part. The microvoid density can vary substantially across the part. Micro-voids, or the inhomogeneousness of Aluminum can lead to these type of measurement errors.

Other common issues with optical measurement systems that have an effect on an online system are the surface conditions. Surface conditions limit the range and resolution such as the maximum slope measured, the specularity of the surface, step size, curvature, and maximum angle resolved can all diminish the measurement accuracy. Common basic setup issues are axial alignment for position referencing, parallelism, and light source variation.

The many issues with optical measurement systems have been researched and resolved to a limited extent, usually at the expense of increased system complexity. For online measurement systems, a heterodyne interferometer shifts the frequency for the displacement signal to avoid affects from low frequency light source intensity variations and noise. Mini-fiber optic interferometers are separate from laser and receiver electronics and are less sensitive to mirror misalignment. Researchers in the past have used multiple commercially available optic sensors to cover the measurement area and use the method of triangulation to overcome step height problems [18].

Induction Sensors

Induction sensors are entrenched in industry and are commonly known as eddy-current sensors. These sensors generate a magnetic field that when approaching the material under inspection will induce a magnetic field in the adjoining material that interacts with the sensor’s magnetic field. The change in the magnetic field is calibrated to the change in the distance between the sensor and the target. The sensor magnetic field is relatively insensitive to dirt, oil, and other contaminants, as well as corrosive environments, but the material must respond to a magnetic field to be calibrated. In this case aluminum is suitable, but other materials like plastic and glass are not.

The main issue with using the inductive sensor for measuring topography can be described through the fundamental theory governing these sensors:

$$\delta = \sqrt{\frac{\rho}{\pi \mu f_{ex}}} \quad [19]$$

This equation reveals the depth of penetration, δ of the magnetic field beneath the surface of the target material. The target position is where the maximum density of the magnetic fields is found and this occurs, where the field penetrates the target material, called a lossless image plane [19]. The only practical way to decrease the depth penetration is to increase the frequency of the magnetic field, f_{ex}. For Aluminum, with a conductivity, ρ of 38 x 10^6 S/m and a permeability, μ of 1.25 x 10^{-6} H/m, a frequency from 10 kHz to 100 MHz will change the penetration depth from 820 μm to 8 μm [19]. This depth penetration is still quite significant in this application, given the presence of voids within the workpiece material.

The higher frequencies create additional issues. With a traditional coil wound inductive sensor, the coil will become quite dense (minimum range, ultimately resolution is limited by minimum physical size of coil, which is 100-500 µm). This higher frequency coil has large parasitic losses from the cable and the interface electronics that causes a high amount of heat generation relative to the tolerances in this application [20]. Heat generation causes a change in permeability in the target material that leads to measurement error. Permeability is highly sensitive to changes in temperature, so inductive sensors are highly sensitive to changes in temperature. A recent study shows that a change in the bridge structure will allow the measurement system to break down the data into the different components comprising the magnetic field fluctuation: inductance and resistance. The ability to measure inductance and resistance separately allows one to measure not only the error in measurement due to the change in temperature, but measure an accurate change in position despite a change in temperature [21]. However, a sensor, which generates heat in this application can affect the workpiece material by changing the workpiece's dimensions and hence influence the measurement.

Other research approaches the temperature issue with a new type of sensor configuration and electronics interface. The inductive sensor with new manufacturing processes can be configured into a flat compact sensor where the parasitic losses are eliminated by combining the electronics interface within the proximity of the sensor. The new sensor can have the required high frequency and lower heat generation, but at the cost of lateral resolution. As well, there is a significant increase in power generation to establish this new system [20].

Looking again at the lossless image plane, there is something else to consider. As the penetration depth approaches zero, the sensor's chief advantage over other noncontact sensors vanishes. The sensor is no longer insensitive to contaminants on the target surface [19]. In fact, since no study has been done on this new phenomenon, at a nanometer measurement level, the sensor may be affected by dust, humidity, and other pollutants entering and moving through the air gap as the measurement is taken.

Tactile probe sensors

Tactile probes, as their name suggests take measurements by physically touching the surface of the component under investigation. In the case of surface finish measurements, the mechanical mechanism is usually a cantilever projectile that moves along the surface of the component. The surface topography causes the cantilever to move vertically. The vertical motion is translated through a transducer that converts the mechanical motion to an electrical signal. The resolution of a tactile sensor is theoretically infinite if the mechanical motion of the stylus is transmitted through a linear variable differential transducer or transformer (LVDT) [22]. With a cantilever configuration, the mechanical motion can be detected as well using piezo resistive sensors or strain gauges to nanometer level resolution. Given that they involve mechanical mechanisms these sensors are prone to hysteresis [23].

A tactile stylus measures the direction normal to the surface of the workpiece. The stylus can take as many measurements of the surface as required to attain accurate surface characterization. The most commonly used machine in industry is the coordinate measuring machine (CMM) that uses a tactile probe to characterize the part. The Gannen XP 3D tactile probing system has a repeatable resolution of 2nm and a 45nm stylus probe diameter [24]. The probe is attached to three slender rods with integrated piezo resistive sensors with a hysteresis of 0.05%. This highly specialized CMM is used for measuring the characteristics of micro components. The CMMs and the Talyscan surface finish machines are offline, fully automated, environmentally controlled and isolated machines. These machines have anti-vibration mounts and environmental enclosures to eliminate floor vibrations and acoustical noise that are reduced to a point where nanometer level measurements are guaranteed [13]. Offline, the tactile sensor is isolated from vibration or noise that would otherwise impede the repeatability of the measurement. The tactile sensor is prone to significant drift from environmental noise especially at micrometer and sub-micrometer measurements.

Even under environmental control, many other errors in measurement must be taken into consideration when using the tactile probe system for sub-micrometer level measurements. Stylus flight is a common problem with tactile probes if the workpiece and process is not flat enough to take measurements. Stylus flight occurs when the probe loses contact with the surface due to the change in surface gradient. Flight leads to missing points and erroneous measured points. High speed, changes in speed (i.e. friction slip-stick), changes in applied forces, damping (impact force), surface height changes, and the spatial wavelength of the surface due to roughness for example can lead to stylus flight [25].

Stylus flight is just one area of measurement error at the nanometer level. The stylus tip will also wear with usage and create a flat. The width across the flat affects the spatial resolution of the sensor. As well, the stylus probe stiffness can lead to indentations and scratches on the surface upon impact, and can cause sliding, and stick-slip issues, if the probe is used for scanning the surface of the part.

Decreasing probe stiffness in relation to material stiffness will make indentation affects negligible, but will lead to an increase in flight and surface sticking induced errors during scanning [24]. Surface finish measurement errors can be minimized by slowing down the speed of the probe during impact or scanning, however this increases the measurement process time. A slower speed can be partially overcome by spiral sampling, instead of the standard rectangular grid method when taking surface finish measurements [26].

A slow measurement process and surface finish damage when scanning a workpiece surface are the main detriments when using a tactile probe system within the framework of nanometrology in a production environment. With the addition of on-machine measurement, the machine vibration becomes a significant source of measurement error from increased stylus drift and flight. As well, special consideration in nanometrology has to be given to changes in mechanical properties, grain boundaries, surface tension, and static buildup. Given all this, tactile probe systems as online measurement systems have major drawbacks that make them unsuitable for ultraprecision online surface finish measurements.

Capacitance Sensors

In this research study, a capacitance sensor is the sensor of choice for surface form measurement online for ultraprecision single point diamond turning of a flat aluminum workpiece. This section will not only cover the operation, advantages, and disadvantages of these sensors at nanometer operation, but this section will go into more depth as to the future of capacitance sensor technology and the applications of commercially available capacitance sensors within the manufacturing machining industry.

Capacitance sensors operate on the principle of capacitance, C. The following equation defines capacitance of parallel plates and the aspects that impact these type of sensor outputs.

$$C = \frac{\varepsilon_0 \ \varepsilon_r A}{d} \quad [19]$$

Where ε_0 is the electric constant, or the vacuum permittivity, 8.854 x 10^{-12} $F.m^{-2}$, ε_r is the electrical permittivity of the material between the plates, A is the sensor's operational face in m^2 and d is the distance between the plates in meters.

The sensor and the target form the plates of the capacitor. A voltage applied to the sensing area of the sensor will cause charge to form on the surface of the sensor and the target. The electric field that is generated from the sensor surface to the workpiece changes as the distance between the plates change or if the dielectric properties of the material between them changes. Thus this sensor is sensitive to changes in the air and surface properties of the sensor and part. The capacitance sensor works when the target is a conductive material such as Aluminum, Brass, or Steel. As long as the material is conductive, the electric field will only sense the surface of the component and will not penetrate below the surface of the material, since the capacitance measures the change in the charge between the plates and there is a constant flow of positive and negative charges, where the distance is measured by a change in the current. A capacitance sensor can detect a non-conductive object and measure the density and thickness of a non-conductor with a grounded conductive material behind the insulator [27]. A non-conductive material on the spindle face would create just this situation. If the conductor could be removed as support, then one would measure the change in the capacitor's fringe field as the sensor moves across the non-conductive surface. Fringing occurs in the absence of a conductive plate and the electric field bends back to the sensor body creating a fringe field. With or without a conductive plate supporting the non-conductor, the capacitor may or may not be detecting the surface.

From the capacitance equation and from a general understanding of the operation of a capacitance sensor comes many of the issues when employing a capacitance sensor. As shown in Figure 8, the electric field generated from the sensor area will emanate from every surface without a guard to surround the sensor body.

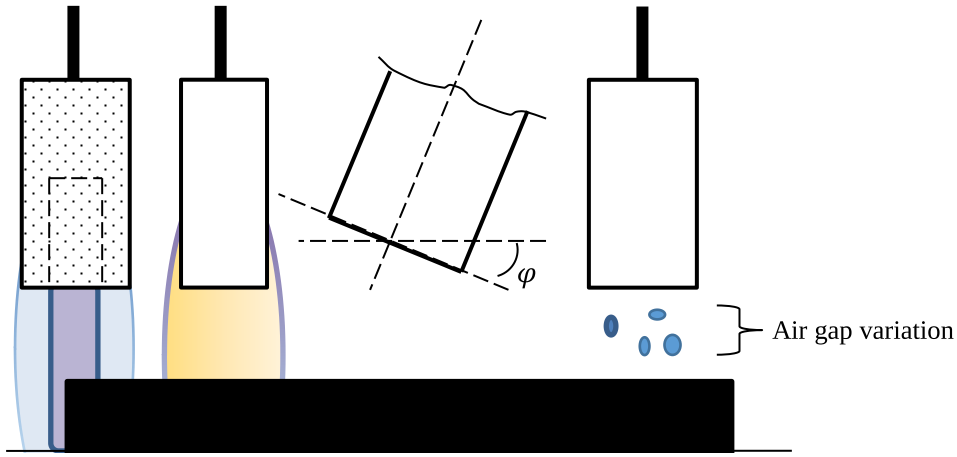

Figure 8: Measurement errors generated by capacitance sensor. A) Shielded sensor at target edge, B) Unshielded sensor, C) Sensor face tilted to target, and D) Air gap environmental variations.

A guard can be used to focus a capacitive sensor and reduce the associated charge interaction with surrounding materials. When applying a capacitive sensor to measure the distance to a target, if the area of the target is smaller than the sensing area or if the sensor is over the edge of a target, then an electric field will be generated from the sides of the target causing an erroneous measurement. To be effective the general operational rule is that the target area is to be 1.3 times greater than the sensing area in order to make this error negligible.

A change in the dielectric properties between the plates can affect the measurement result. This effect is shown in Figure 8d, the charge is affected by a change in the humidity between the plates. The dielectric between the target and the sensing area in this research study will be air. The number of atmospheric ions or the dielectric constant of the air in the gap is directly affected by the relative humidity. Relative humidity is a measure of water in the air and is affected by changes in temperature and pressure. According to [28], moist air obeys Ohm's law where the atmospheric electric fields between the plates is directly proportional to the current generated as long as the voltage applied is less than 1000 V. Below 50-60% relative humidity, the atmospheric ions are too great in number compared with the water molecules to have an effect on the capacitance. The capacitance sensor will not be affected by changes in the dielectric constant of the air as long as the temperature, humidity and pressure are controlled. A capacitance sensor does show signs of hysteresis when humidity changes. Humidification followed by dehumidification to the same initial relative humidity will give different measurements [28].

The equation above for capacitance is for parallel, flat plate electrodes. In this research, the sensor will have a flat face connected to a cylindrical body with a likewise flat plate target. If the capacitance sensor electrode face is tilted to the plate, a non-linearity error is introduced into the measurement. As well, at a nanometer level measurement, the surface roughness of the electrode face can produce a non-linearity error depending on the measurement range and the sensing area size. The tilt and the surface finish error have the same effect on the linearity of the measurement system. The resulting error does not affect relative measurements, but the gain error or fixed offset error can decrease the performance of the sensor system [29] [30]. In [29] the research provides an equation by which to determine the allowable surface finish waviness or change in vertical height that makes the effect of the surface finish of the electrode negligible as follows:

$$\Delta e < D.\varphi \ ,$$

where Δe is the surface waviness allowed as long as the product of the diameter, D, of the sensing electrode and the tilt, φ (rads) is larger (φ = arctan(Δe/L)) which for this study means that the surface finish is negligible, since the electrode diameter is quite large compared with the measurement range.

In addition to being sensitive to fluctuations in temperature and pressure, or changes in the air permittivity, if the capacitance sensor is not properly calibrated for the application, then when the sensor is moving across the target, the electrode can experience electrostatic overcharging that results in low frequency variation.

These are the main drawbacks to using a capacitance sensor for measuring nano-metrology surface finishes on the machine. Most research to reduce these effects focus on a capacitance sensor's usage on a lithography machine, or where precision sub-nanometer assembly is required. Within these research studies, they have changed the reference capacitance to reduce temperature drift effects and fitted the sensor with a stepper thermal collar for alignment error reductions. However, these modifications are not commercially available, in regards to the collar, or the capacitance sensor interface attachment, and therefore are outside the scope of this research.

There have been relatively successful attempts at using commercially available capacitance sensors to measure the surface of ultraprecision parts meant for in-situ on the machine measurement systems. Research in 1995 ([31]) uses an array of capacitance sensors to incorporate a reference line when measuring the flat surface. More recently research conducted in 2013, and outlined in [32], had the goal of measuring surface finish using one of two techniques. The one technique employs two micro-epsilon capacitive sensors. The paper uses one sensor as a reference to compensate for Abbe error, an error inherent in all translating measurement systems, as shown in Figure 9.

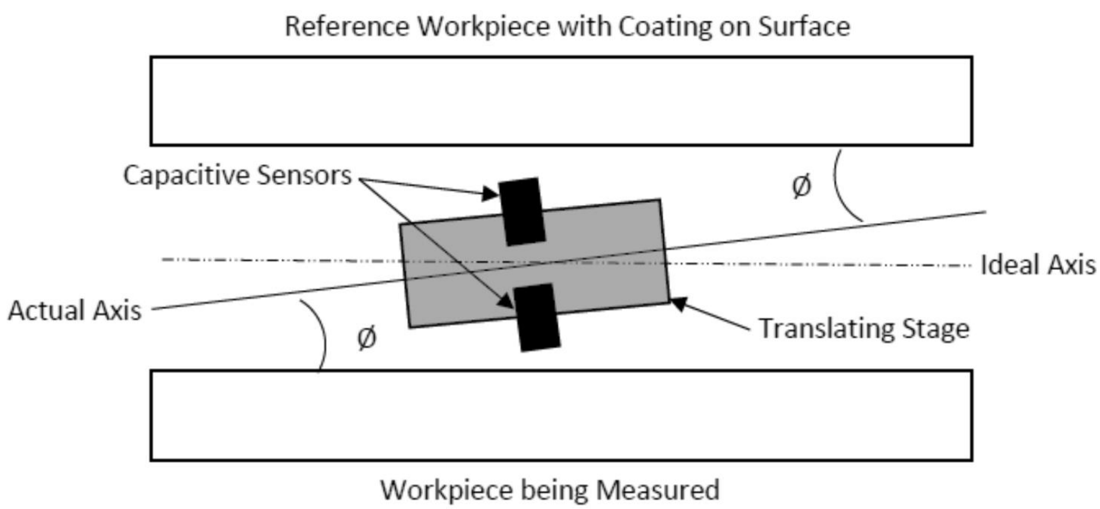

Figure 9: Diagram of Abbe Error as seen through the experimental setup in [32]. The Ø represents an error associated with the measurement system that is canceled out by the reference when the setup is properly aligned.

The reference sensor measures an ideal workpiece and can be used to filter out the effects of the air gap, or thermal drift of the measurements. The results are quite repeatable and attains a resolution of 1nm, but the testing was within a controlled environment and the setup is quite different from the machine environment.

Considerable research has been done in an attempt to use a capacitive sensor, an array of capacitive sensors, or a combination of sensors with a capacitive sensor that either directly or indirectly measures the topography of the surface of a workpiece within the precision machining industry. Table 5 provides a summary of some of the studies that come close to the research outlined in this thesis.

Year Pub.	**Source**	**Comparison Summary to Current Research Study**
2011	[33]	Use a calibrated 0.5mm diameter sensing area electrode from Lion Precision. Calculate average value from stylus reading to compare to capacitive value as done in [34]. Study takes measurements every micrometer for comparison to stylus. Study takes measurements from ground, milled, and shaped pieces. Closest measurements between systems is seen with milling.
2011	[35]	Study uses a stylus pressed onto the drum of a cylinder with a cantilever spring and capacitance sensors are arranged along length of stylus arm and measures 0.1 micrometer profile depth.
2007	[36]	This study develops a linear regression model by comparing the measured Ra with the spindle Ra from the designed cylindrical capacitance sensor. The linear regression model is used to predict the Ra given the capacitance sensor reading from the spindle. This model is applied to milling.
1998	[34]	This study takes measurements on the machine following turning process in order to correct machining errors. Use fringe field of capacitance sensor and calculate average value to compare with Ra. Measurement system is not sensitive to material type, coolant or lubricant spray, and other disturbances are low. The study found that the pneumatic heads clean surface of the lubricant well enough that the measurements are not corrupted.

Table 5: Summary of recent research focused on on-line measurement of workpiece surface topography.

Summary

A commercially available capacitive sensor is compact, relatively inexpensive, and has the potential to take sub-micrometer surface finish measurements of the workpiece on the ultraprecision single point diamond turning machine. The main drawbacks can be largely overcome with proper calibration of the sensor with the capacitance sensor interface. The tilt has been studied and shown to be inconsequential for relative measurements as long as the tilt to the target is within reasonably achievable setup limits, [30] which is the case for most optical components. Previous research has taken measurements from the workpiece following various machining processes and only compared the measurement with the Ra value from other measuring equipment. Recent research has not measured the qualitative surface finish of an ultraprecision turned workpiece, while on the machine. This study sets out to use a commercially available capacitance sensor that is compact, has a small electrode diameter, and nanometric resolution and qualitatively determine the sensor's ability to detect mid to low spatial frequencies present on the workpiece with the workpiece still mounted on the fixture of the machine.

Chapter 3. Experimental Work

The remainder of the research report will outline the system developed to take measurements on a production ultraprecision single point diamond turning machine and the measurements taken. The single capacitance sensor took measurements of a turned workpiece following finishing. Finishing being defined as a mirror grade surface that has a flatness and parallelism error of less than 0.5 micrometers across the entire part in the direction of the tool path. This would be well within industry standards for a well-operated, finished turned ultraprecision component and would allow for the usage of a high resolution capacitance sensor, where higher resolution usually means a lower working range.

The sensor will be set-up to take two types of measurements. Firstly, measurements will be taken as the sensor moves radially across the workpiece following the same path as the tool would take radially across the workpiece. Secondly, the sensor will be set up to take measurements at various points as the workpiece rotates and thereby take circular measurements of the components. These two measurements should capture all the low to mid spatial frequency errors, more commonly referred to as profile or form errors.

Test Equipment

The data acquisition system connected to the capacitance sensor that was implemented for this study is shown in Figure 10.

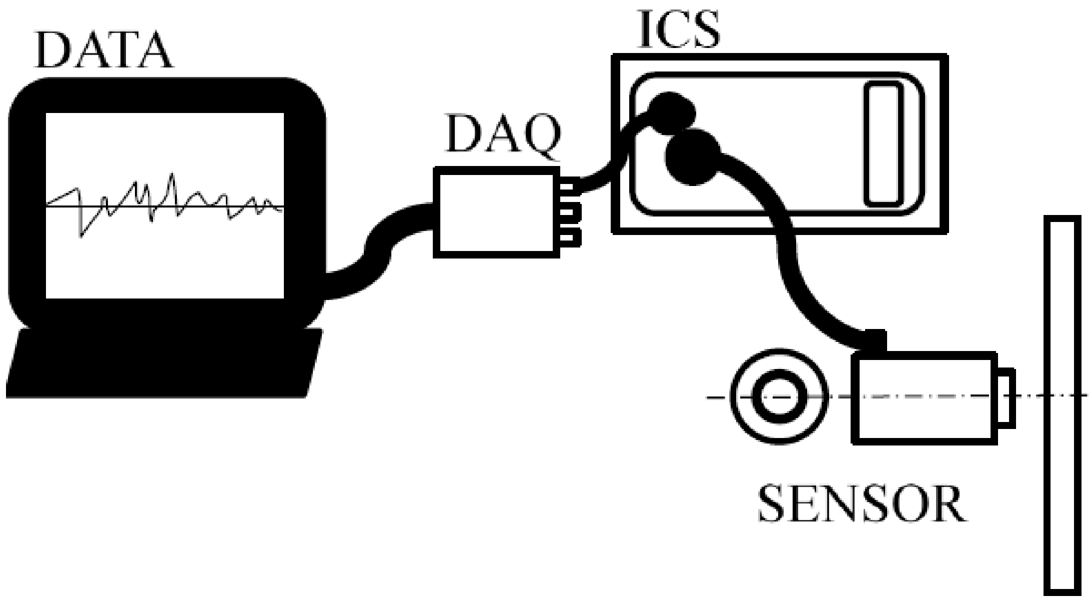

Figure 10: System for Data Acquisition

The capacitance sensor is a Lion Precision C5R-0.5-2.0 coupled to a DMT10. The sensor was chosen from amongst others based on it having the smallest lateral resolution commercially available at 0.5mm diameter, a high resolution at a high frequency: 0.2 nm at 5 kHz. The capacitance sensor works over a 10 micrometer range at a standoff of 10 micrometers from the target, or in this case the workpiece surface. The more important sensor capabilities and the interface unit specifications for the sensor are listed in Table 6 and Table 7, respectively.

Table 6: Capacitive Probe, C5R-0.5-2.0 Capabilities [37]

Specification	Value
Electrode Diameter	0.5 mm
Min. Sensing Area	0.65 mm
Range for 2nm p-p	10 µm (±10 VDC)
Near gap	10 µm
Bandwidth	15 kHz
Resolution @ 15kHz	2.4 nm
Resolution @ 5kHz	0.2 nm
Sensor Dimensions	(5 Dia. x 17 long) mm
Amphenol cable	2 m ±25 mm

Table 7: Probe Driver, DMT10, Capabilities

Specification	Value
Output Voltage	±10 VDC
Bandwidth	20 kHz (set for this study)
Differential Voltage	yes

With a capacitance sensor, one looks for a sensor with one tenth the requirements of a production process resolution, so while the sensor has a nominally reported 0.2nm resolution in a well-controlled environment, one would expect under less than ideal conditions the resolution due to influencing factors would be ten times more, or in this case, 2nm at 5000 Hz.

For data acquisition, the analog to digital converter is a NI 9234. Given the 20 V output of the sensor and the required resolution and high bandwidth, this analog converter is capable of a ±5 volt range with a 1.2 microvolt resolution with 24 bits and a maximum of 51.2 kHz sampling rate. The sampling rate and the resolution is more than enough to overcome the error associated with the sampling process. The sampling rate is based on an integer value that must be adhered to in order to minimize sampling error as the analog converter takes in data continuously during the measurement process. The main drawback of the NI 9234 is the small voltage range. This further limits the range of the capacitance sensor.

Another important quality for this study provided by the NI 9234 is the differential voltage. This allows connection of different types of sensors to the same unit with grounding that allows for continuous measurements and diminishes cross-talk, or electrical interference making other units impossible to use. A list of the more important qualities of the analog to digital converter are listed in Table 8 that make this unit the best option for this application.

Table 8: DAQ, NI 9234, Capabilities

Specification	Value
Voltage Range	±5 VDC
Max. Sampling Rate	51.2 kHz
Min. Sampling Rate	1.652 kHz
Bits	24
Resolution	$20/2^{24}$=1.2μV
Differential Voltage	yes

Sensor Fixture

The main drawbacks with regards to the mechanics of setting up and using a capacitance sensor requires a well-designed flexible sensor fixture. The required parallelism of the sensor face to the target, the inability to see the near gap, or the range visually, the need to calibrate the sensor, the rigidity of the surrounding machine, the fact that single point pressure, or too much clamp force must be avoided when holding the sensor, and the requirement of flexibility of design due to inexperience creates some challenge when designing a fixture for a capacitance sensor. Additionally, the sensor must be set-up (for the purposes of this study) within the same space as the tooling used to turn the workpiece, and the measurements will be taken as closely as possible along the tool path in order to minimize measurement error related to the kinematics of the machine axis. The useable footprint with and without the tooling is shown in Figure 11, which has a picture of the machine's current set-up for turning. As one can see the space for the sensor is quite small.

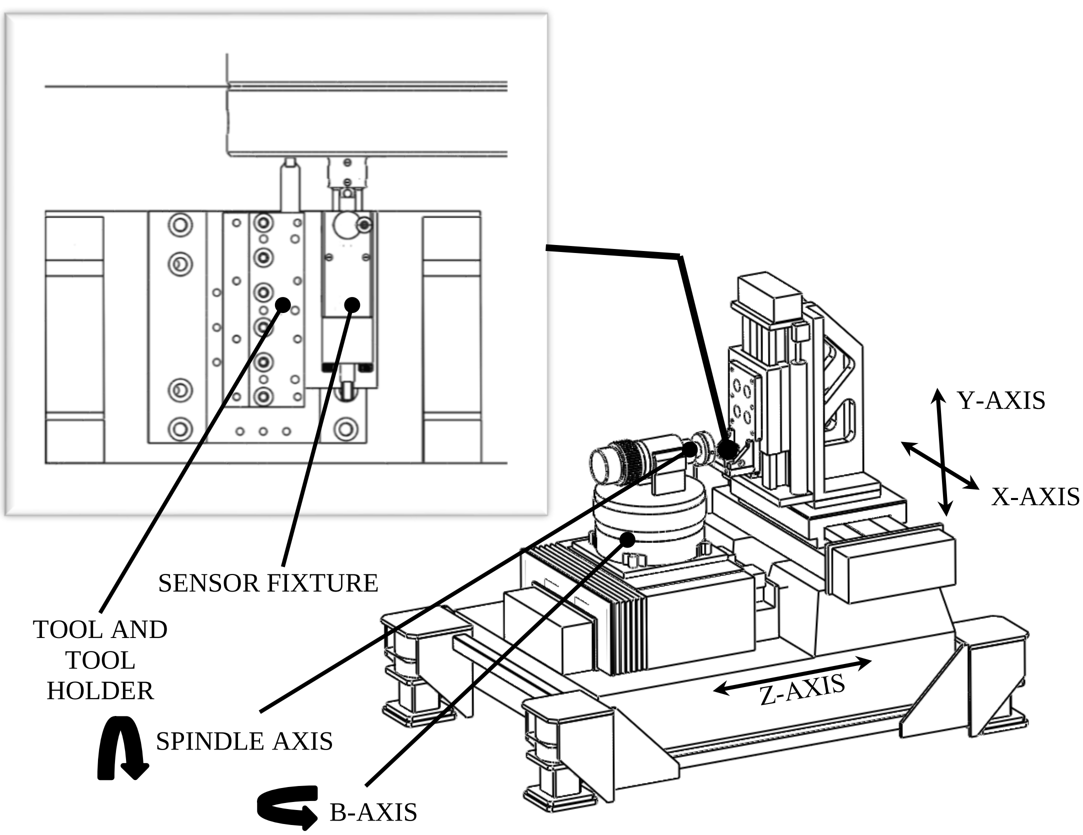

Figure 11: Current Machine Set-up Spatial Constraints

The sensor comes from the supplier uncalibrated, so before designing the fixture for the tests, the sensor was set-up on a vibration isolation table, and the sensitivity of the sensor was measured using a realistic workpiece material. Consistently, the sensor was found to have a range of approximately 10 micrometers over 7 volts. The near gap for the sensor is indeterminable in practise as 20 μm is very difficult to see. Thus the sensor is set-up in an off position. The sensor is placed flat against the target, then moved back from the target, until the sensor voltage begins to change. At this point, the sensor is active and is within working range. If the sensor is turned on, while pressed against the target, then the sensor will be overcharged and will not work. At this point the sensor must be turned off and allowed to rest for a few hours. Therefore, the exact near gap of the sensor is not known, but is believed to be approximately 20 μm. From this information, the sensor fixture must be adjustable to a point that the sensor can be moved to the middle of the working 10 μm range.

A picture of the sensor fixture is shown in Figure 12 and the specifications of the sensor fixture are in Table 9. The sensor is adjustable through a differential screw that has a resolution of 1 μm per 6 degrees of revolution and a total travel of 1mm. A wrench is used on the back of the fixture to allow for minute adjustments and a spring is used within the mechanism to pick up the backlash in the thread pitch.

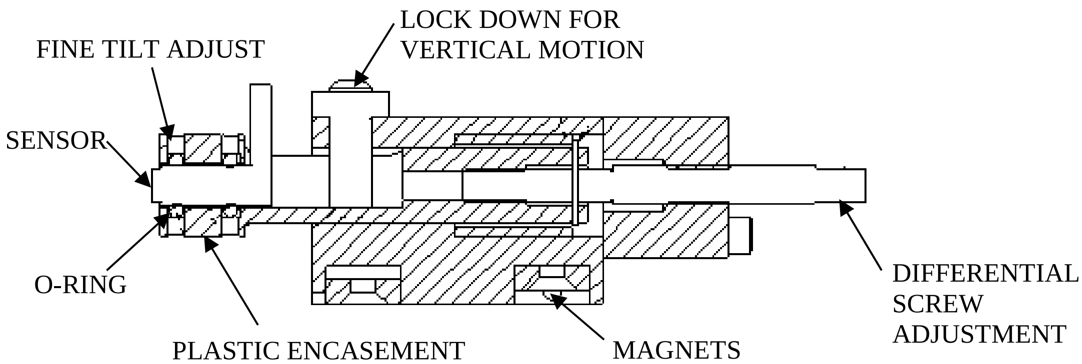

Figure 12: Sensor Fixture

Table 9: Sensor Fixture Specifications

Specification	Value
Adjustable Tilt	Yes
Linear Resolution	1 µm / 6 degrees revolution
Linear Travel Range	±1 mm
Minimum Magnet Pull force	<0.5 lb
Maximum Magnet Pull force	3.5 lb

The sensor is held in place by o-rings that apply pressure along the circumference of the sensor in two places along the length of the sensor. As well, set screws are located at ninety degrees along the circumference of the o-rings to allow for minor tip and tilt adjustment of the sensor. The sensor fixture is also adjustable through the use of magnets to hold the fixture in place. As the forces and vibrations within ultraprecision machining are minimal, the magnet force is very small and is negligible about 2mm from the steel mounting plate. This allows one to place the sensor against the target very easily and then drop the magnets into place to fix the fixture in place. This makes visually aligning the sensor parallel to the target easy to set-up and re-set-up as required. To make the sensor fixture more rigid once fixed into place a stop is pushed into the sensor guide and locked, in order to keep the sensor from vibrating vertically.

Calibration of Capacitance Sensor

The capacitance sensor for this study did not come calibrated from the supplier, so measurements were taken on this setup to determine the linearity, sensitivity, resolution, and the frequency response of the sensor. These measured values were then used for the rest of this study.

Analog to Digital Converter

First, the analog to digital converter was tested to make sure that a high sampling rate would re-produce the captured signal from the sensor. A wave generator was used to test the analog to digital converter. For data frequency analysis, the bare minimum to detect a sine wave is to sample at twice the frequency of the sine wave. At this sampling rate, one will get two points for every cycle. However, in practice, for minimal error when randomly sampling, one should sample between five to ten times the maximum frequency one expects and this is especially true if the shape of the wave form is important. Using NI9234 and a wave generator, the sampling of five times the generated sine wave of 5 kHz reproduced the sine wave and clearly demonstrated that the analog to digital converter was working. For this testing, the converter will be continuously sampling. In this mode, if the sampling is not set at an integer multiple of the internal master frequency base of the analog to digital converter as described in the manual [38], the sampling rate will contain errors. The sampling rate will not be consistently correct and if using the timer, the time will dip into negative values.

Sensor Performance

A normally functioning capacitance sensor mounted in a fixed position will output a voltage value that when captured over a few seconds will provide a voltage value that fits within the expectations of a normal curve. Data was captured from the capacitance sensor over about 10s and then the data was sorted in order to see if the data would fit within a normal curve. Figure 13 shows the distribution of 40,000 samples taken from the sensor.

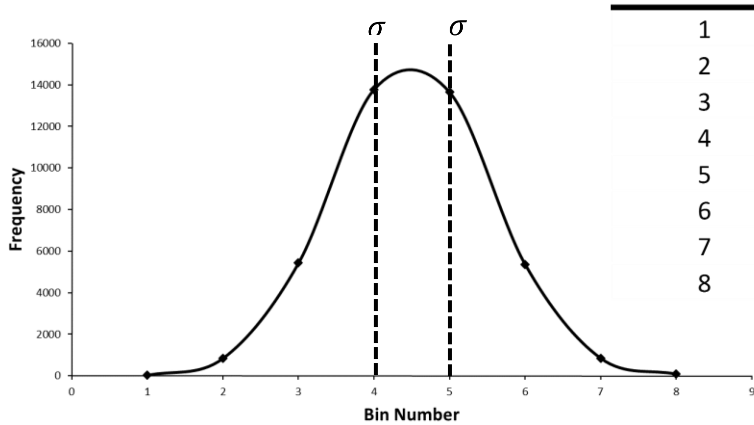

Bin Number	σ *(V)*	*Frequency*
1	-4.593	27
2	-4.582	842
3	-4.572	5425
4	-4.561	13774
5	-4.550	13639
6	-4.539	5358
7	-4.529	849
8	More	87

Figure 13: Distribution of Voltage Values Sampled in Single Position

Each bin represents one standard deviation from the mean of the group of samples. The sensor follows the three-sigma rule, or 99.7% of the data lies within three standard deviations. The normal curve is neither skewed left or right, so the mean of the data will give the voltage value for this position.

Sensor Linearity and Hysteresis

The sensor was set-up on the machine and measurements were manually taken using an oscilloscope to determine the sensor's linearity and if there was any hysteresis present. Using a silicon wafer fixed to the spindle face, the spindle was moved away from the target in increments of 500 nm. Data points were taken from when the sensor first responded (close to the target) and taken until the sensor no longer responded. As one can see from Figure 14, this occurred at approximately 7 volts consistently. These same measurement points were taken as the spindle moved closer to the sensor.

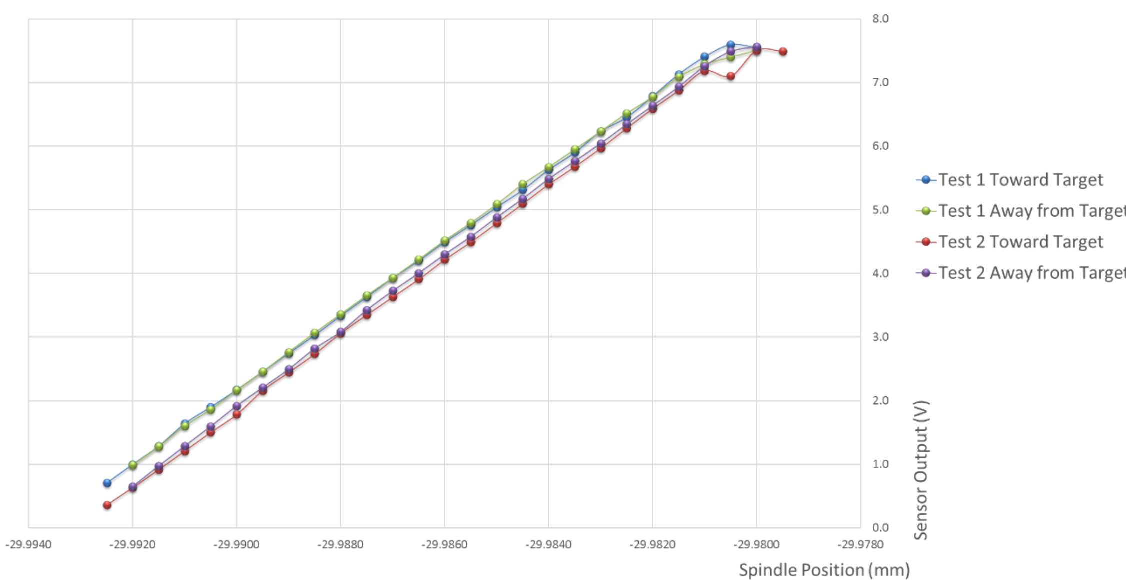

Figure 14: Behaviour of Sensor Moving Toward and Away from Target Surface

The two tests in Figure 14 show that the sensor exhibits linear behavior with no noticeable hysteresis over the course of the two tests as one should find with a capacitance sensor.

The sensor shows linear behaviour when taking measurements on the machine, however when the sensor is set in one position and voltage readings are taken over a long period of time, the voltage reading fluctuates as shown in Figure 15. The voltage fluctuation seems to be greater on the isolation table then on the machine.

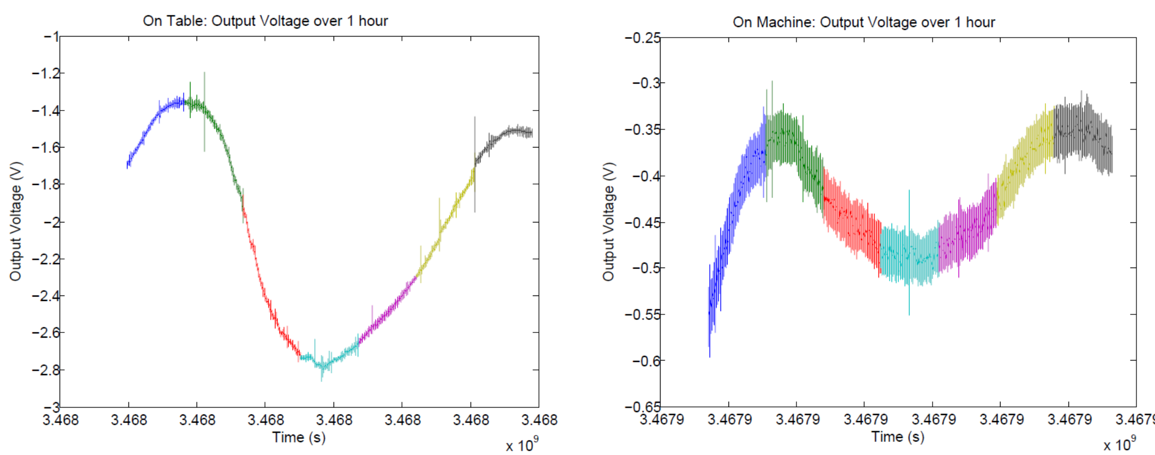

Figure 15: Voltage reading of static, single point over one hour on a) the vibration isolation table and b) the machine with each coloured segment representing 1 million samples, or approximately 10 minutes at 1652 S/s.

The slow variation fluctuation may be a result of a slowly drifting change in temperature or pressure in the room. Temperature is controlled in the lab, but temperature will vary as the air conditioner cycles on and off. The isolation table is open to the lab environment, while the machine is enclosed and thus will fluctuate less than the surrounding temperature controlled room. If a single measurement is taken over too long of a period of time thermal variation will start to affect the measurement. The measurements, whether or not they are relative, or absolute measurements will be meaningless if taken over a long enough period of time.

Sensor Frequency Response

Foregoing the static characteristics of the sensor, measurements taken from the sensor in a single position on the machine and on the vibration isolation table were analyzed to determine the noise difference and the frequency response of the sensor. Both situations are shown in Figure 16.

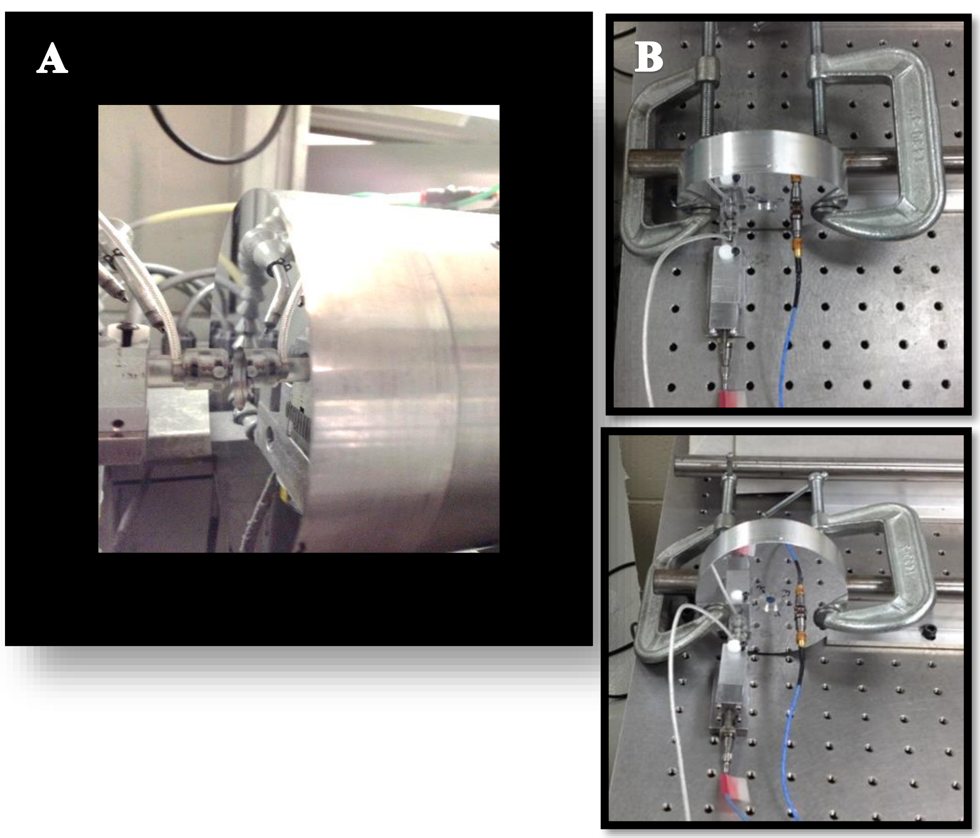

Figure 16: Frequency response test set-up for a) on machine and b) on isolation vibration table.

In each case the measurements were taken using the same workpiece with the same machined surface. Figure 16a depicts the sensor set-up on the machine in approximately the same way the sensor was set-up for on-machine measurements of the workpiece surface.

Approximately twenty seconds of captured, detrended noise per measurement is shown in Figure 17 at a sampling rate of 10,240 samples per second for both situations: on the machine and on the vibration isolation table.

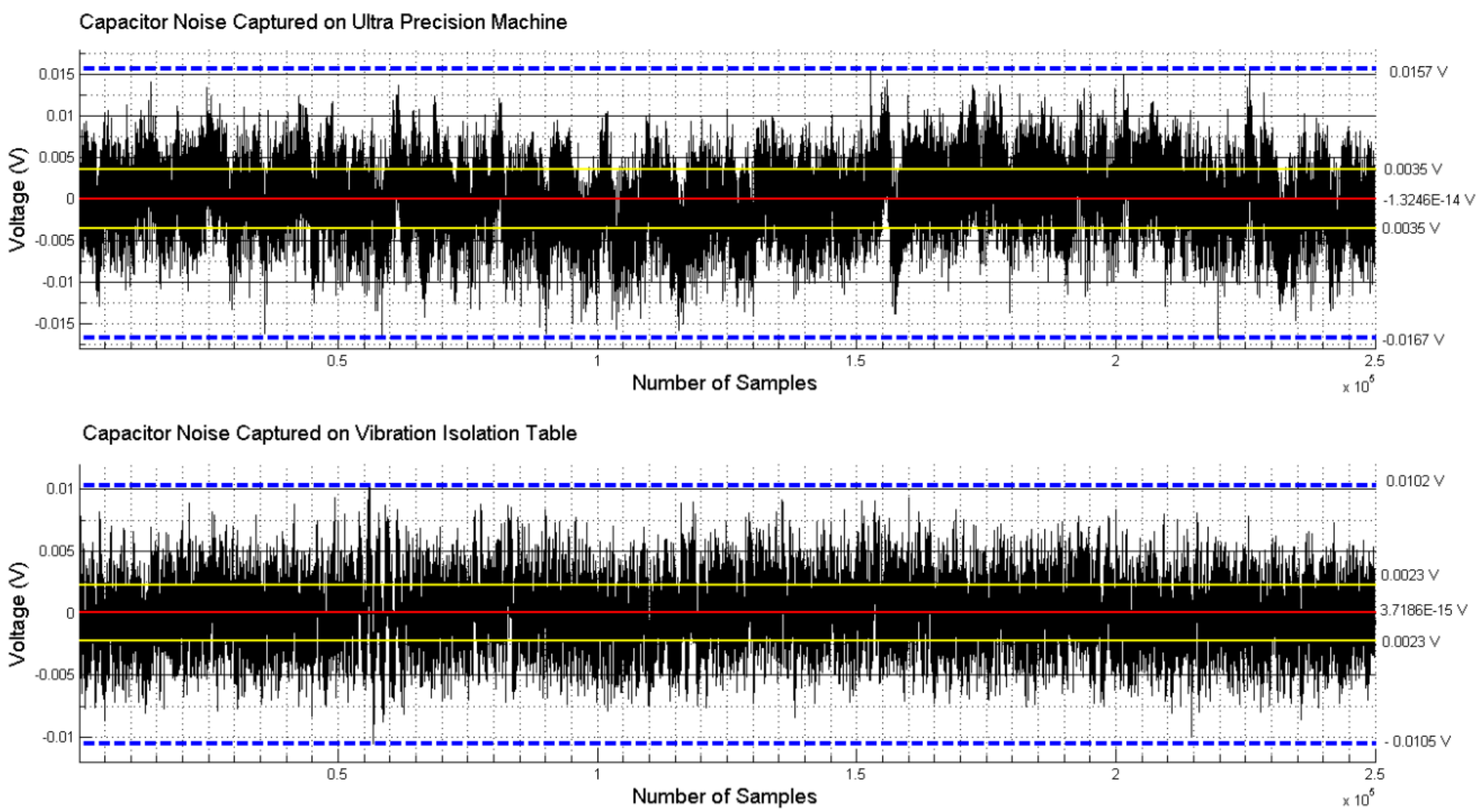

Figure 17: Capacitor Noise Captured on a) the UP-SPDT machine and b) the vibration isolation table.

The lines on the graphs indicate the mean (red), two standard deviations (yellow), and the maximum and minimum points (blue). The spread of the noise is forty percent greater on the machine and the mean voltage is a factor of 10 greater than the mean on the vibration isolation table. As expected the machine is noisier and the sensor is capable of depicting that difference. The signals in Figure 17 have been broken into a frequency power spectrum shown in Figure 18.

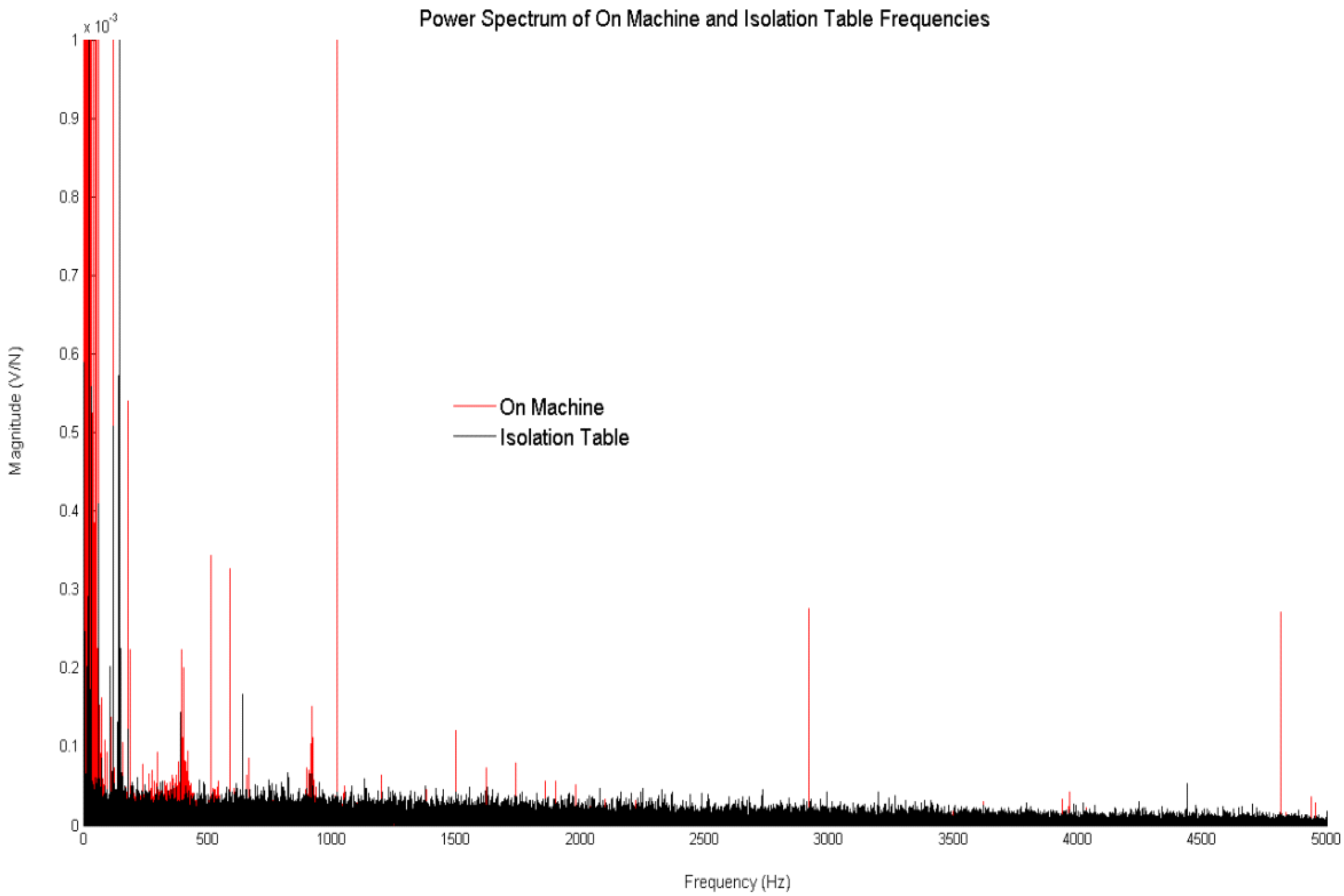

Figure 18: Power spectrum of on-machine and isolation table frequencies.

The power spectrum exaggerates the amplitudes of the frequencies seen by the sensor, but one can clearly see that with a cut-off frequency of 5 kHz and a sampling rate of 10.24 kHz that the sensor is picking up very high frequencies, while positioned on the machine. Amplitude usually diminishes with frequency, so the capacitance sensor is demonstrating an ability to pick-up high frequencies with small amplitudes.

On Machine Resolution: 2, 5, 10, 20 Nanometer Increments without Frequency Filtering

The vertical displacement measurement that the sensor will be measuring is along the z-axis or the spindle axis of the machine. Here along this axis, the machine has the most linear resolution of 2nm.

The sensor was setup on the machine with an aluminum workpiece as the target. With a feed rate of 0.001 mm/min, a dwell at each measurement point of 2 seconds, and a sampling rate of 10240 S/s the machine axis was moved away and toward the sensor in 2 nm, 5 nm, 10 nm, and 20 nm increments. The results of the measurements are graphed in Figure 19. For each test, the spindle (fixed to the z-axis) moved toward the sensor in a set increment with ten increments in one direction, then ten increments away from the sensor. At each set increment, the spindle would dwell in the position for 2 seconds providing approximately 20000 samples per increment.

A moving average filter was applied to each data set and the initial starting point is set to zero. The graphs have been truncated at the start to eliminate this error. When using a moving average filter, the amount of smoothing to eliminate the noise and to clearly see what the sensor sees depends on the window size, or the amount of data points over which the filter will average the surrounding data points. Too large of an averaging set will lead to rounding at the transition points. The averaging window has been set for the smaller nanometer resolutions based on the window sizing required to see the transition points for the larger nanometer steps such as 500 nm and applied to the 2 nm, 5 nm, etc. step sizes. Clearly from Figure 19, one can see the steps at 10 nm and 20 nm, but while one can see that the spindle is moving away and toward the sensor there is too much machine noise to see the 5 nm and 2 nm steps.

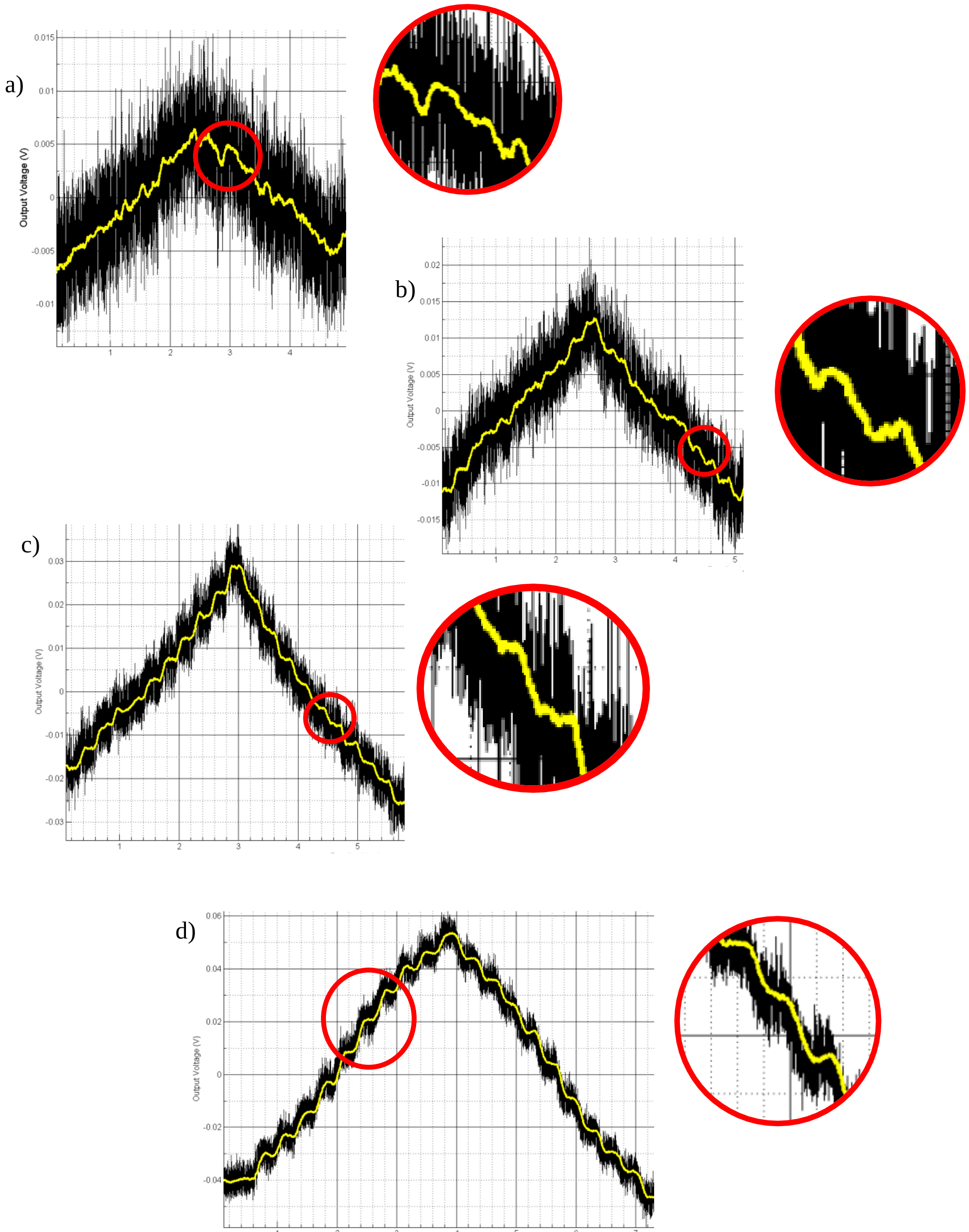

Figure 19: Raw capacitance data (black) at nanometer increments with a moving average plotted in yellow. No frequency filtering based on noise testing. a) 2nm increments, b) 5nm increments, c) 10 nm increments, and d) 20nm increments.

The sensor will not be able to resolve in a static or dynamic situation profiles below 10 nm. The environmental noise of the machine makes taking measurements below 10 nm from the workpiece surface profile impossible.

Conversion of Capacitor Voltage to Nanometers

In order to determine the resolution of the sensor when measuring the profile and compare the profile taken by the sensor with the profile measured by the laser interferometer, the sensor voltage must be converted to metric units.

Measurements were taken by the sensor on the machine with the spindle moving away from the sensor in 500nm increments with a two second dwell at each increment before moving a subsequent 500nm away from the sensor. After two micrometers the spindle would move toward the sensor in 500nm increments. The measurements taken are shown in Figure 20. The neon green line represents the detrended raw data taken. The black line running through the green neon line is the effect of the moving average filter.

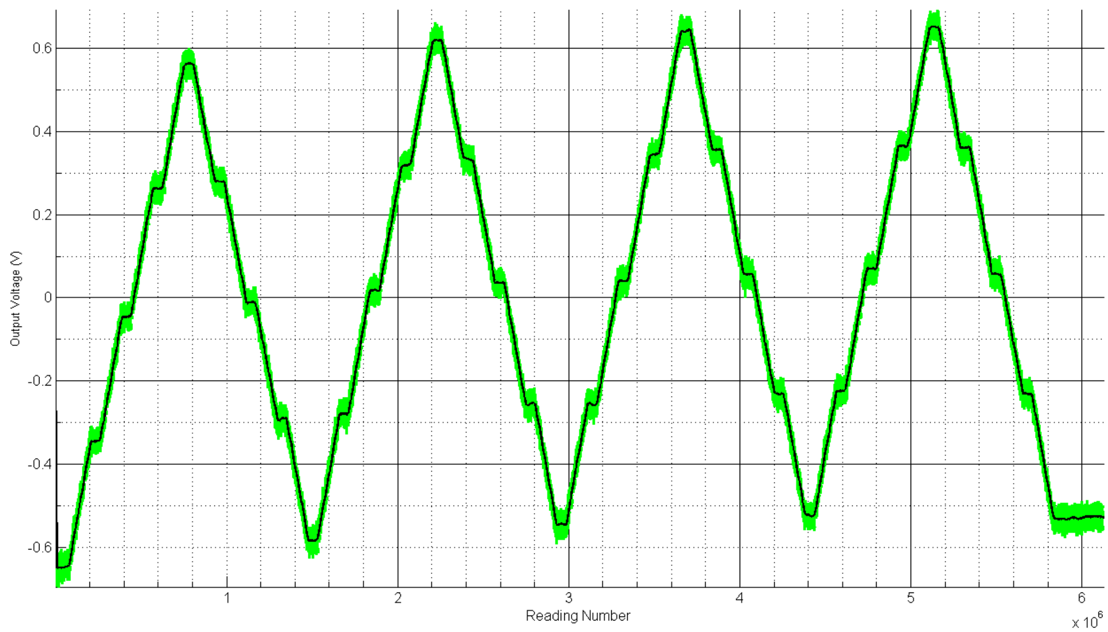

Figure 20: Raw capacitor data (green) with 500 nm steps with a moving average (black) plotted through the data.

First Derivative Signal Processing

The measured data in Figure 20 went through the following process in order to determine the average voltage value for each step regardless of feed rate, sample rate and to gain a consistent set of data given that the start and end point of the steps are ambiguous.

First, the moving average filter smooths out the original signal. The first derivative of the sloping upward or sloping downward portions of the filtered data is taken. The graph of the first derivative is a square wave as shown in Figure 21.

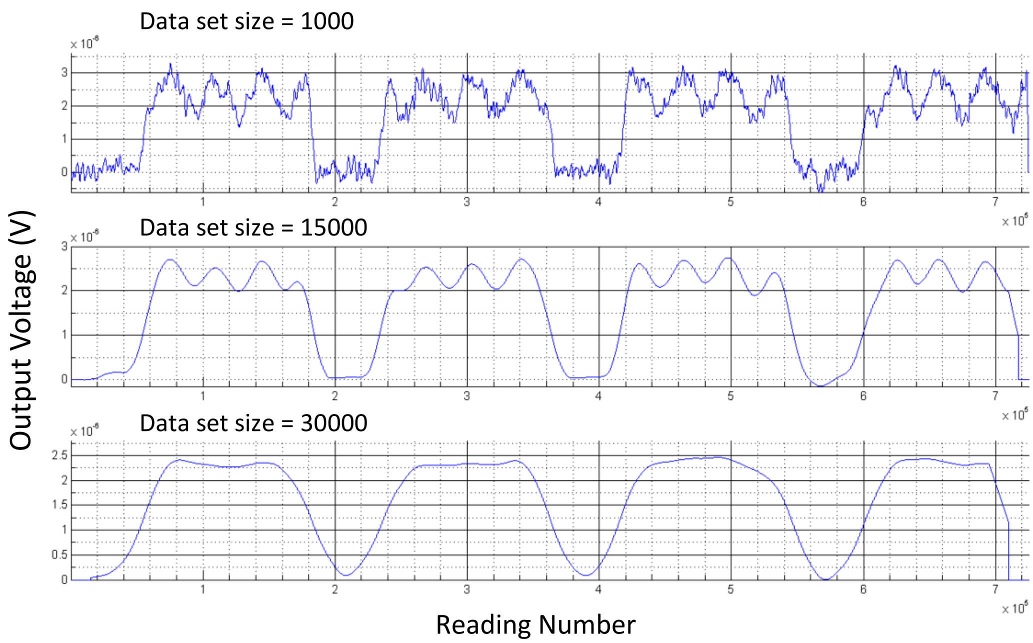

Figure 21: First derivative of filtered raw data with each graph representing a moving average applied twice with a different data group size. The last graph with a data set of 30000 data samples is the size used to obtain peak points for calculating voltage average at each step.

From Figure 20, the point of dwell virtually demonstrates a flat line, therefore the derivative of this line should be a constant zero and the slopped line should be a constant value of the slope. Figure 21 shows the constants forming a square wave.

In Figure 21 and Figure 22b the signal has been smoothed using a moving average twice causing triangulation. The triangulation of this dwell ends in a peak, which is the tip of a symmetric triangle waveform. The peak transposed to the original data, forms the midpoint of the dwell step as shown in Figure 22a and Figure 22c.

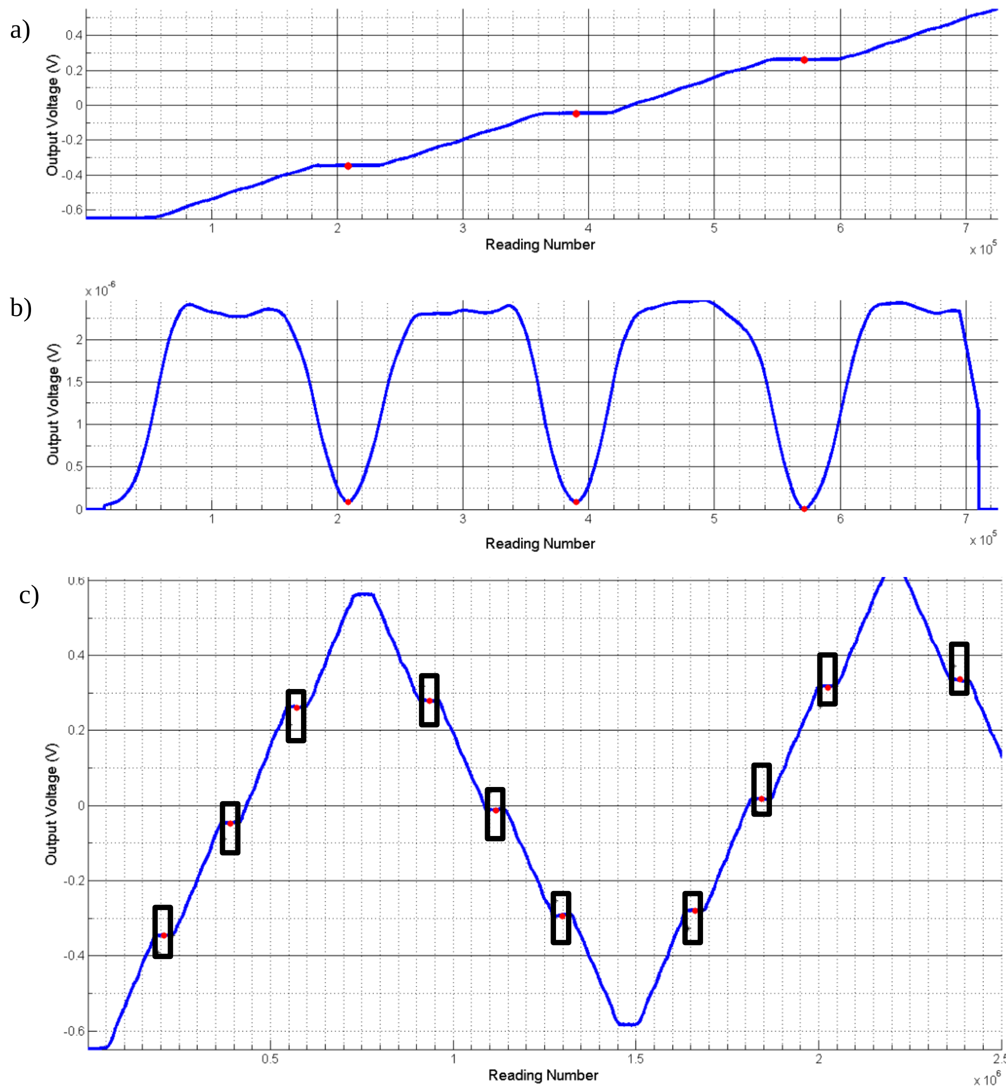

Figure 22: Process of finding the approximate mid-point for creating the point spread for each step to calculate the average voltage value at each dwell point: a) original filtered data with midpoint of the point spread for the average on each step, b) the smoothed first derivative with the peak point, and c) the transposed points and the window for the average.

Once the midpoint has been found using the first derivative of the signal along the constantly unidirectional changing portion of the measurements, then a window of data of

±10,000 data points from the midpoint is taken to calculate the mean and standard deviation of the voltage at each dwell point as depicted in Figure 22c.

Mean and Standard Deviation for 500 Nanometer Steps

Taking twenty-three averaged points from the 500 nanometer measurement test and taking the difference between the calculated points, the mean of ten voltage differences is 0.2929 Volts using the unfiltered data of the 500 nanometer steps. Table 10 shows the results for the filtered and unfiltered 500 nm steps. Using the signal-to-noise ratio for the filtered steps, the resolution of the sensor on the machine is approximately 1 nm at one standard deviation with an error band of ±5nm at any one time. This 10nm is with a 20 kHz probe driver bandwidth setting. When considering a continuously moving sensor as will be the case for measuring the form error, the resolution at a conservative six times the standard deviation will be closer to 6nm.

Table 10: Voltage values derived from 500nm steps from Figure 22.

	Filtered	**Unfiltered**
SNR	48	42
Mean (V)	0.29486	0.29294
Std (V)	0.00609	0.00700

Comparative Indicator versus Capacitance Sensor

When the data for the 500nm steps was taken with the capacitance sensor, at the same time, data was taken with an electronic indicator that provides a voltage value per range (in nm) setting. Both sets of data are graphed in Figure 23. The indicator was on the back side of the spindle face during the entire test measurement to eliminate cross-talk between the sensors. Due to the set-up, the voltage increase and decrease for both sensors was in the same direction. The indicator data voltage to displacement conversion as shown in Figure 23 was calibrated according to the equipment settings on the indicator at the time of the test of 100nm/Volt, the highest resolution setting for this sensor.

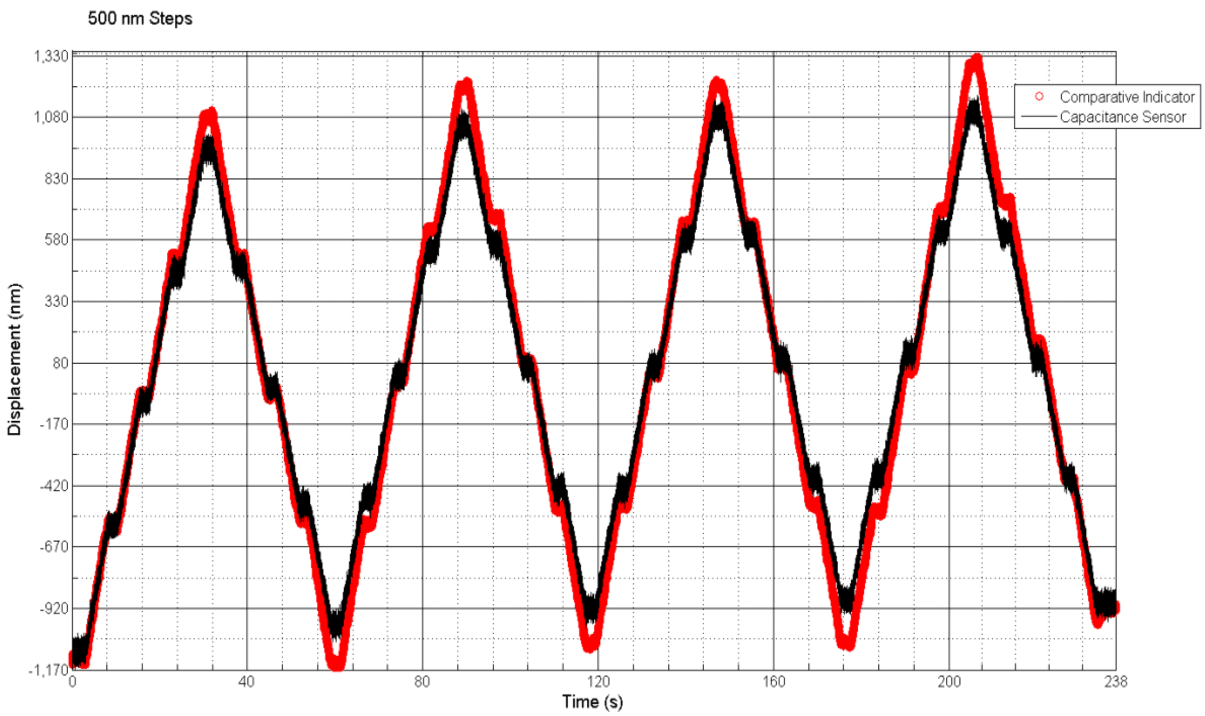

Figure 23: Indicator and Capacitance Sensor taking Same Measurements

Both sensors have given the same displacement for each step and thus provide validation of the capacitive sensor's performance. However, the indicator shows some hysteresis with the measurement varying drastically when the spindle changes direction.

Not taking calibration measurements prior to the test due to cosine error may have added some error to the measurements.

Workpiece Specifications

The workpiece on the UP-SPDT machine is affixed to the spindle using a vacuum. A vacuum not only provides for an easy way to attach and detach the workpiece, but also provides the means by which the part can be centered to within microns with respect to the spindle rotation. Workpiece functionality requires a sub-micron surface finish form and sub-nanometer surface roughness. The amount of imbalance is a large contributor to the performance of the machine even when machining a flat surface. According to the manual for the ultraprecision freeform machine to meet minimum performance criteria set out in the manual and company literature, the workpiece must be concentric to the spindle center to within two micrometers. Outside this range, the supplier cannot guarantee the precision of the machine.

The issue

The main issue with the vacuum is the unknown impact it will have on reshaping the part to conform to the vacuum chuck surface. The vacuum causes the workpiece to deform as shown in Figure 24 and the cutting process leaves residual stresses related to this deformation.

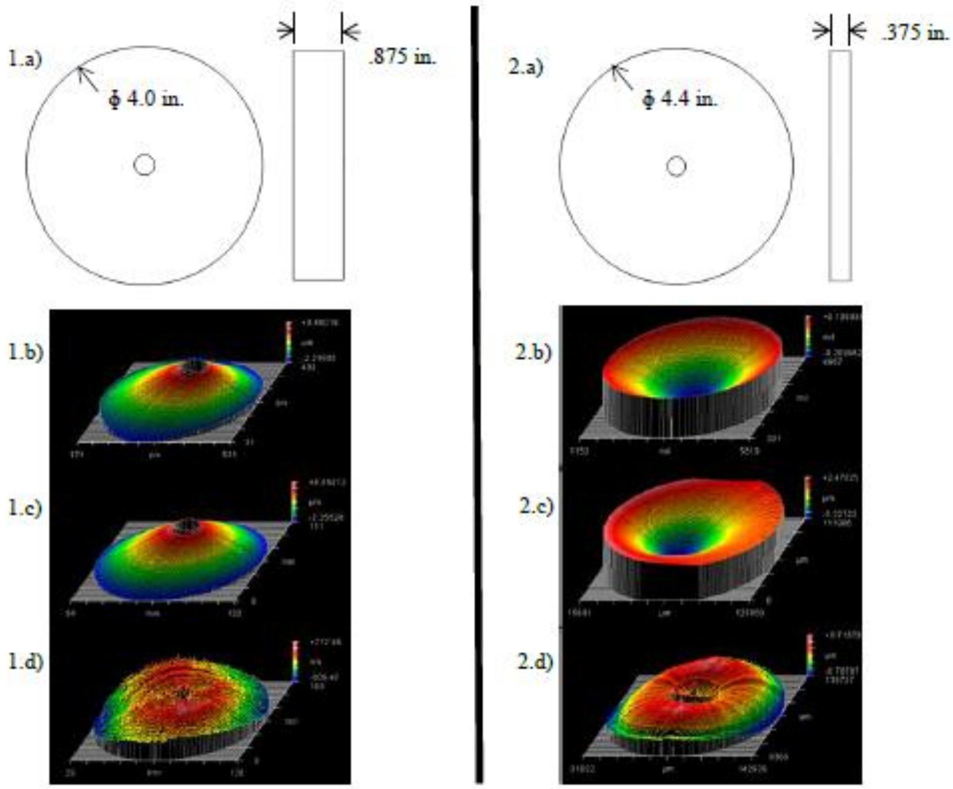

Figure 24: Standard workpieces, each of a different thickness machined with constant parameters (b and c) and machined using a constantly changing parameter (d). 1.a-d is the 7/8 in. thick, annealed, 6061 Aluminum workpiece and 2.a-d is the 3.8 in. thick, 50% CR, 6061 Aluminum workpiece.

The vacuum causes a 4-inch diameter workpiece (the maximum work holding diameter, given the current set-up) to deform. The degree of spring back, or the shape of the residual stresses seen on the surface of the workpiece varies. With the thicker aluminum workpiece, the profile consistently produced a cone, while the thinner aluminum workpiece's shape was consistently an inverted cone. These profiles were produced using constant speed, feed, and depth of cut across the entire surface. When the parameters are not constant such as the feed rate, the profile changes or the residual stresses on the surface of the work piece change. The vacuum is the major cause, but there may be other variables that lend to producing this shape. An FEA analysis done using SolidWorks software further supported that the vacuum was a main source of the shape. When the workpiece was modelled and the vacuum pressure applied to the workpiece surface, the vacuum caused the workpiece to deflect into a similar shape as given by Figure 24a. This model considers an ideal surface and the workpiece may not always lay flat against the vacuum chuck and the cone may shift in shape. As well, at issue is the unpredictable amount of spring back that would occur when the part is removed from the machine to be measured by the laser interferometer. Since the measurements taken by the capacitor are to be compared to the measurements taken by the laser interferometer, the form of the workpiece created from machining the workpiece surface must be maintained after the workpiece is removed from the vacuum chuck. Therefore, a workpiece fixture was designed to reduce the sensitivity of the vacuum chuck on the workpiece profile.

The Workpiece Fixture Design

The workpiece fixture must reduce the vacuum effect and not introduce any new sources of error. To do this, the workpiece will stand off from the vacuum and be held on with a fixture the same size as the spindle face with a protrusion to which the workpiece will be glued along the perimeter of the protrusion. Details of the workpiece and the fixture as well as the assembly process is outlined in Figure 25.

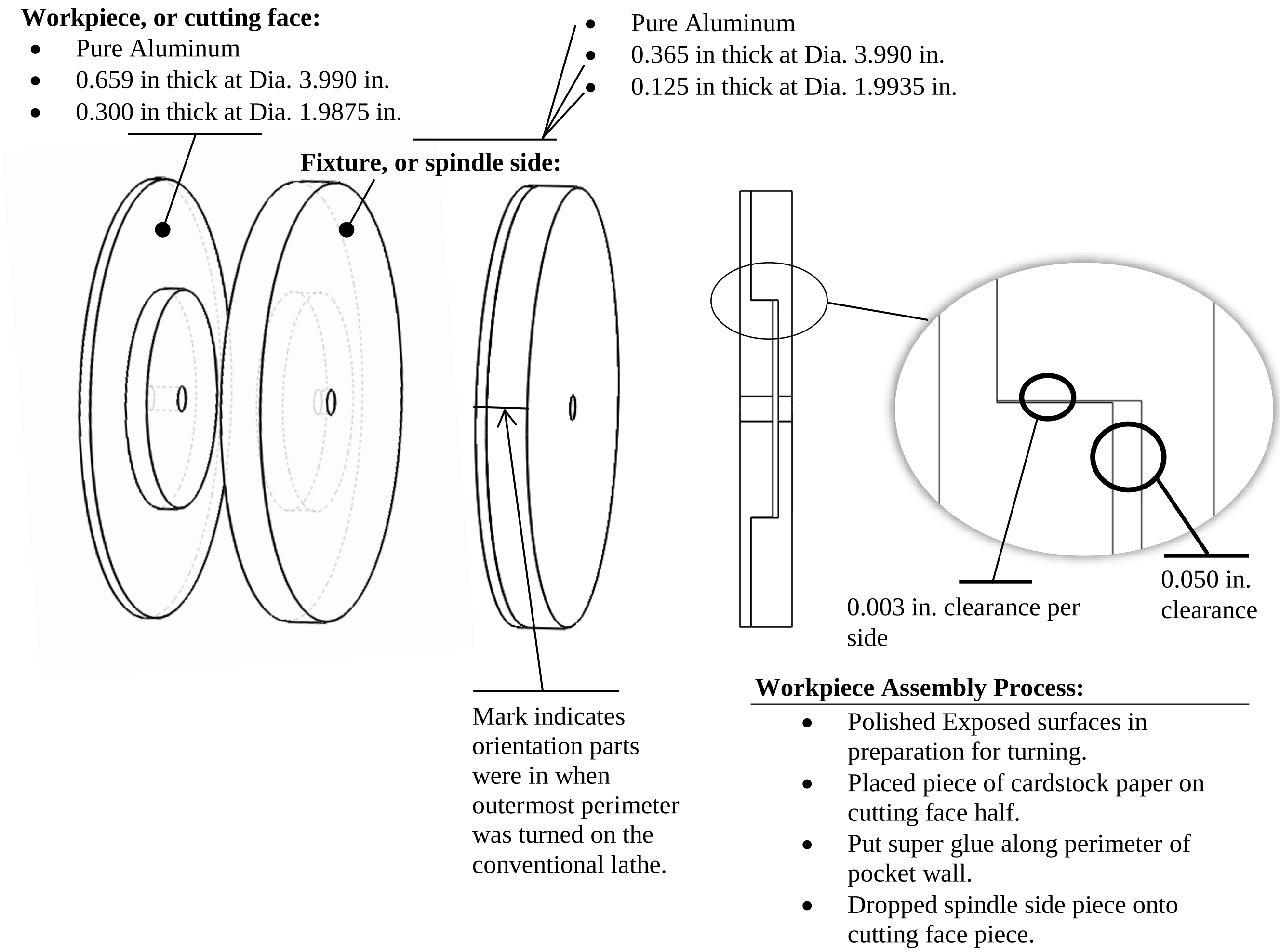

Figure 25: Workpiece fixture construction (drawings not to scale).

The fixture and the workpiece were machined on a standard lathe separately to the geometry shown in Figure 25. Once the protrusion and the pocket were machined. The fixture and the workpiece were placed together and pressed against the face of the standard lathe. Here the fixture was turned as one piece to within a micron of out of roundness. A mark was made as indicated in Figure 25, in order to maintain the same center of mass as produced on the lathe going forward to the UP-SPDT machine, and reduce the effect of imbalance from having two separate pieces on the spindle.

Once glued together using super glue, or cyanoacrylate, the face affixed to the spindle was machined to a mirror image. The resulting finished spindle face of the fixture is shown in Figure 26a.

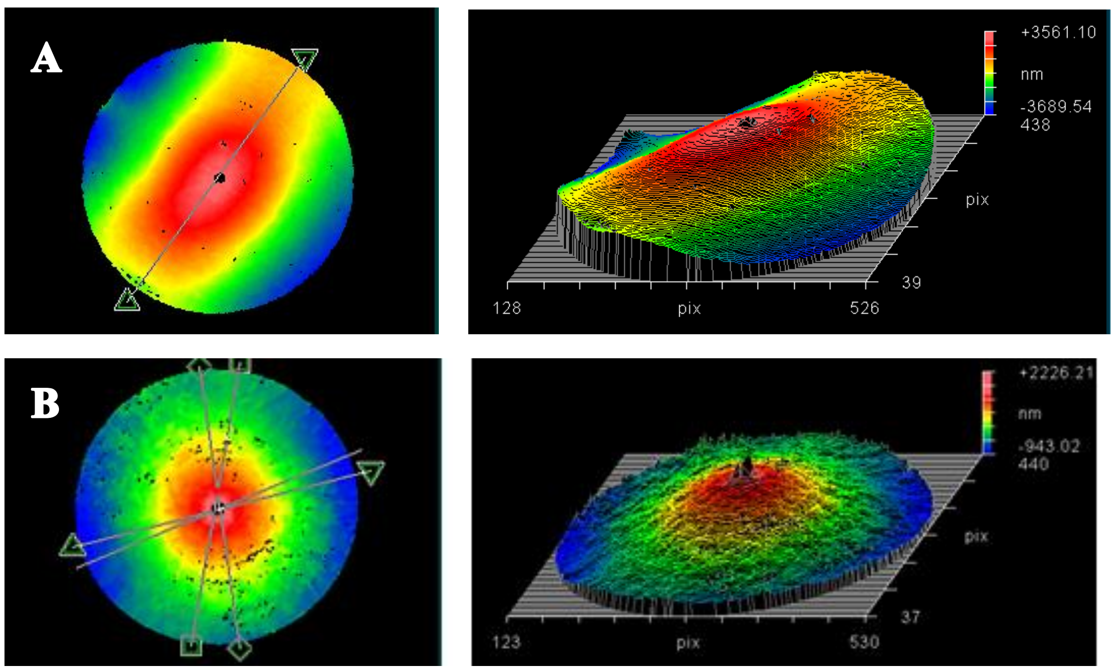

Figure 26: A) Fixture, or spindle side surface after diamond turning the face to a mirror finish and prior to turning workpiece face and B) Workpiece side affixed to fixture. Four consecutive passes across the workpiece surface with a PCD roughing tool.

The face is no longer a cone and shows the spindle imbalance that occurs once per revolution of the spindle. In Figure 26b, the rough machined workpiece surface is shown following four consecutive passes. The cone shape is not as visible as with Figure 24, but the imbalance is clearly present.

The finished surface of the workpiece was machined to a mirror finish. The process took five consecutive passes with the machining parameters of 5 mm/min feed rate, 1000 rpm, and two micrometers depth of cut per pass. Following this, the workpiece was removed and the surface observed with the laser interferometer. To ensure that the workpiece fixture was indeed not affected by the vacuum chuck and showed a consistent profile, the workpiece fixture underwent this process five times. The results of the four of those five runs are shown in Figure 27. Each workpiece in Figure 27 provides a similar profile with error within 1µm. The profile is the expected profile of a part face turned on an ultraprecision air bearing spindle as studied in [39].

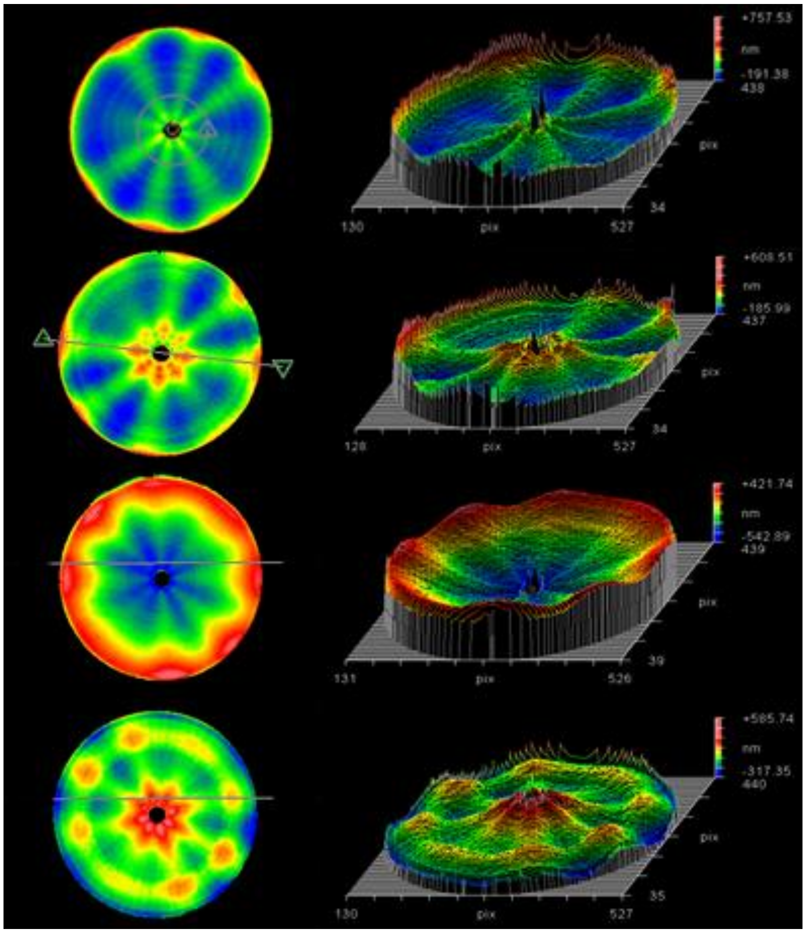

First Run
PV: 0.949 um

Third Run
PV: 0.794 um

Fourth Run
PV: 0.965 um

Fifth Run
PV: 0.903 um

Figure 27: Final fixture and workpiece with gap between fixture and workpiece.

Radial Form Error

The radial form error measures across the diameter of the workpiece. The sensor will measure multiple radial lines of the finished workpiece on the machine. These profile lines will be compared with the profile line measurements taken from the laser interferometer. The entire test procedure, data processing, and the profile are presented below.

Testing Procedure

The objective of the procedure for setting up the test equipment is to reduce and minimize the kinematic errors. The radial line will approximately be the same path the cutting tool took as the tool moved across the face of the workpiece. The sensor radial line will then be measured by the indicator and the laser interferometer and then compared.

The procedure for setting up the equipment for the radial error form measurements is pictorially outlined in Figure 28.

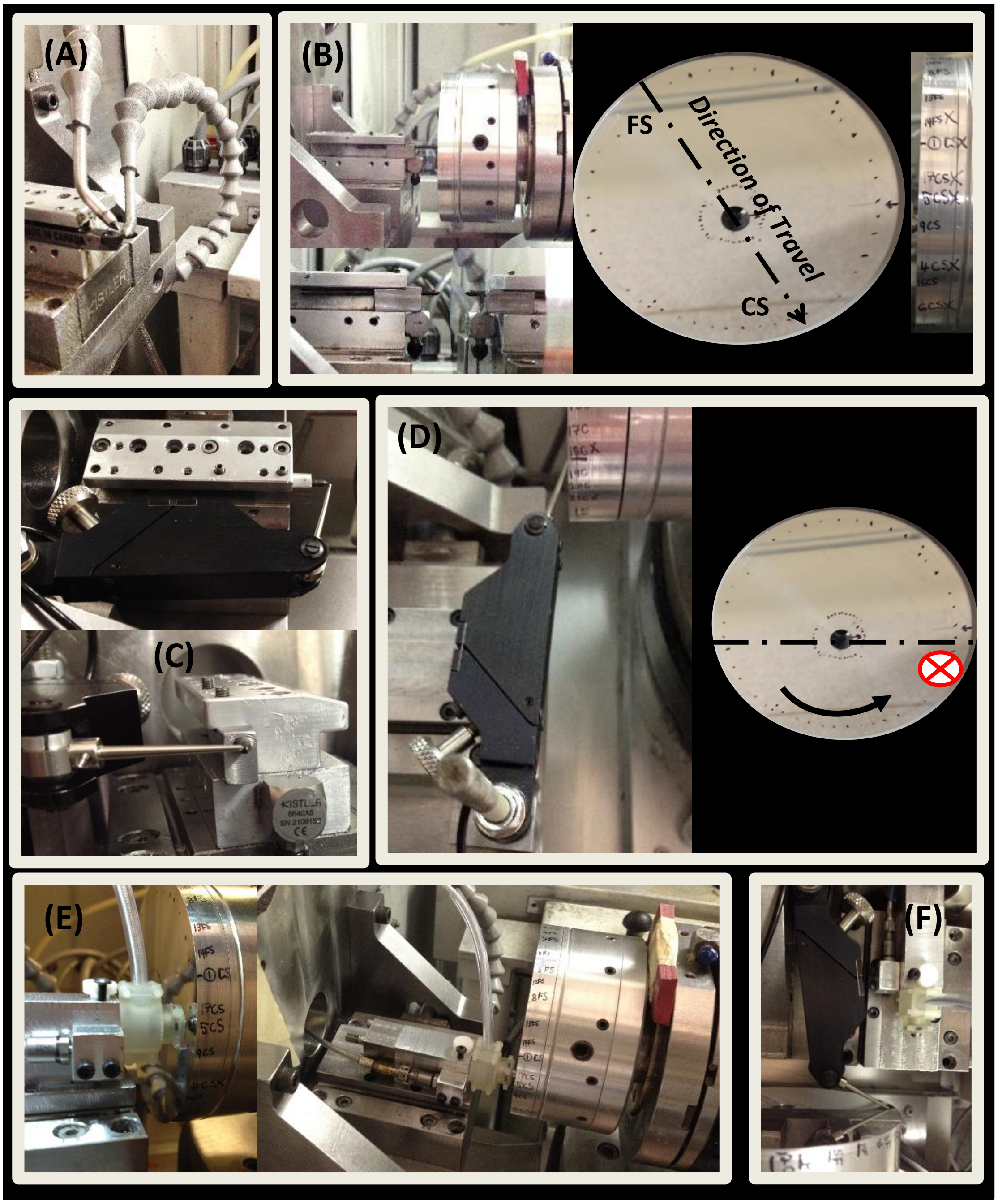

Figure 28: Measurement process for radial error measurement. a) set-up for cutting measurement surface, b) creating transfer punch holes on measurement surface, c) aligning Precitech sensor with punch height, d) re-aligning punch holes and locking spindle at correct height for radial measurement of line, e) capacitance sensor measurement set-up, and f) electronic indicator spindle measurement.

Before beginning the process, the spindle and the tool holder were cleaned in order to provide a flat surface with minimal inclusions that may distort the fixture, or the cutting tool's contact angle.

The fixture was then attached to the spindle and centered on the spindle using the dial indicator to within 1 micrometer alignment error using the larger workpiece circumference.

The machine's axes are cycled for an hour with the workpiece to thermally stabilize the machine. Upon initiation of the cycle, the acceleration and deceleration of the loaded spindle was optimized at the cutting speed of 1000 rpm (M90 S1000). Once warmed-up, the air hoses were positioned overtop of the cutter to effectively and efficiently remove chips from the cutting area.

The finishing, cutting process takes five passes with the final two passes having oil applied to the surface of the workpiece. After approximately five passes, the workpiece is visually devoid of concentric circular grooves and a rainbow effect cannot be perceived when shining a light upon the surface. As well, monitoring the cutting through the vision system, one can see that the cutter is continuously cutting the surface and a new surface has been generated. Working with a freshly prepared surface ensures that the sensor is easier to setup as its range is very limited.

The cutting parameters used were not to ensure an optimal surface finish or form and were based upon current lab practices. The specifications for the diamond cutting tool and the machine parameters used to cut the surfaces for the radial and the circular form error measurements are listed in Table 11.

Table 11: Finishing Diamond Tool, 207712 Specifications

Tool Height	3.984 mm
Radius	1.512 mm
Cutter Material	Single Diamond Crystal
Spindle Speed	1000 rpm
Feed Rate	5 mm/min
Depth of Cut	2 micrometers

Once a mirror surface has been achieved, the cutting tool is removed from the tool holder and the work environment is cleaned of all debris. The workpiece surface is cleaned with a degreaser to eliminate any oil residue and cutting debris from the surface. Other solvents cannot be used as they degrade the bond between the fixture and the workpiece.

A transfer punch holder is mounted in the same position as the cutting tool. A transfer punch is inserted into the punch holder and a rubber stop with extra grip is placed between the spindle and the spindle housing to keep the spindle from rotating, since the spindle does not have a built in brake system. The rubber acts as a spring stop and is placed in the center at the top of the spindle (Figure 28b). This wedge is to minimize distortion that may affect the measurements and the future performance of the highly sensitive air bearing spindle.

With the transfer punch in place and the spindle locked, the spindle was moved to the z-axis position of the last cut made. Dimples were then made by the transfer punch at approximately 10mm from the circumference of the workpiece at both ends of the radial measurement line. The dimples are deep enough to distinguish them from any other surface finish features and will provide a radial line reference when setting up the indicator and when taking measurements with the laser interferometer.

The dimples were then marked with a permanent marker and an “F” and a “C” plus a line number were left on the circumference of the workpiece. The markings are important. The dimple mark ensures that a dimple was made. The other markings are to note the direction of travel and proper position of the workpiece when the measurements are taken. The x-axis is not parallel with the radial lines running from one side of the spindle diameter to the other side, or if the “F” and the “C” are interchanged, then the indicator will not cross both points during a measurement.

The “C” added onto the end of the number indicates the position closest to the operator on the machine, or the side of the spindle that did not see the cutter. “F” is the linear position farthest from the machine operator. Figure 28b shows this step in the measurement process.

With all the radial line dimples taken, the electronic indicator was set-up on the tool fixture on the x-axis as shown in Figure 28c. The height of the indicator was adjusted to the height of the transfer punch, then the tool holder was removed from the machine and the capacitance sensor fixture was installed. The capacitance sensor fixture height was adjusted to the height of the tool by including a steel plate beneath the capacitance fixture.

As well, the load cell area is non-magnetic and a steel plate was bolted to the load cell to create a magnetic surface to attach the capacitance sensor fixture too.

With the electronic indicator in place as shown in Figure 28d. The workpiece was spun into place using the indicator to find the correct height of the dimple for the radial line to be measured. Once the dimple was at the same height as the indicator, the spindle was locked into place and the indicator was moved to the other dimples across the workpiece to ensure that the radial line was in the correct position.

With the spindle locked into position and the spindle moved to the z-axis position of the last cut taken, the sensor was brought against the surface of the workpiece to where the "x" is in Figure 28d. The sensor was against a clean surface and far enough from the dimple to not detect the dimple. The sensor was adjusted visually using the camera until the sensor face was visually flat against the surface of the workpiece. Then, the sensor fixture was locked down using the magnets and the sensor was moved back from the spindle face using the differential screw.

Once in place, the sensor power was turned on and using an oscilloscope, the sensor range was adjusted until the sensor was in the middle of the positive range for the analog to digital converter. Then, with the LABView program running, a trial run of the sensor moving across the workpiece was done to ensure that the measurements were within range across the entire diameter of the workpiece and to ensure that the sensor crosses the dimples. Then a machine program was initiated in conjunction with the LABView program and the capacitance sensor crossed back and forth across the diameter of the work piece twelve time. Each pass would be denoted with the sensor traveling off the workpiece to take the sensor out of range before traveling back across the workpiece.

Measurement Procedure for Electronic Indicator

Once the measurements were taken with the capacitance sensor, the electronic indicator was set-up and a single measurement was taken across the same radial line. The tip of the electronic indicator is missing the ball at the end of the indicator, so the indicator leaves a visible line when moving across the workpiece surface. The fixture for the indicator is shown in detail in Figure 29. A magnet on the bottom of the fixture fixes the sensor to the machine.

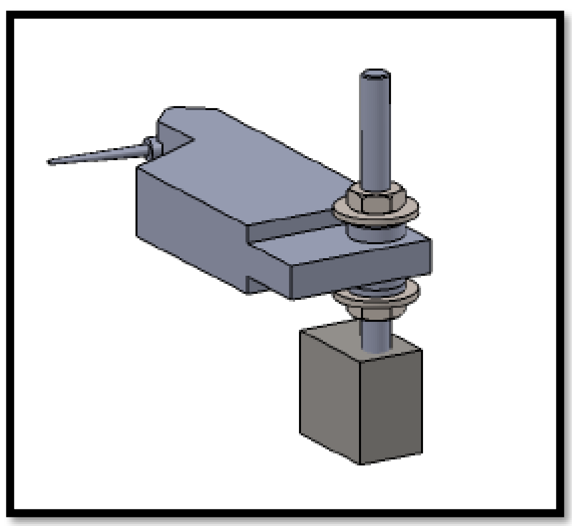

Figure 29: Electronic Indicator Fixture for Radial Line Measurements

As previously noted, the indicator was already at the proper height for measurement and was not adjusted. With the indicator on the x-axis and the x-axis at the starting position of the cutting process, the spindle was brought into position and the indicator was brought in, until the indicator provided a reading at the dimple farthest from the operator as shown in Figure 28f. Then the indicator was calibrated. The calibration for each line discussed in this report is given in Appendix A-1.

The settings for the test have been set through previous trial and error measurements. The most stable measurements were obtained when moving the indicator at the lowest speed of 20mm/min and with the indicator range set to ±10 μm, where one Volt equals one micrometer. Once the calibration measurements were taken, the indicator was brought in to the start point and the voltage was zeroed. The indicator was brought away from the surface by moving the spindle away in a controlled movement. Then, the program given in Figure 30 was enacted and the indicator moved across the workpiece.

00FGCPR1.PGM

G01 ;COMMAND FOR LINEAR INTERPOLATION

G71 ;PROGRAM UNITS ARE IN METRIC

G90 ;ALL MOTIONS ARE ABSOLUTE

G1 F5.0 ;FEEDRATE TO MOVE CLOSER TO SPINDLE

Z-74.000 ;INITIAL SPINDLE POSITION

G1 F100.0 ;FEEDRATE TO MOVE TO START X-AXIS

X-105.000 ;X-AXIS ZERO RANGE POINT

G1 F5.0 ;FEEDRATE TO MOVE INTO SPINDLE POSITION AGAINST WORKPIECE

Z-74.657 ;SPINDLE POSITION FOR INDICATOR TEST

G1 F20.0 ;FEEDRATE DURING TEST

G04 F2.0 ;DWELL AT X-105 FOR 2 SECONDS

X-110.0 ;X-AXIS START POINT

M00 ;WAIT AT X-110 UNTIL OPERATOR PUSHES START BUTTON

G1 F5.0 ;FEEDRATE MOVING TO TOUCHPT.

Z-74.640 ;MOVES OUT SLIGHTLY

Z-74.657 ;MOVES TO TEST POSITION

G1 F20.000 ;FEEDRATE OF TEST

X-208.000 ;FINAL POSITION AT END OF TEST

G1 F5.000 ;SPEED MOVING AWAY FROM SURFACE

Z-74.000 ;FINAL INDICATOR POSITION

Figure 30: Indicator Test Measurement Program for Radial Lines

Figure 31 shows the generic results of this test procedure and the portion of the test where the indicator was taking measurements along the workpiece.

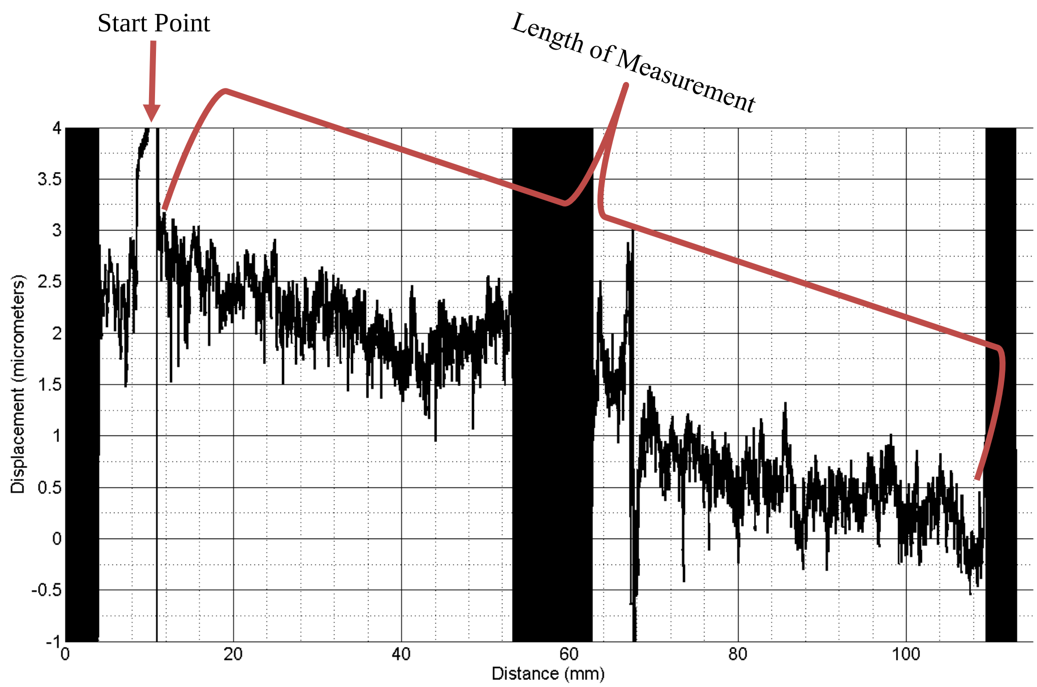

Figure 31: Indicator Measurement for a Single Radial Line

Processing of the Capacitance Data

The data collection and initial data processing steps are a result of the limitations of the analog to digital converter and the maximum feed rate of the x-axis.

For repeatability, the test completed ten radial measurements per radial line. To get ten good passes, the sensor took the measurement twelve times. The sensor started off the surface of the workpiece, then crossed the diameter of the workpiece until the sensor was completely off the farther side of the workpiece, then returned and repeated this for twelve passes. Allowing the sensor to fall out of range at the start and end of each measurement gave a clear indication as to where one pass ended and another began and helped to break the measurements into twelve passes when processing the data.

The time to complete this test depends on the feed rate. The sensor reading drifts over time as previously shown in Figure 15. Given the circumstances, the feed rate was set to the maximum allowable of 200 mm/min. Above 200 mm/min the machine sometimes did not comply with the inputted speed command.

To see if the measurements were affected by the feed rate, prior to testing, measurements were taken along one radial line at various speeds and the results are shown in Figure 32, where each graph represents a different feed rate. Here a band pass is used to eliminate any unnecessary noise at frequencies above 5 kHz and frequencies below 10 Hz. Only in the lower feed rate of 20 mm/min is the drift significant over five complete passes.

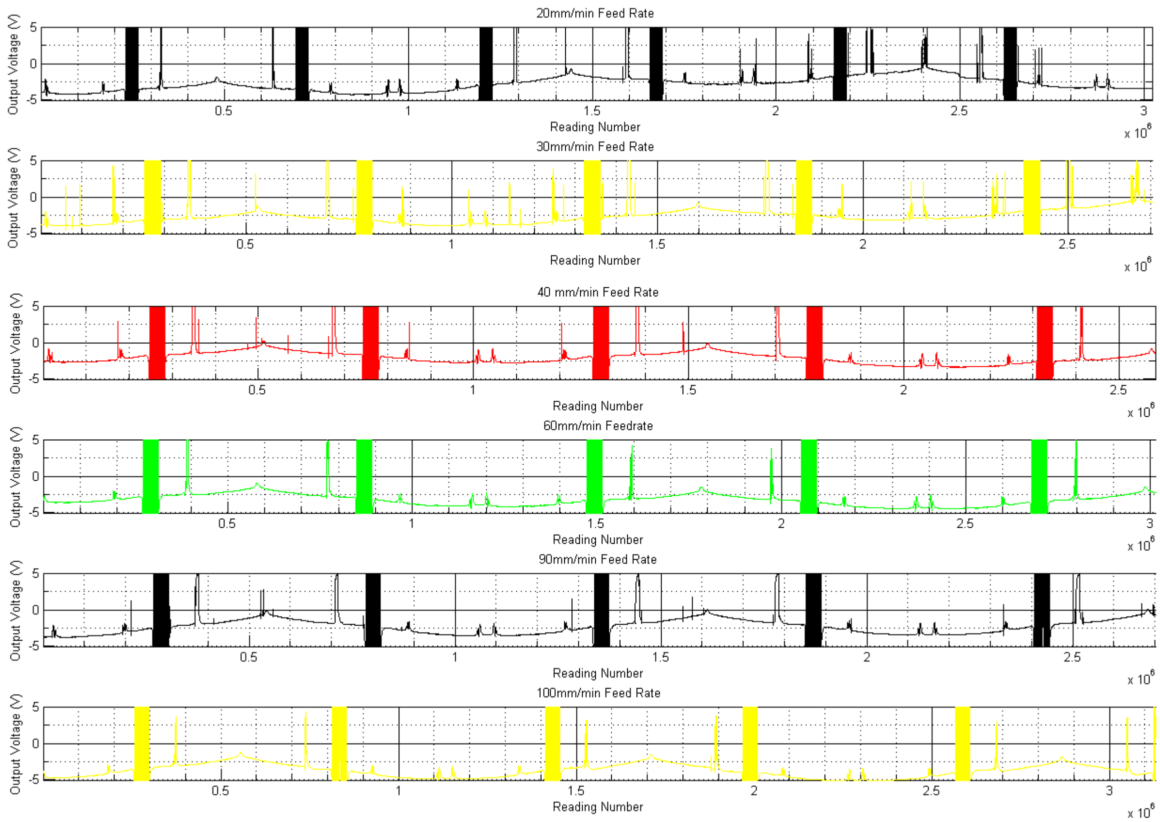

Figure 32: Analog bandpass filtered data at various radial feed rates.

For consistency of comparison, the sample rate set for the capacitance sensor is based on the achievable performance for the electronic indicator. The electronic indicator must move slowly across the workpiece due to vibration generated due to sliding when taking the measurements, but not too slowly due to measurement drift. The indicator moves linearly across the workpiece at 20 mm/min and running at the lowest allowable multiple frequency on the DAQ of 1652 S/s to minimize data intake. At this feed rate and sample rate, the electronic indicator should get 5.452 samples/nm. More than enough resolution to capture the form error typically present on a workpiece.

The data collected in Figure 32 confirmed that the data was being sampled as calculated in Table 12. Table 12 gives the amount of time required to do twelve passes and shows that as the feed rate increases the sampling rate would have to be the DAQ's maximum allowable frequency of 51,200 S/s.

Table 12: Effect on Using Various Feed Rates on Data Collection

Feed rate (mm/min)	Sample Rate (S/s)	DAQ Sample Rate (S/s)	Time/Pass (s)	Total Time (min.)	No. of Samples
20	1652	1652	282	56.4	5590368
30	2726	2844	188	37.6	6416064
40	3635	3657	141	28.2	6187644
60	5452	5689	94	17.4	6417192
90	8174	8533	62.67	12.5	6416816
100	9087	10240	56.4	11.28	6930432
120	10904	12800	47	9.4	7218200
200	18173	25600	28.2	5.64	8663040

Digital Filtering Post Measurement

The following section outlines the data processing techniques used in order to generate the averaged radial line seen in Figure 33c.

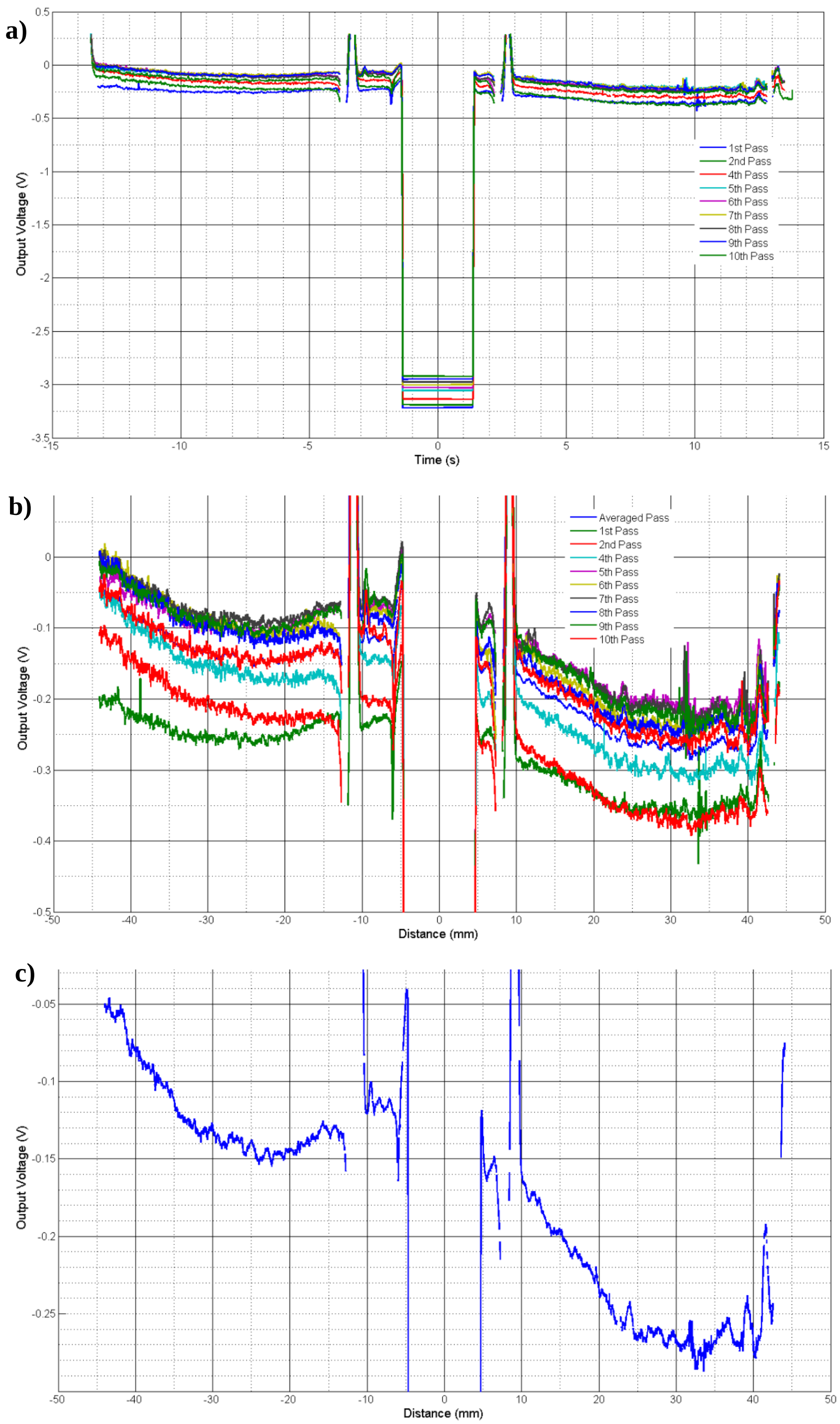

Figure 33: Averaging together the ten passes into a single pass. a) The ten passes of centred yet unequal, b) the ten passes centred and of equal length, and c) average of the ten equal, centred passes.

The data collected from the sensor was filtered using standard functions provided by MatLab. In Figure 34a, the top most picture, the detrended, raw data of one radial line test is shown. The entire measurement involving all twelve passes were detrended at this point. The detrend function removed the dc component and the linear slope of the measurement, so no absolute position information is retained and the slowly changing thermal profile of the machine is removed.

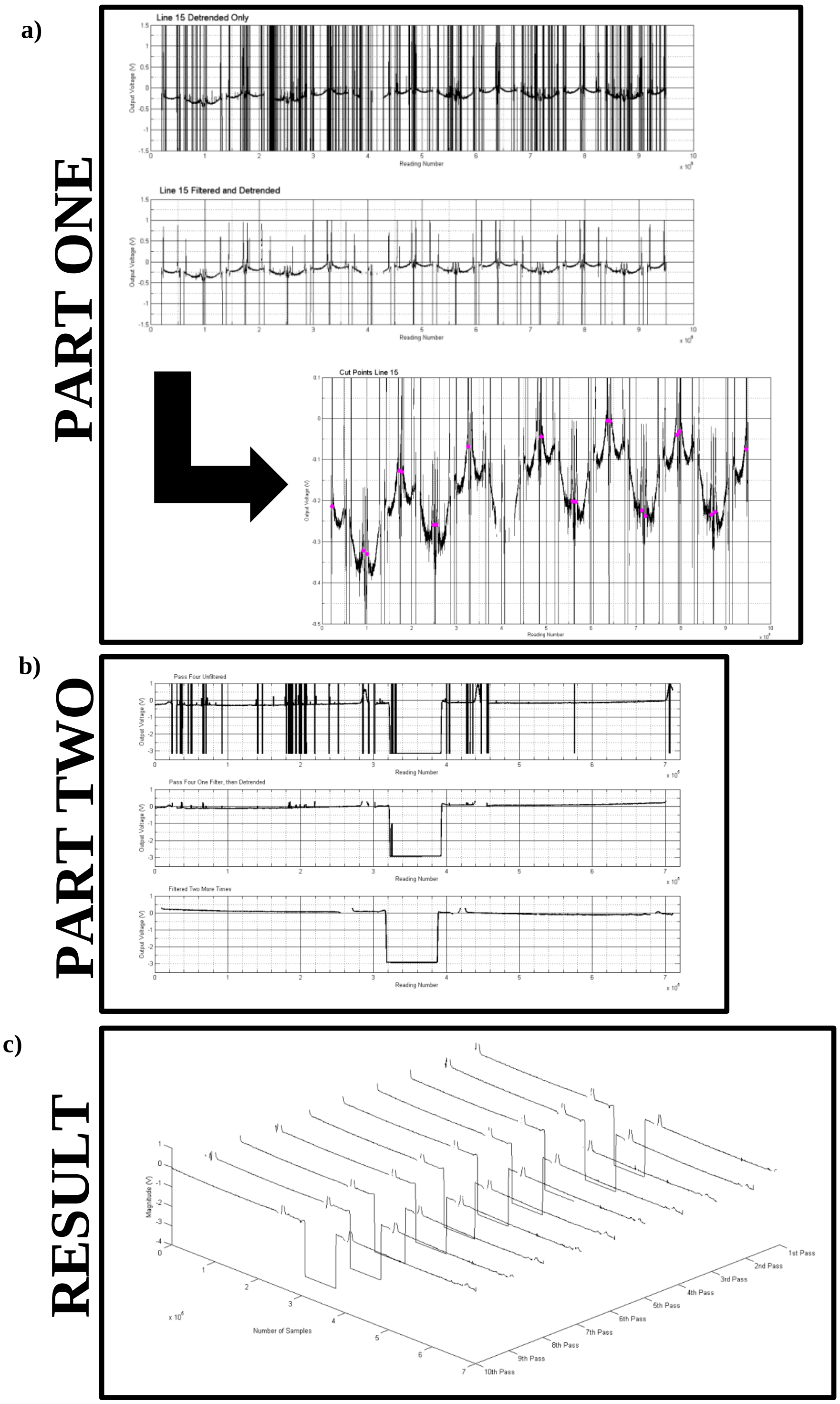

Figure 34: Filtering process prior to modifying capacitance data. a) Breaking continuous measurement into the twelve passes, b) filtering each pass, and c) all ten passes after filtering.

The ten passes were broken into their constituent parts manually by picking the end points of the lines. Here one can see that the break lines are not easily perceivable. There are innumerable spikes in voltage across the entire reading. These spikes are not pits because the voltage is in the wrong direction and they are not protrusions, since the voltage is quite high and larger than the foreseeable profile error. These spikes are usually caused by low frequency noise related to the sensor's environment [40]. Digital band passes do not function like their analog counterparts, therefore more appropriate digital filtering functions provided by MatLab were used to provide clarity, in order to mark the endpoints. The function medfilt1 was used to take out the spikes across the entire measurement. With more clarity, the end points were chosen as shown in the third graph, as part of Figure 34a.

Once broken into radial lines, each line was individually filtered and the spikes and unwanted protrusions were removed. Within a loop of 100,000 data points (due to memory limitations of the function), the function calculates the median of 100 data points. Points that were outliers were replaced with the median value of the surrounding data. Each line underwent the filter once to take out the random spikes. The spikes, though are grouped together at times. To bring the median value down, a cut-off voltage was established based on profile error expectations. Beyond this voltage value, the data point would be replaced with 'NaN'. The 'NaN' would not be used in the median calculation and essentially creates a break in the group. Any spikes after this process would be filtered out by once again using the medfilt1 with the same constraints. The different stages of the filtering process are shown in Figure 34b. Each pass was flipped after being filtered if the pass does not go in the same direction as the cutting process.

Averaging Capacitance Data

After filtering the ten passes, the data was configured, in order for the ten passes to generate the average measurement for the radial line. The averaged radial line was created to compare the radial line measured by the electronic indicator and the laser interferometer.

The average was calculated by taking the average of the sum of the ten passes. To do this, each pass must be the same length and centered. Once centred, the voltage values were converted to spatial values. The process allowed for the data arrays to be aligned and each array point to be averaged over the ten passes. Figure 33 shows the data centred, then centred and of equal length, and then the final averaged radial line.

Removing Spindle Tilt Error

The last artefact to be removed from the now averaged radial line was the spindle tilt, a result of the measurement process. The spindle tilt was found in the radial line past the cutting zone, or past the center of the part, where the tool did not cut. The x-axis was not perfectly parallel with the spindle face so a slope can occur in part of the measurement segment. This slope occurs as follows: the tool cutting the workpiece generates a surface, which is parallel to the x-axis. This parallelism only occurs across the cutting half of the spindle. Therefore, when the sensor crosses the center of the workpiece surface the noncutting side of the workpiece surface was no longer parallel with the x-axis and there was a noticeable tilt in the averaged data shown in Figure 33c.

To remove the tilt from the second half of the radial line, the difference between the second and first half of the data was taken. Figure 35a plots the difference and using linear regression, a line has been plotted through the data. Other than the location of the dimple and the hole, the difference closely follows a linear line. The difference was then removed from the second half of the data.

a)

Pass	Slope (V/mm)
1	-0.00286
2	-0.00528
3	N/A
4	-0.00412
5	-0.00342
6	-0.0043
7	-0.00403
8	-0.00433
9	-0.00422
10	-0.00371
Average	-0.00419
Median	-0.00412 V/mm
Average	-0.00405 V/mm

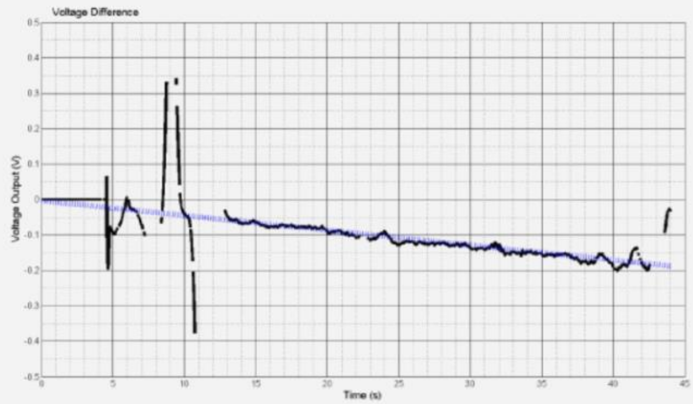

b)

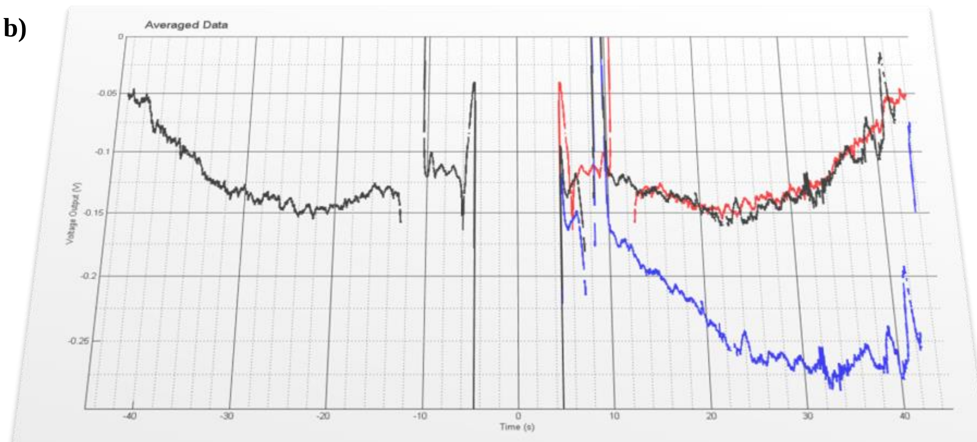

c)

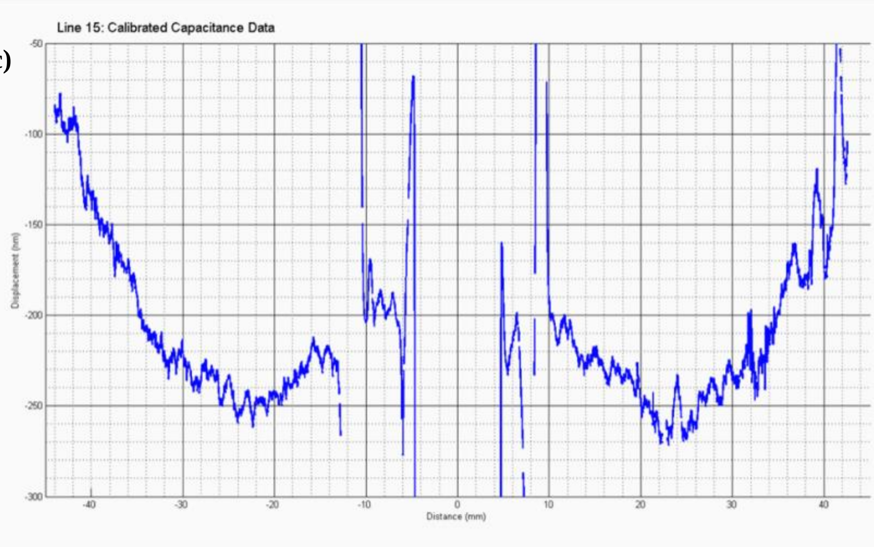

Figure 35: Removing the error from the average due to the spindle tilt.

Figure 35b plots the first half of the data (in black), the original data (in blue), and the corrected data (in black). The red line is the first half of the data mirrored onto the second half of the data. The completed, modified data is shown in Figure 35c.

Processing of Laser Interferometer Data

Figure 36 provides three measurements taken from the laser interferometer along the same path the capacitor would have followed. Two measurements were taken along the outer most edges of the dimple and one measurement was taken along the approximate center of the dimple.

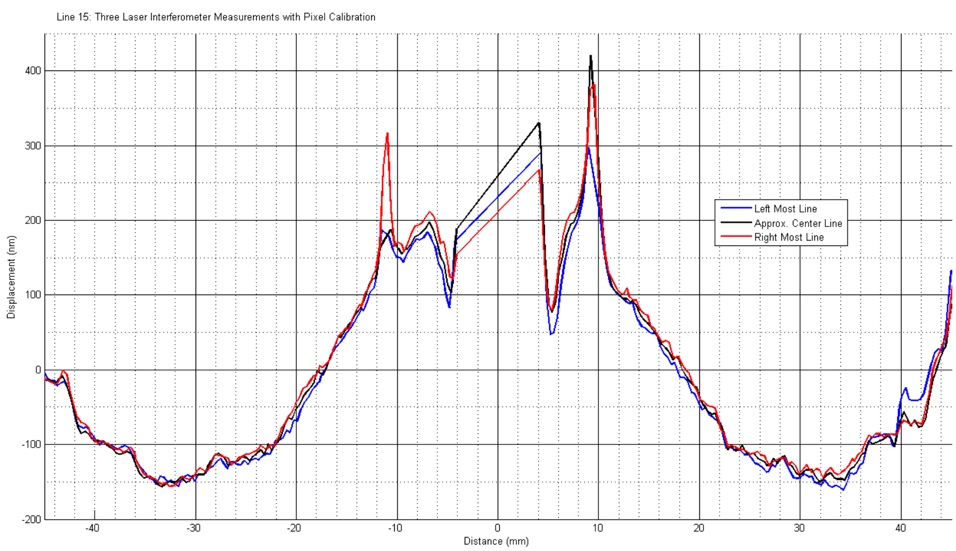

Figure 36: Laser interferometer measurements for line 15.

Conversion from pixels to mm is based on measuring the center hole which was roughly drilled out. The drill size is measured to be 11/32 inches. Looking at Figure 35c and Figure 36, the hole size the capacitor measured and the laser interferometer hole size are approximately the same. The capacitor hole as expected would be a bit larger by about 30 percent, since the reading would drop off as the sensor reached the edge.

Circular Form Error

The circular form error will measure the circular form of the workpiece surface. The sensor will measure concentric circles at various points along the radius of the workpiece. The measurement, as was done with the radial error form, will be compared with the laser interferometry measurements. The test procedure, data processing, and the resulting profiles will be provided in this section.

Test Set-up and Procedure

The circular measurements were taken following the radial error measurements. Therefore, the workpiece was already set for generating a new surface from which to measure circular form error.

Once the workpiece was centered to within one micrometer of the center of the spindle using the dial indicator as done previously with the radial error measurement, the machine's working axes were run through a dry cycle continuously for an hour. Upon activation of the dry cycle, a M90-code (a user defined function) at the start of the program optimized the acceleration and deceleration of the loaded spindle rotation at the cutting process final cut speed as previously discussed. Once again, the M-code helps to make the spindle more stable during cutting.

A new finished, diamond turned surface was generated after five passes with a similar cutting process setup as shown in Figure 28a. As before, the last two passes had oil applied to the surface prior to cutting the surface. The result was a mirror finish as shown in Figure 37a.

Once the surface was acceptable, the tool was removed and replaced with the transfer punch holder and the transfer punch as shown in Figure 37a. The spindle was brought in to the last cutting position and locked in place using the rubber wedge as shown in Figure 37c.

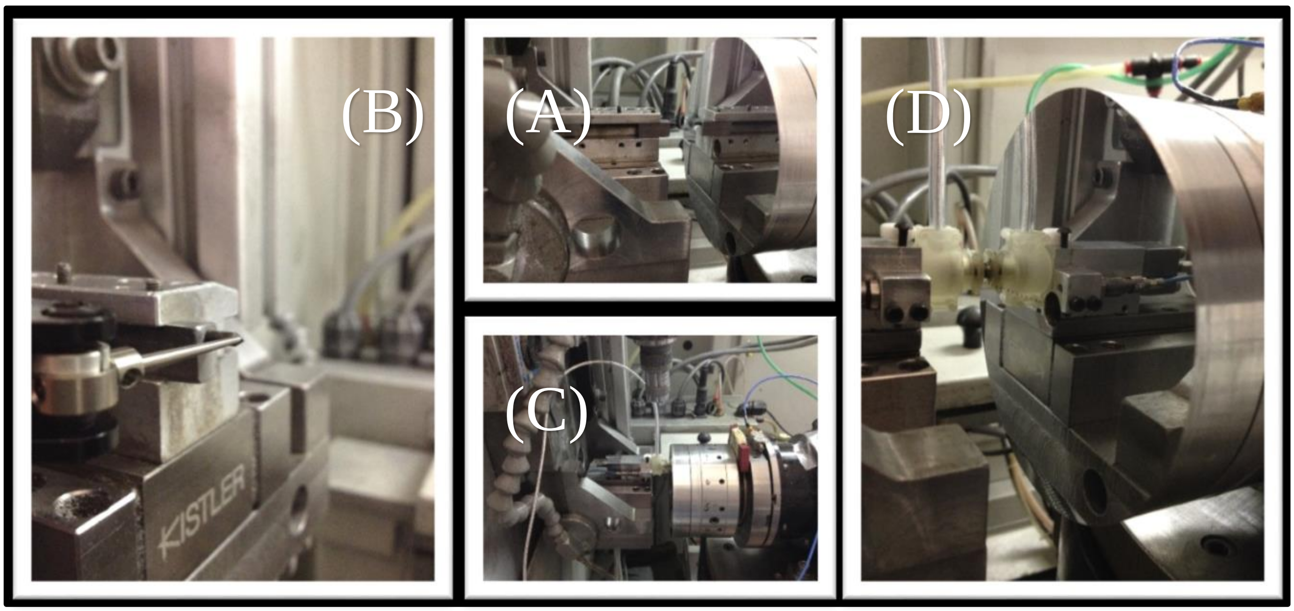

Figure 37: Capacitance sensor circular error form measurement set-up: a) dimpling with transfer punch, b) adjusting indicator to proper tool height, c) set-up of capacitance sensor, and d) capacitance sensor measurement.

At approximately three millimeters from the outer edge of the workpiece at the x-axis position of 108 mm, the part was dimpled with the transfer punch. The transfer punch, or the x-axis moves in three millimeter increments and a dimple was made every three millimeters to x-axis position 149 mm (approximately three millimeters from the center hole of the workpiece). Each dimple position was noted, the wedge then removed, the spindle rotated approximately sixty degrees, and then the wedge was put back into position. Another set of dimples was created at the same x-axis positions. The two points per circular measurement were used to create a circle of the data points at that position on the laser interferometer. The marking on the side and the dimples also provided clues as to the direction of travel on the spindle, when taking the measurements from the laser interferometer.

With the spindle brake still in place, the electronic indicator was adjusted so that the height of the indicator was at the same height as the transfer punch. Then the tool holder was removed and the capacitance sensor set-up. Adjusted to the tool height, the capacitance sensor face was placed against the first outer most dimple and adjusted until the sensor face was parallel to the workpiece face. The sensor magnets were then locked into place and the sensor was adjusted back from the face of the workpiece. The sensor equipment was turned on and the range was adjusted with the oscilloscope. Once adjusted, the wedge was removed and a trial run was done to ensure that the sensor was capturing both dimples.

For each circular measurement, the capacitance sensor took measurements at that position over a range of spindle speeds. At each speed, enough data was collected to obtain ten revolutions of the spindle. The data was collected at 25,600 samples per second at all spindle speeds. The lowest speed the spindle turned at was 20 rpm, which is only permissible with a light load on the spindle face and no cutting. The highest spindle speed run was 3000 rpm, which is above the rpm used during the cutting process. The measurements were taken at various speeds within this range as shown in Figure 41. For each circular position, the spindle was turned at these speeds counter-clockwise (the direction of cutting) and clockwise for each marked position.

Measurement Procedure for Electronic Indicator

After taking the capacitance measurements, the electronic indicator was set-up to take a one shot measurement of the circular error at each of the marked positions. First, the correct height of the dimples was obtained using the electronic indicator as shown in Figure 38a.

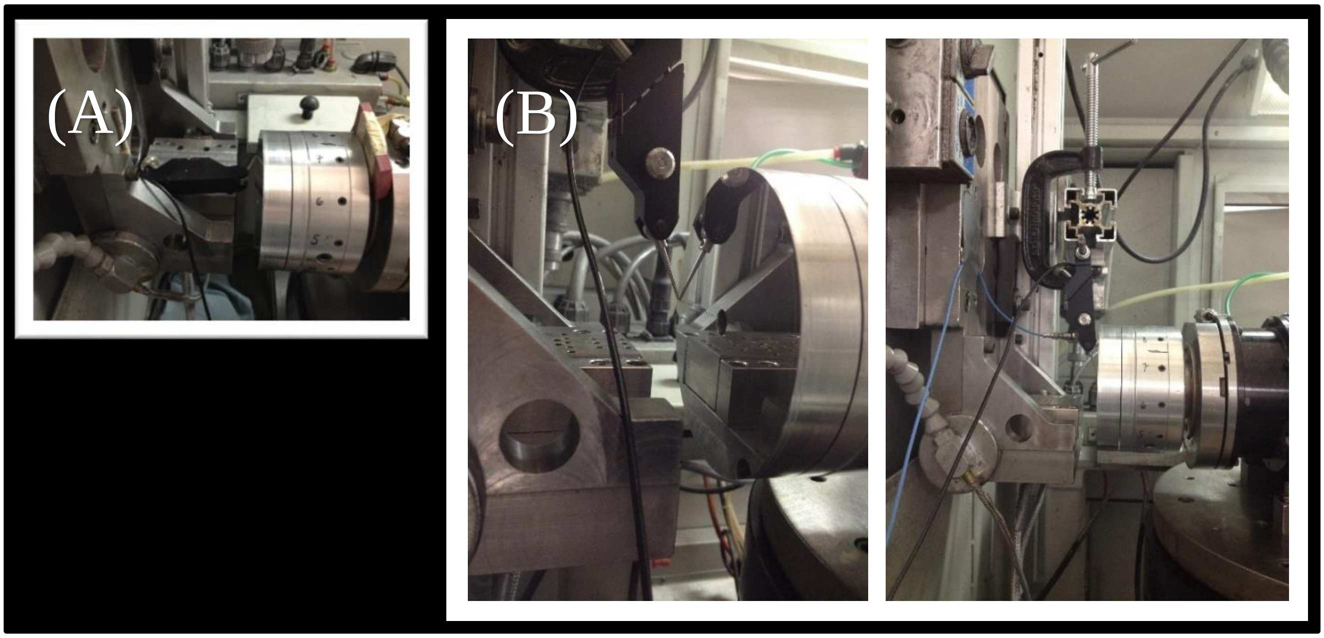

Figure 38: Electronic indicator circular error form measurement set-up: a) locating dimple height and b) fixturing and locating indicator to proper height for measurement.

Once found, the spindle was locked into place with the wedge. Then, the electronic indicator was fixed into place as shown in Figure 38b. The height of the fixture was adjusted until the tip touched the location of the dimple at x-axis position 108. The fixture was rigid and the layout of the indicator created minimal cosine error. In this position, the electronic indicator was calibrated. The calibration measurements can be found in Appendix A-2.

Once the calibration was completed the tip of the indicator was lightly coated with oil. Oil was applied to the indicator tip prior to each measurement taken. As can be seen in Figure 40, when the motor of the spindle was set into motion, the indicator was jolted before the surface moved more smoothly beneath the indicator. In earlier testing it was found that this stiction was large enough when oil was not present to jolt the indicator out of range. To reduce the frictional effects of this and ensure a successful measurement, since there is only one opportunity to get the measurement, prior to each measurement, oil was applied. Once applied, the indicator was brought into position against the workpiece surface and the voltage was zeroed to place the measurement within the center of the range. The settings for these measurements are ±10 μm with one Volt per micrometer for the indicator and the spindle speed was 20 rpm. Immediately after zeroing the indicator, the program in Figure 39 was enacted and the results were typically as shown in Figure 40. The voltage does not go past -5 V and does not continue to -10 V (the range limit of the indicator). This limit is imposed by the analog to digital converter. NI 9234 has a voltage range of ±5 V, so this portion of the graph is a characterization of this limit.

```
0FCIRCLE.PGM

G90       ;ALL MOTIONS ARE ABSOLUTE
G0        ;POINT TO POINT POSITIONING, RAPID FEEDRATE

Z-75.791  ;FULL THROTTLE
Y-63.0    ;FIXED
B-1.95    ;FIXED

M3S20     ;TURN SPINDLE ON CLOCKWISE AT 20MM/MIN

G1 F5.0   ;FEEDRATE OF AXIAL MOTION
G4 F3.0   ;DWELL IN PROGRAM EQUAL TO CYCLE TIME FOR
            20MM/MIN
Z-75.000  ;MOVE FROM SPINDLE FACE
G4 F1.0   ;WAIT TO TURN MOTOR OFF
M5        ;TURN OFF SPINDLE
G1 F200   ;FULL SPEED
Z-50.00   ;POSITION TO ADD OIL FOR NEXT CIRCULAR
           MEASUREMENT
M30       ;END PROGRAM
```

Figure 39: Indicator Program for Circular Measurements

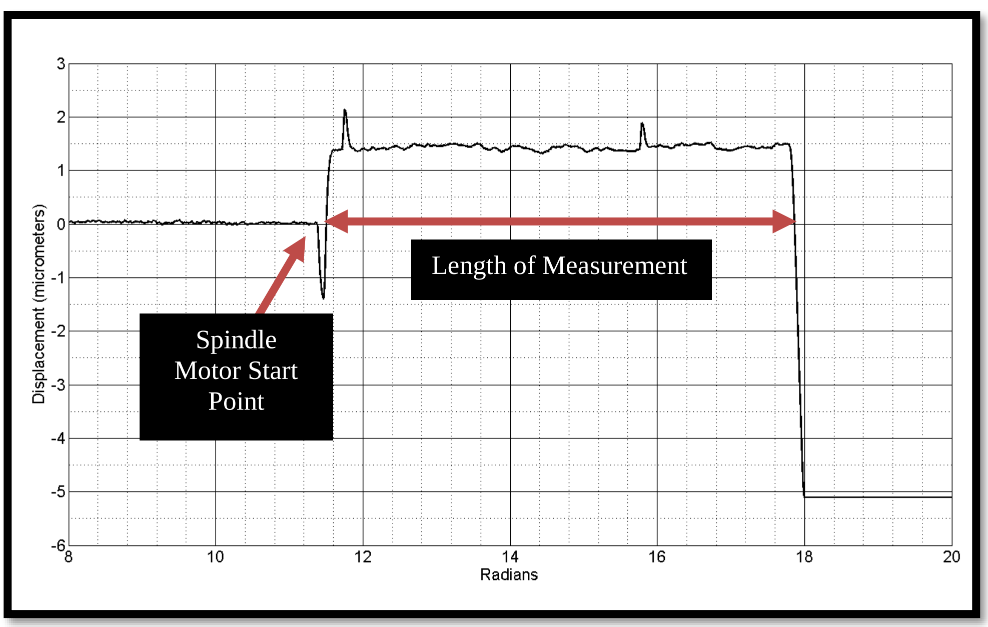

Figure 40: Resultant Circular Measurement with Electronic Indicator

Processing of Capacitance and the Interferometer Data

The expected form error when maintaining a spindle speed of 1000 rpm is seen in Figure 27. The circular form error at a constant 1000 rpm generates an eight lobe wave pattern across the surface of the workpiece and was expected to be generated and be measured by the capacitance sensor and the laser interferometer and forms the basis for determining the extent of data processing required to compare measurement systems.

Determination of Spindle Speed for Comparison Analysis

Figure 41a and Figure 38b show all the measurements taken by the capacitance sensor per circular position. To determine the optimum speed at which to compare the form error, or at which the data most clearly shows the pattern of eight waves, a frequency response analysis was conducted on each measurement for both the counter-clockwise and the clockwise data sets.

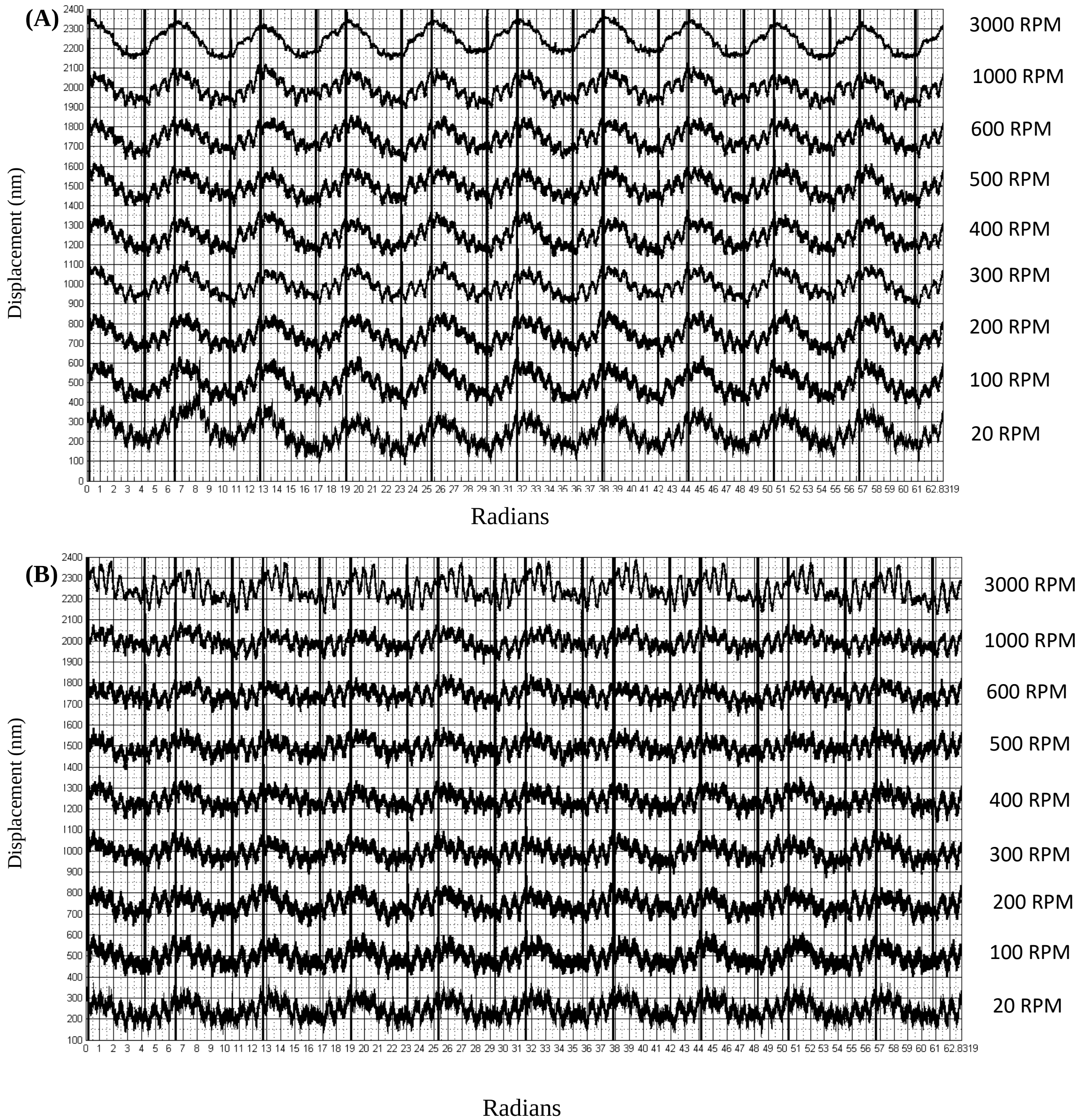

Figure 41: Ten Revolutions of Spindle at Various Speeds: a) clockwise and b) counter-clockwise

As part of the frequency response analysis to determine the spindle speed at which to conduct the circular profile measurement comparison analysis, the bin resolution of the sampling algorithm must be understood. The bin resolution decreases as the speed increases as shown in Table 13. At 3000 rpm the bin resolution for ten cycles is 1 Hz. The maximum frequency resolved will not go above the sampling rate, but the frequency that can be deciphered with the FFT becomes greater with the more samples collected over time. At the higher rpms, ten revolutions may not be enough data to resolve the frequency spectrum and either more data must be collected or the sampling rate must increase. Figure 42 and Figure 43 provides the frequency response spectrums of the data given in Figure 41a and Figure 41b, respectively. Within these FFTs, one can see that the resolution improves with more sampling time.

Table 13: Frequency span and resolution for one cycle at a given spindle speed.

Spindle RPM	Cycle Time (s)	Sample Points (#)	Bin Resolution for One Cycle (Hz)	Total No. of Bins for One Cycle	Last Bin Freq. for One Cycle (Hz)	"8" Pattern Freq. (Hz)	Bin Resolution for Ten Cycles (Hz)
20	3	76800	0.33	38400	12799.67	12.67	0.033
100	0.6	15360	1.67	7680	12798.33	13.33	0.167
200	0.3	7680	3.33	3840	12796.67	26.67	0.333
300	0.2	5120	5	2560	12795	40	0.5
400	0.15	3840	6.67	1920	12793.33	53.33	0.667
500	0.12	3072	8.33	1536	12791.67	66.67	0.833
600	0.1	2560	10	1280	12790	80	1

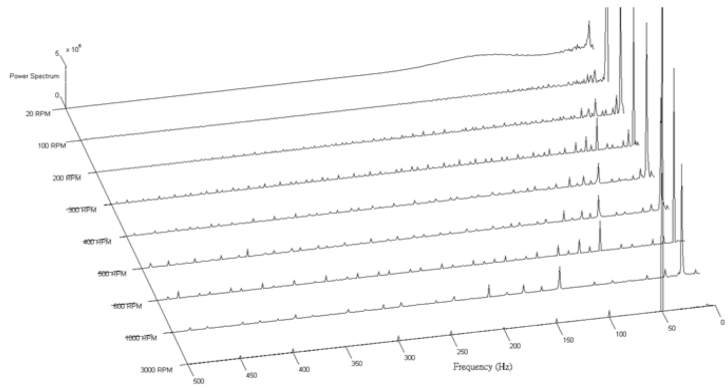

a)

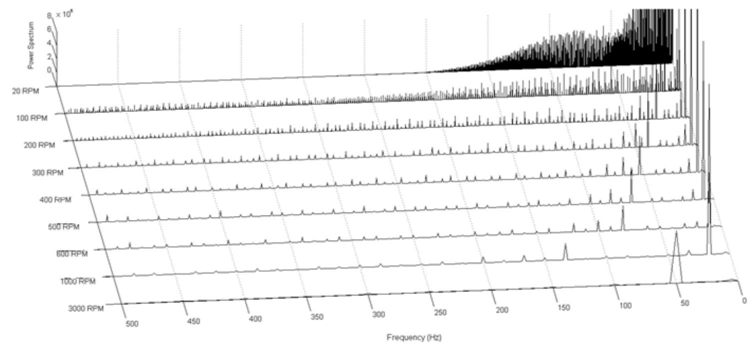

b)

Figure 42: Position X108 Frequency Spectrum for spindle moving clockwise: a) One Second of Data and b) Ten Revolutions.

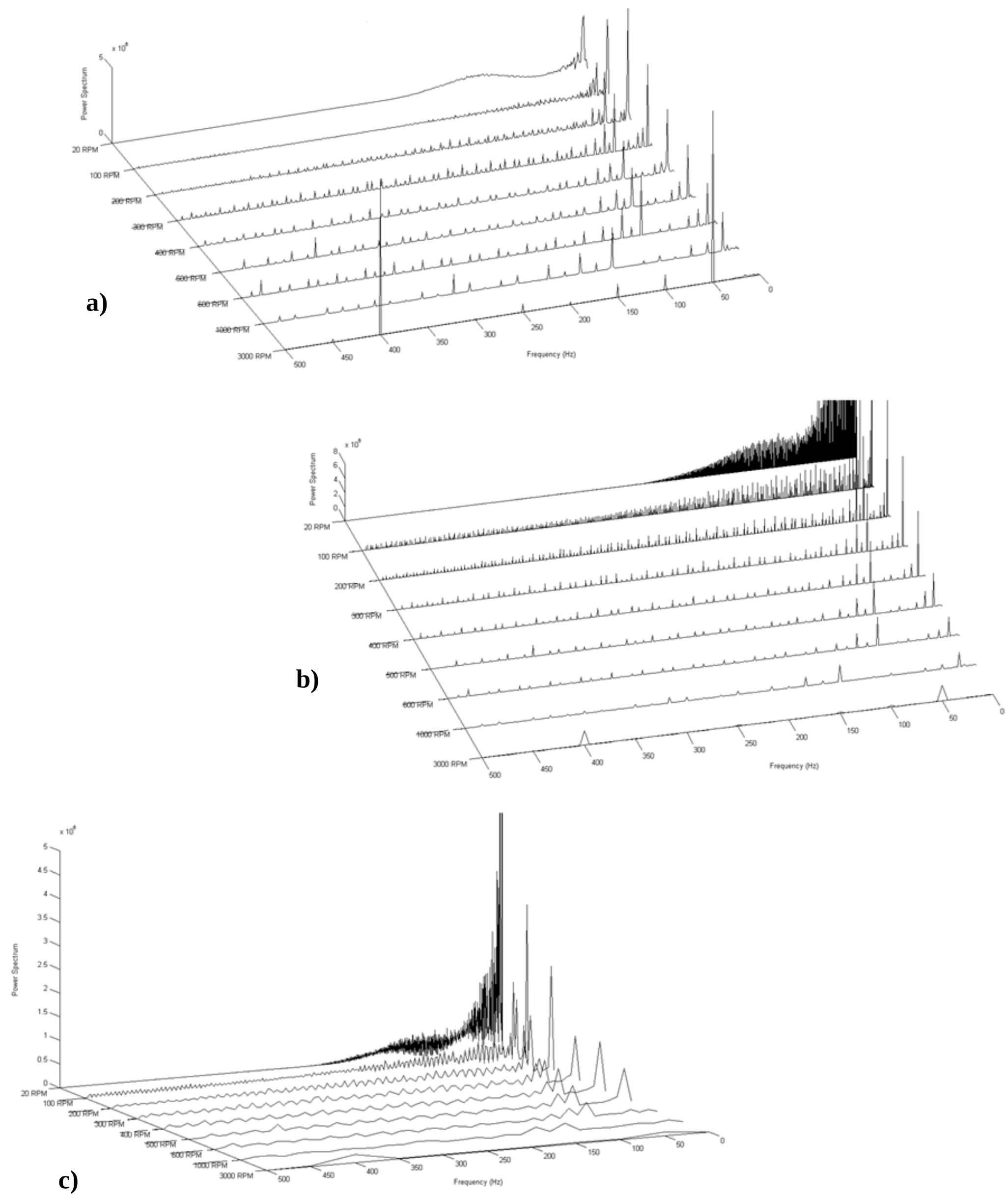

a)

b)

c)

Figure 43: Position X108 Frequency Spectrum for spindle moving counter-clockwise: a) One Second of Data and b) Ten Revolutions, and c) One Revolution.

However, whether the data collected is for ten revolutions, one second of data, or one revolution, the wave pattern is observable at 400 Hz in all the FFTs presented in Figure 43, but not in Figure 42. In Figure 42 at 3000 rpm with the spindle moving clockwise, the 400 Hz disappears. The frequency is strongest in Figure 43 when the spindle is moving counter-clockwise at 3000 rpm. Given this information from the frequency response, in order to compare circular form error with the measurements from the laser, the data from the capacitance sensor will be taken from the 3000 rpm spindle speed moving counter-clockwise (opposite direction to the cutting direction), where the waviness pattern has the greatest resolution.

Aligning Capacitance and Laser Interferometer Data

To compare the capacitance data with the laser interferometer data, the two sets were aligned, first using the dimples as data directional references and for coarse alignment. Then, to achieve precise alignment, the data was processed into frequency bins, whereby both sets of data were filtered of all frequencies except for the frequency at which the wave pattern occurred as shown in

Figure 44b. Once filtered, the first peak of both signals were found and the difference in the position of the lag value was found. The laser interferometer wave captured the static wave and the lag was added or subtracted from the capacitance wave to bring the capacitance wave in alignment with the laser interferometry data. Once re-configured both sets of raw data, as clearly shown in Figure 44a, were aligned.

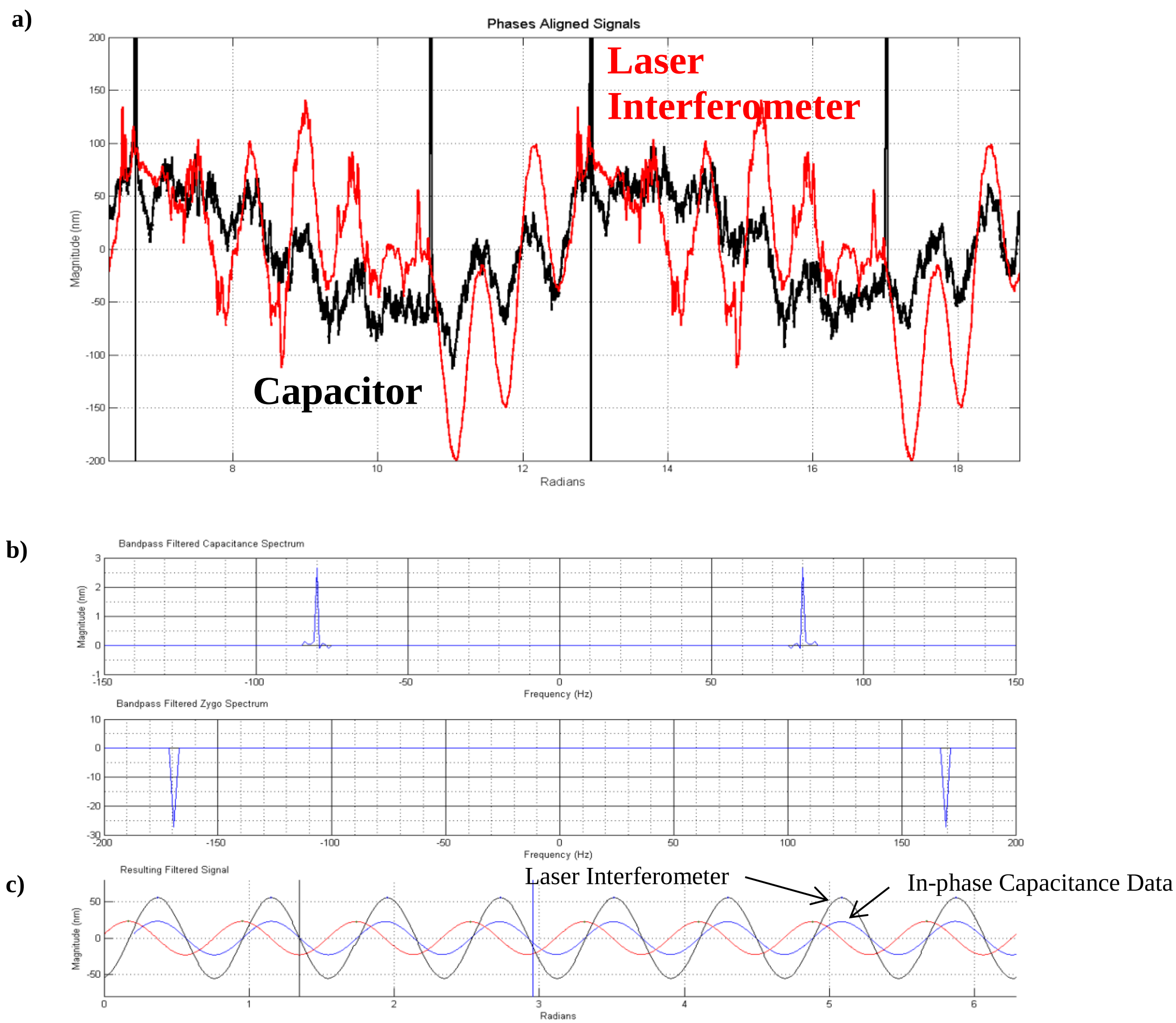

Figure 44: Aligning Laser Interferometer and Capacitor Data for 600 RPM: a) the raw data sets aligned, b) filtering out all frequencies except 400 Hz, and c) aligning the 400 Hz in both sets of data.

Figure 44a and Figure 45 show the filtered wave forms of both sets of data with the red wave depicting the capacitance sensor data prior to alignment. The blue wave in Figure 45 is the capacitance sensor wave after modification and aligned to the laser interferometer data (black line). Figure 45 shows how that alignment can be consistently found and corrected at different spindle speeds and direction of rotation.

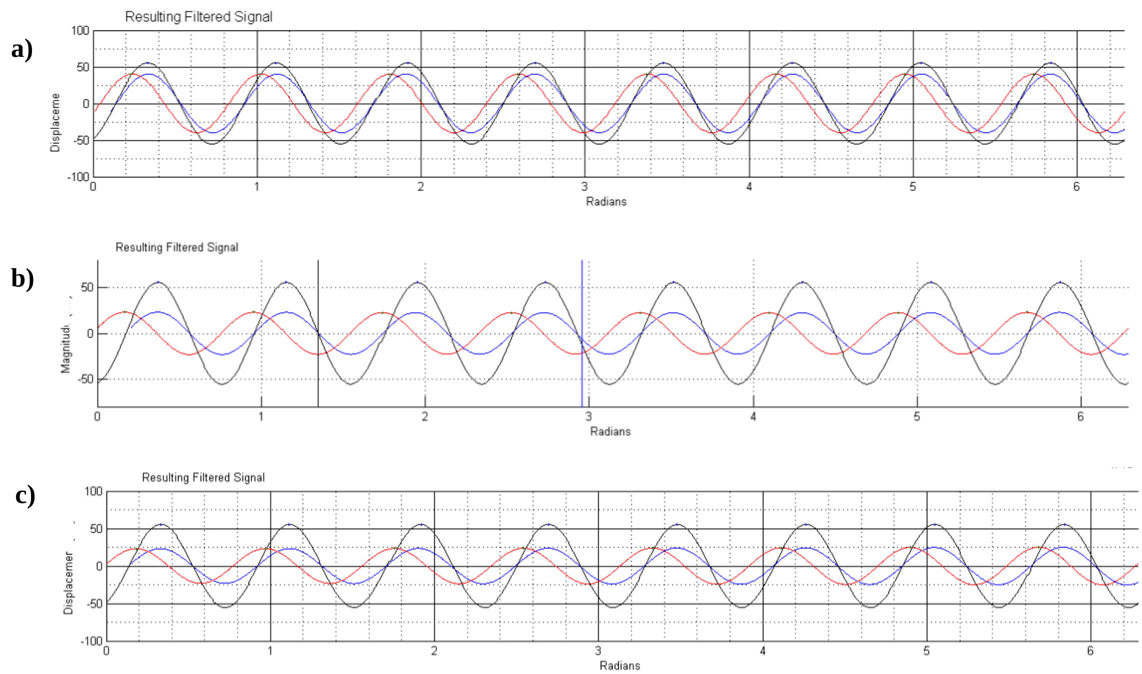

Figure 45: Phase Aligned Data for X108. a) CCW data at 3000 RPM, b) CW data at 600 RPM, and c) CCW data at 600 RPM.

Chapter 4. Discussion

The results of both measurements of the profile error: radial measurements and circular measurements are presented in part within this section. The section will first discuss qualitative aspects of the radial form error measurements: the imperfections in the processed capacitance data and the qualitative correlation between the online capacitance and the offline laser interferometer data. Then, this section will discuss the qualitative aspects of the circular form error measurements in the same manner as the other measurements taken. Finally, the section will discuss the broader implications of online measurements as they relate to previously done research, where two different measurement systems measure the same surface finish quality. Beyond this, the section will briefly discuss the results of the online measurements using the electronic indicator for the radial and circular measurements.

Radial Form Error

Radial form error has been measured with a single capacitance sensor set-up on the same machine, where the workpiece has been finished by a single point diamond turning machine tool. During the measurement process the workpiece remained on the spindle in the same position as the last pass that the tool took across the workpiece surface. The only preparation that took place was the cleaning of the workpiece surface and the removal of the metal chips the machine environment.

The Processed Capacitance Data

Figure 46 shows the complete surface profile of the workpiece as seen through the laser interferometer (the right picture) and the profile lines that will be discussed within this section as seen on the workpiece and through the laser interferometer. All the plotted data profile lines will be presented in the direction in which the measurement was taken. The same direction in which the diamond cutter finished the surface of the workpiece.

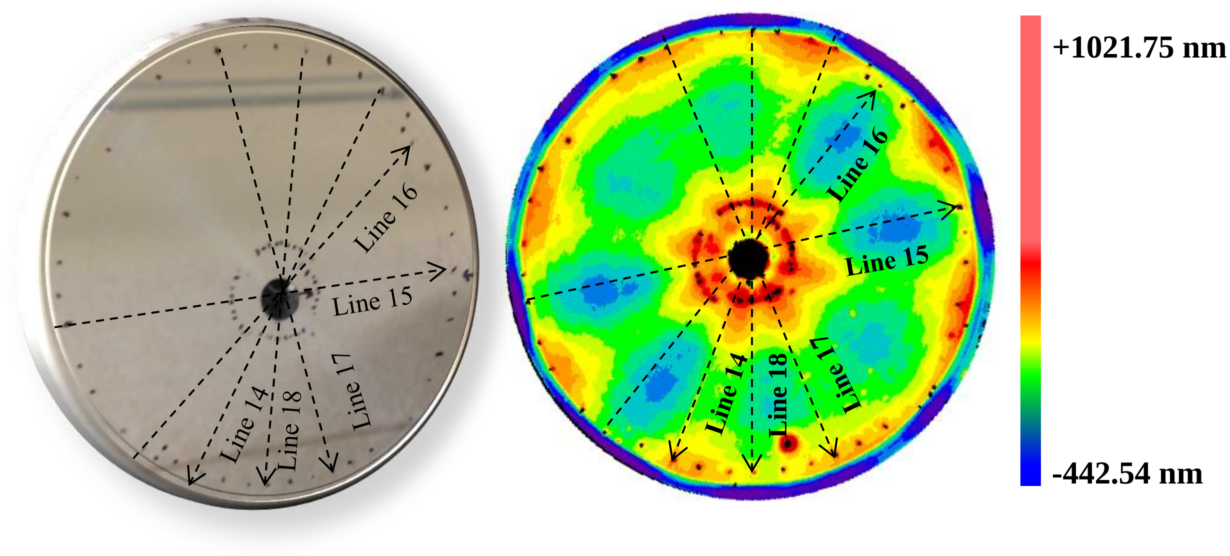

Figure 46: Workpiece measurement surface (left side, photo shows part at an angle) and laser interferometer image of workpiece surface (right side) with lines of measurements taken and given in report. Arrow indicates direction of measurement.

All the data discussed in this report has been captured as the sensor moved at 200mm/min across the workpiece surface, which was the fastest allowable feed rate. Figure 47 shows radial line 14 captured at 100mm/min (Figure 47a) and captured again at 200mm/min (Figure 47b).

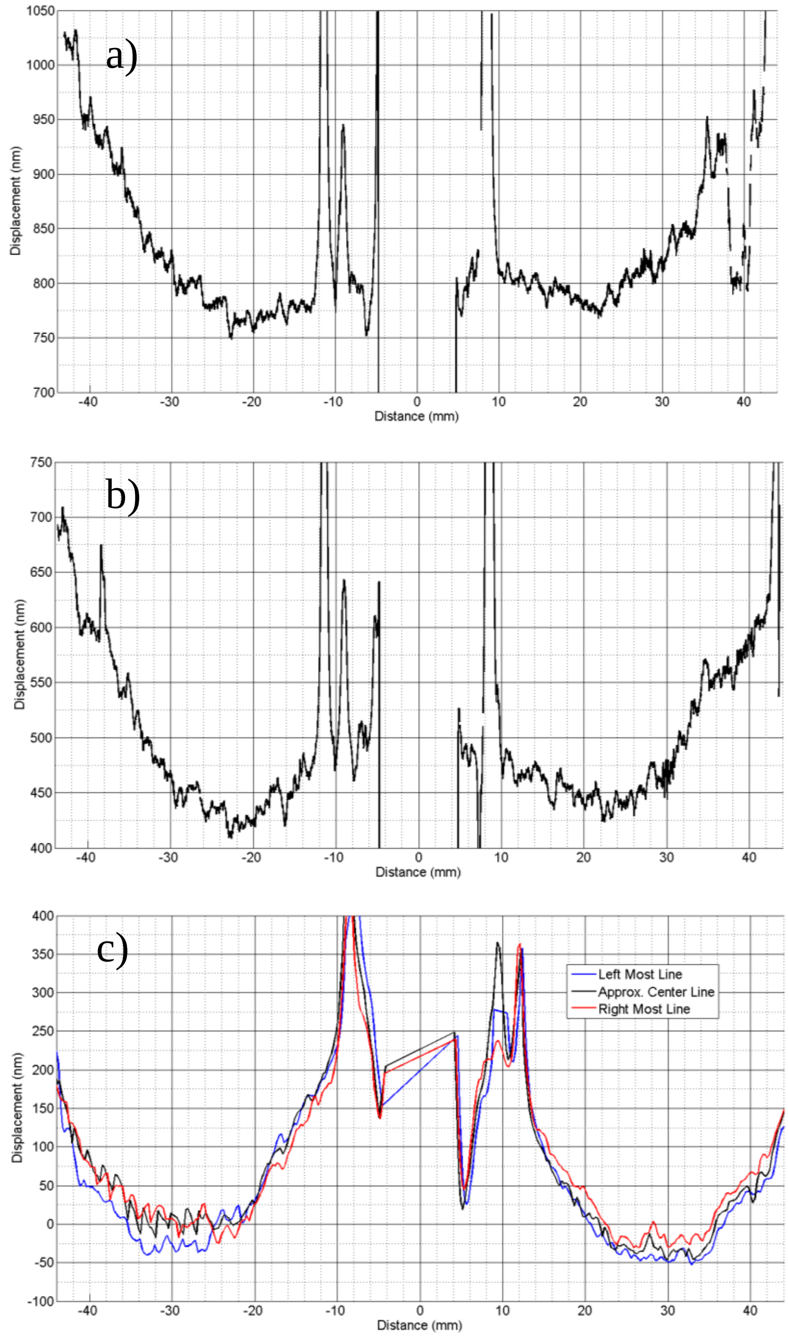

Figure 47: Line 14 Measurements at Different Speeds. a) 100 mm/min, b) 200 mm/min, and c) laser interferometer data.

At either feed rate, both sets of data underwent the same amount of post data collection processing. The only notable difference is the vertical resolution seems to increase as the speed decreases. However, the inflection near the center in comparison to the laser interferometer data does not improve. The motion of the sensor across the surface may be decreasing the vertical resolution of the profile, but does not significantly impact the charging and discharging of the sensor that can lead to results such as those shown in Figure 48.

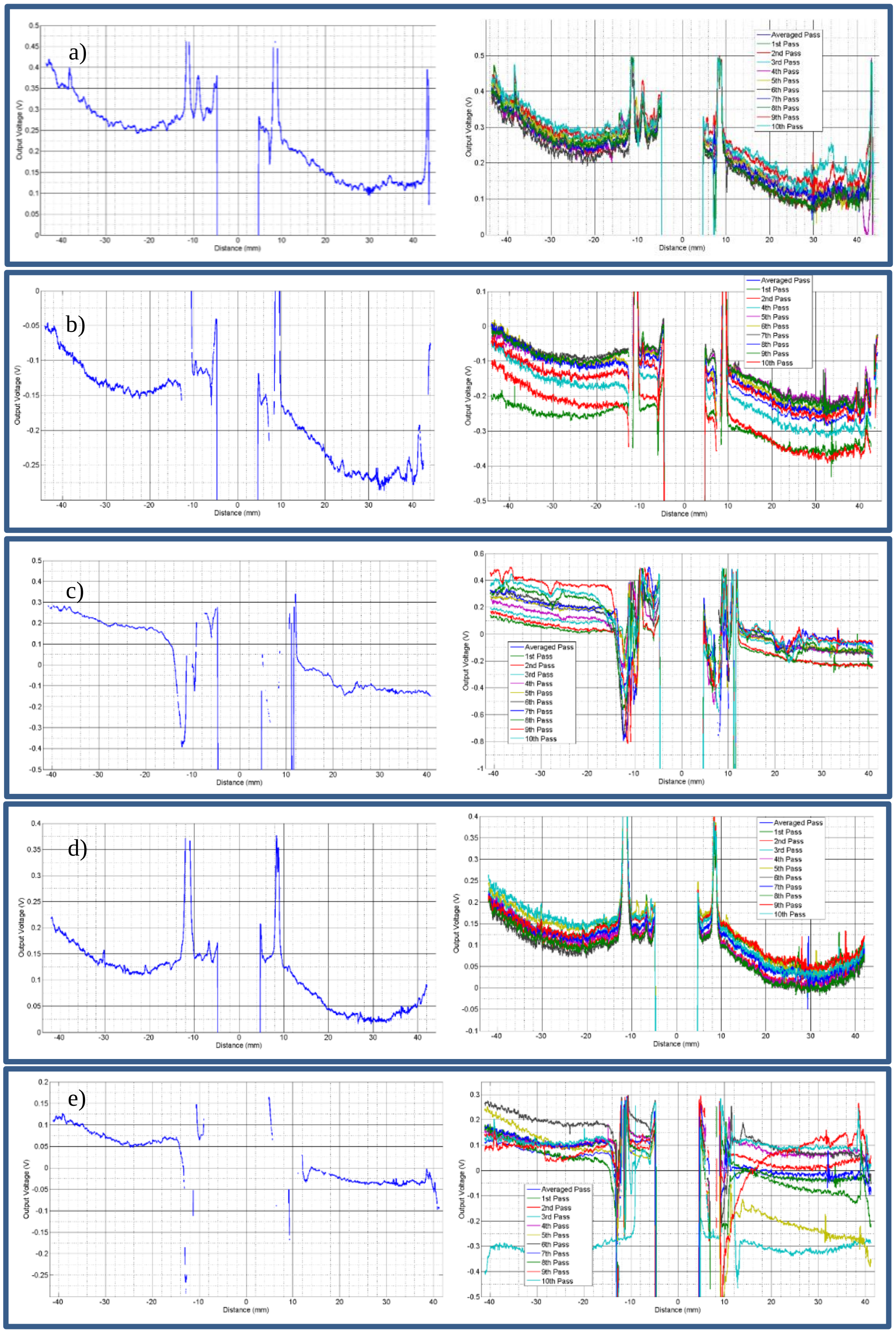

Figure 48: Each pair of plots represents ten passes of a radial line (right) and the average radial line (left); all centred and of equal length: a) line 14, b) line 15, c) line 16, d) line 17, and e) line 18.

In Figure 48, the results of five radial lines captured by the capacitance sensor are shown. The average of ten quality passes from the original twelve passes is shown on the left and the ten passes used to calculate the average pass are shown on the right. All the data was captured at 200 mm/min and the machine took approximately 5.64 minutes too complete twelve passes. These measurements were taken over the course of approximately three days.

There may be one of many reasons for the discrepancy in measurement spread between Line 14 and Line 17 and the remainder of the lines shown in Figure 48. Line 14 and line 17 according to Figure 46 occur over the flatter portion of the workpiece and the other lines are taken over the more topographically changing portion of the workpiece. With all the lines, more sensor charging was observed as the sensor moved across the tilted portion of the spindle. The relative tilting of the sensor and the topographical changes in the surface may be causing uneven charging that leads to immense drifting and extreme changes in the measurement. Another reason for the extreme drifts in the measurement passes or the increase in spread in the measurements between radial lines could be the lack of environmental control within the vicinity of the measurements. During the radial measurements the door to the machine was kept open to try to keep the interior of the machine from warming up, since the measurements were much longer to take than the circular measurements. The air conditioning vent for the machine is right in front of the opening and the humidity of the room is not controlled. Drafts and fluctuations in humidity can be felt in this vicinity and may have affected the measurements depending on the activity in the vicinity and the cooling of the room. Environmental factors and measurement time could have played a role in the inconsistencies between radial lines depicted in Figure 48.

Future measurements would need to look at shortening the measurement period, more closely controlling the temperature of the machine environment (as done in a production environment), and quantifying the effects of the spindle surface tilt on sensor performance.

Comparison of Laser Interferometer and Capacitance Data

Figure 49 and Figure 50 show plots of both the capacitance data and the laser interferometry data. The data has been represented with both sets on the same plot and with the data sets in each of the separate plots due to scaling errors that can give an erroneous perception of the data. Based on the discussion in the previous section, only Line 14, Line 15, and Line 17 are discussed when comparing data sets.

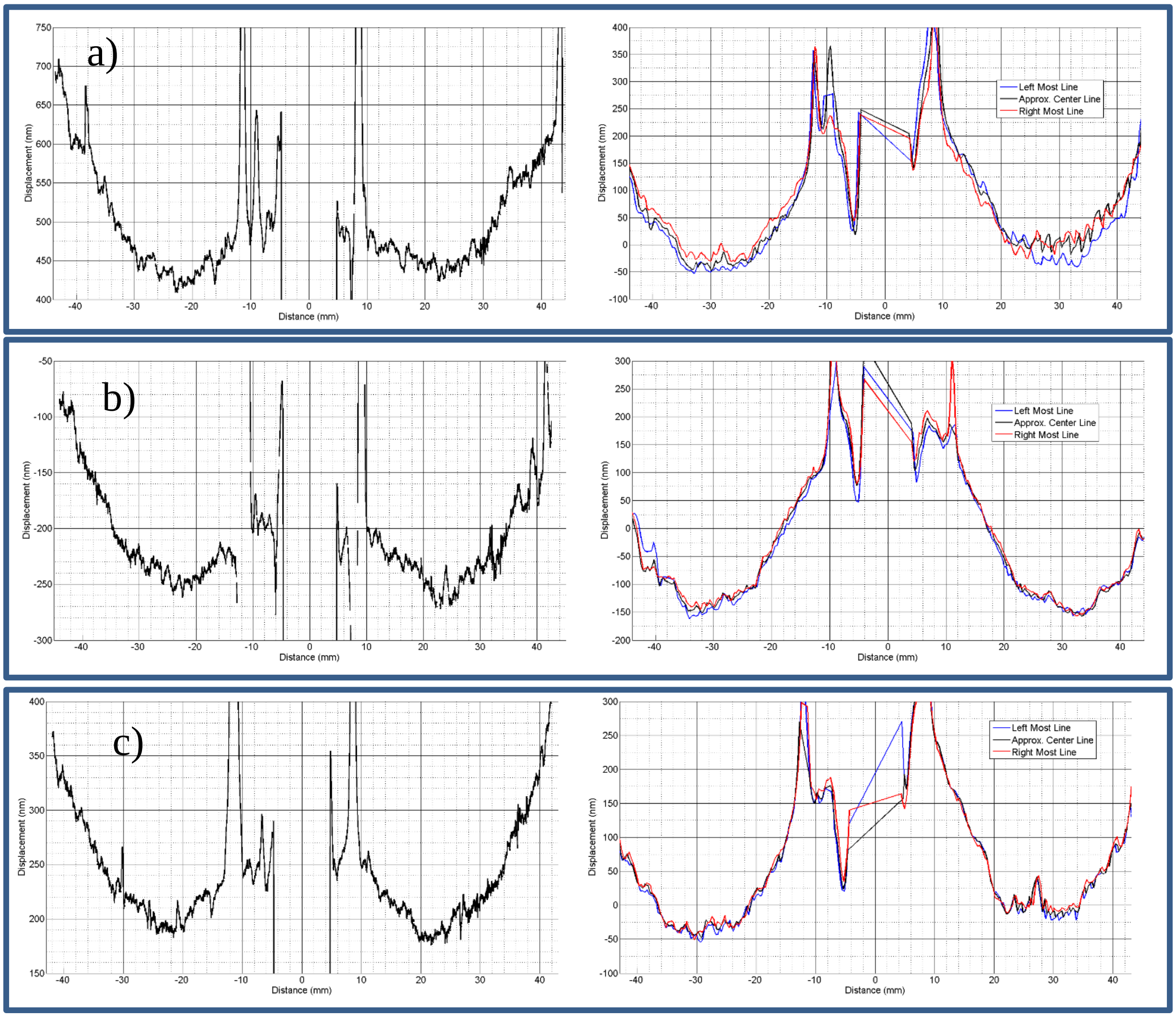

Figure 49: Radial Measurement Data from Capacitance Sensor and Laser Interferometer Side-by-Side. a) Line 14, b) Line 15, and c) Line 17.

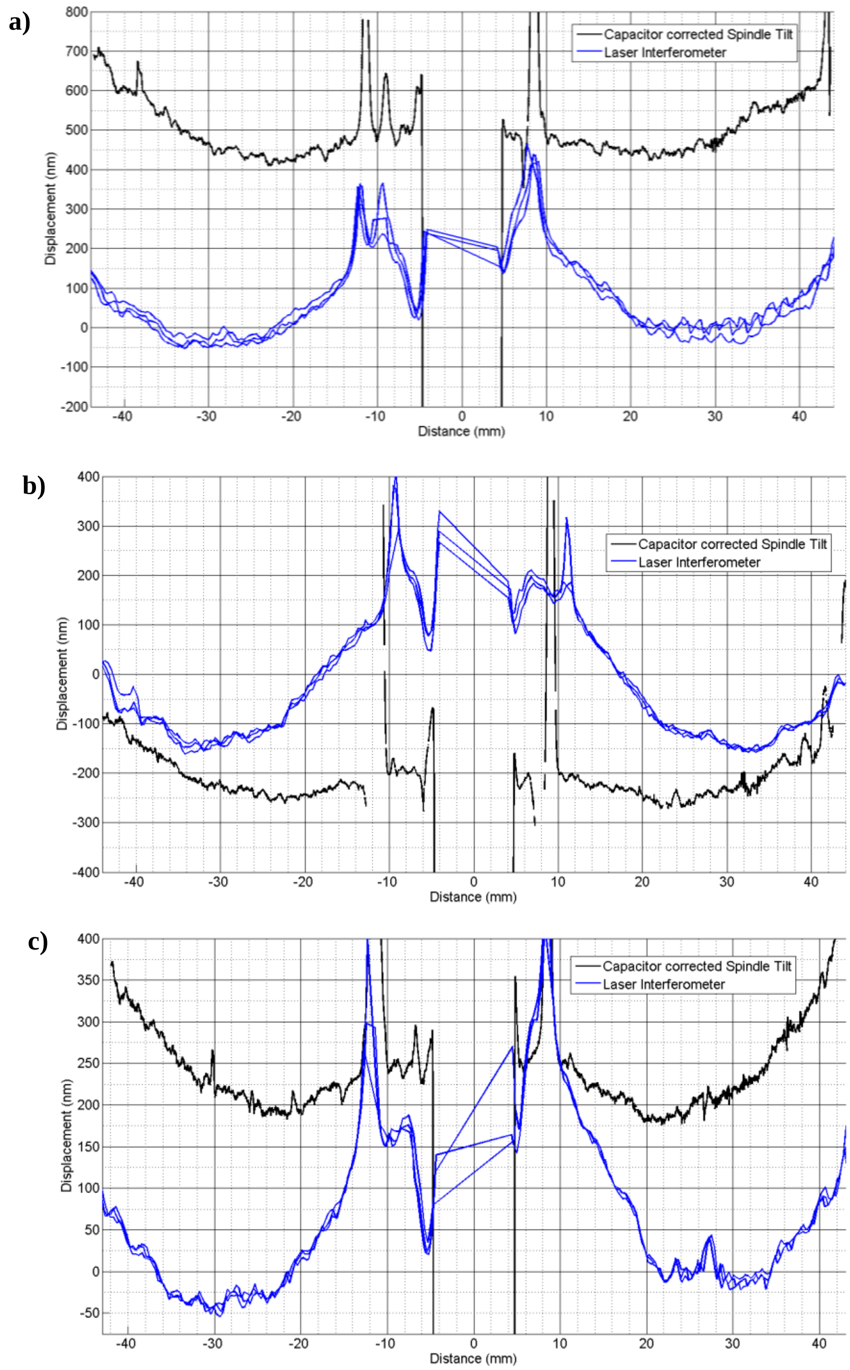

Figure 50: Comparison of laser interferometer and capacitance data without tilt on same plot. Showing a) line 14, b) line 15, and c) line 17 data sets.

In either figure, there was a strong indication that the workpiece had deformed after removal from the spindle. The data sets were inflections of one another near the center. The slope on the perimeter of the data was similar, but the laser data showed a strong incline in the data at +/-20 mm from the center of the part. Over the same spread, the capacitance data had a slight inclination and does not correlate as strongly as the data did beyond the 40 mm diameter.

The shaft of the spindle and the boss of the fixture holding the workpiece on the spindle were both approximately 50 millimeters in diameter. The fact that the inflection in deformation occurred in approximately the same locations, where the fixture attached gives credence to the fact that the discrepancy was a work holding issue.

Despite this, at an ultraprecision level removing the influence of the work holding fixture is challenging, but the capacitance sensor still qualitatively measures the profile of the workpiece and is thus a useful tool for an operator to use to tune the machining program.

Circular Form Error

Figure 51 is a topographical picture of the surface finish as seen through the laser interferometer. The figure provides all of the points of measurement taken with the capacitance sensor and one can clearly see the dimples made by the transfer punch at each measurement location.

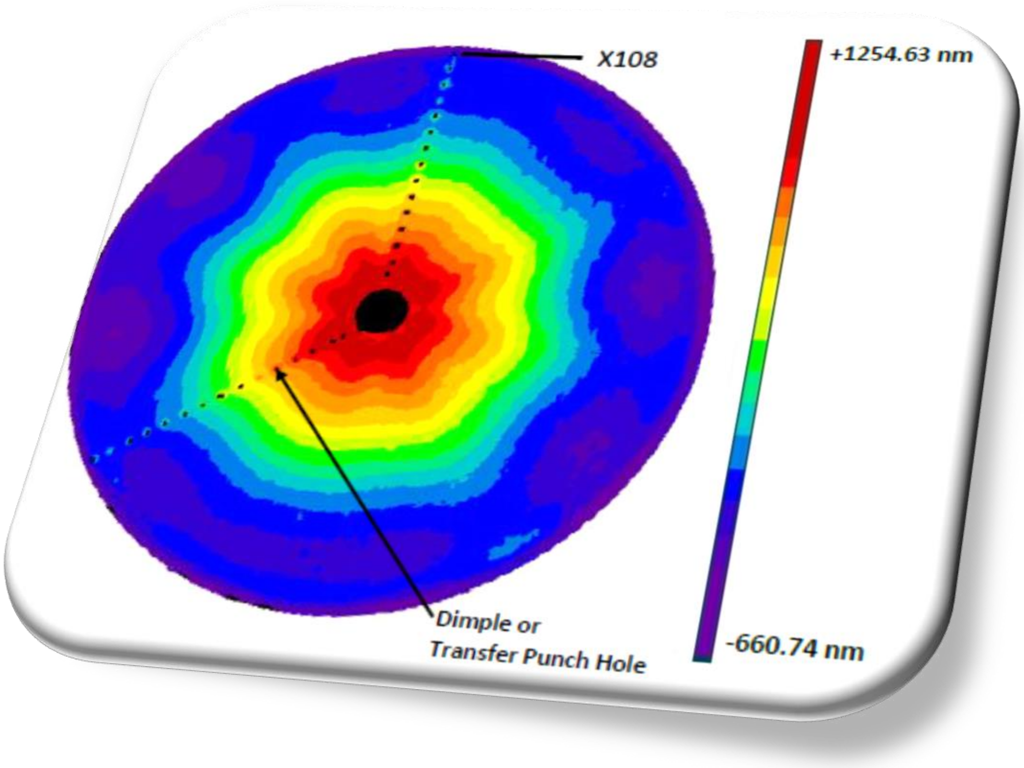

Figure 51: Laser Interferometer Measurement of Circular Form Error with Measurement Locations

As discussed in the procedure section, all data comparisons between the laser interferometer and the capacitance data are done with the data from the capacitance sensor being captured with a spindle speed of 3000 rpm counter-clockwise. At this direction and speed, the wave pattern that is clearly observable on the surface of the workpiece from the laser interferometer data is clearly seen with the capacitance sensor. A comparison of the two set of data is shown in Figure 52.

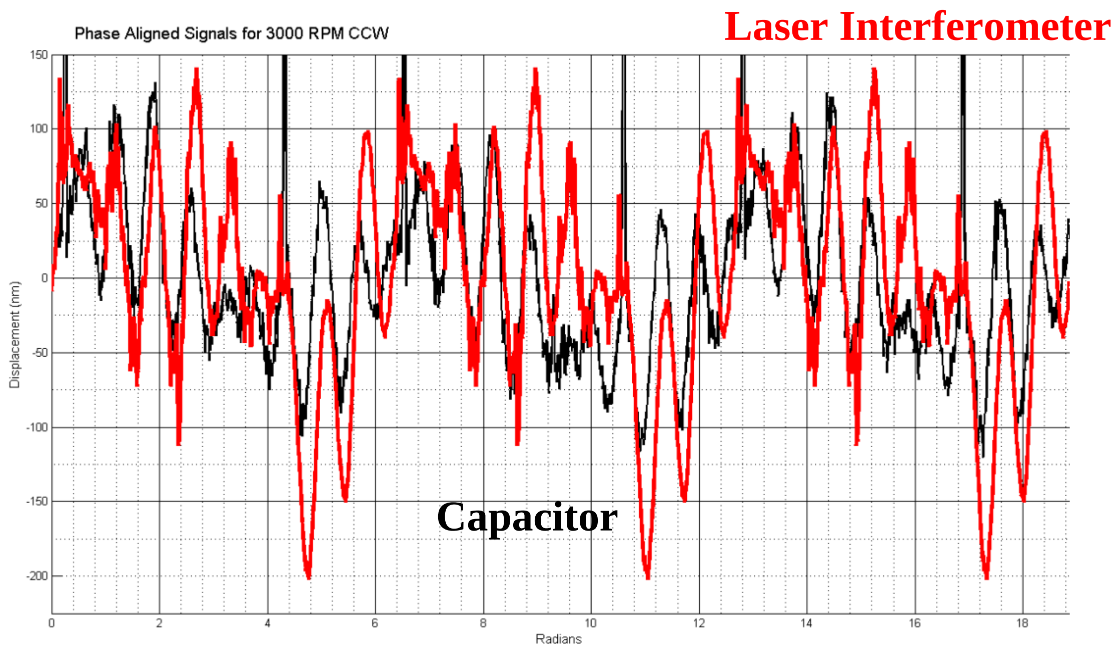

Figure 52: Position X108 with Laser Interferometer Data (red) and Capacitance Data (black) at 3000 rpm CCW

The amplitude of the waves and pattern are visually similar for both sets of data. Differences in the two sets of data are from the vibration of the machine. In fact, the processing of the capacitance data has uncovered an issue with the online measurement testing procedure.

As shown in Figure 41 through Figure 45, a dominant vibration in the spindle exists at 400 Hz. This dominant frequency causes the waviness to disappear through destructive interference when the spindle moves clockwise (the direction of cutting) and the dominant frequency causes constructive interference when the spindle moves counter-clockwise. The amplitude of the constructive interference was almost the same amplitude as given by the laser interferometer as shown in Figure 45a. The cause of the dominant frequency is unknown, but seems to be 90 degrees out of phase when the spindle moves counter-clockwise and comes from the spindle, since the phase of the vibration matches the waviness pattern on the surface of the workpiece seen by the laser interferometer.

This dominant frequency uncovers a potential problem for this measurement system. For the measurement system to move into a production environment and potentially be used to diagnose manufacturing issues, the dynamics of a normally operating spindle must be clearly known beforehand, or a system of analysis must be constructed that will determine the frequency components that distort the surface profile measurements. As shown with this testing, if the measurements were taken at 3000 rpm clockwise, then the capacitance sensor profile measurement would provide a false reading.

A spindle speed and axial feed rate must be set prior to taking the measurement and the measurement cycle time must be minimized. If possible the measurement could be taken using more than one spindle speed, but a range of speeds and feeds for a measurement system could make the process cumbersome depending upon the production time requirements.

Another avenue, could be to use the x-axis and the y-axis in combination to create a circular pattern. Although, this avenue is more complex, this approach would eliminate the spindle vibration issue as the sampling path would break up the vibration pattern.

Measuring Surface Profile on Machine with an Electronic Indicator

As previously noted, an electronic indicator followed the same path as the capacitance sensor. The electronic indicator took measurements along the same radial and circular paths as the capacitance sensor. Both types of sensors provide a relative measurement and were affected by drift and are sensitive to vibration. The electronic indicator, however, left a visible mark in the wake of the measurements and so is not suitable for measuring a final surface.

Figure 53 provides the results of the indicator for line 14, 15, and 17.

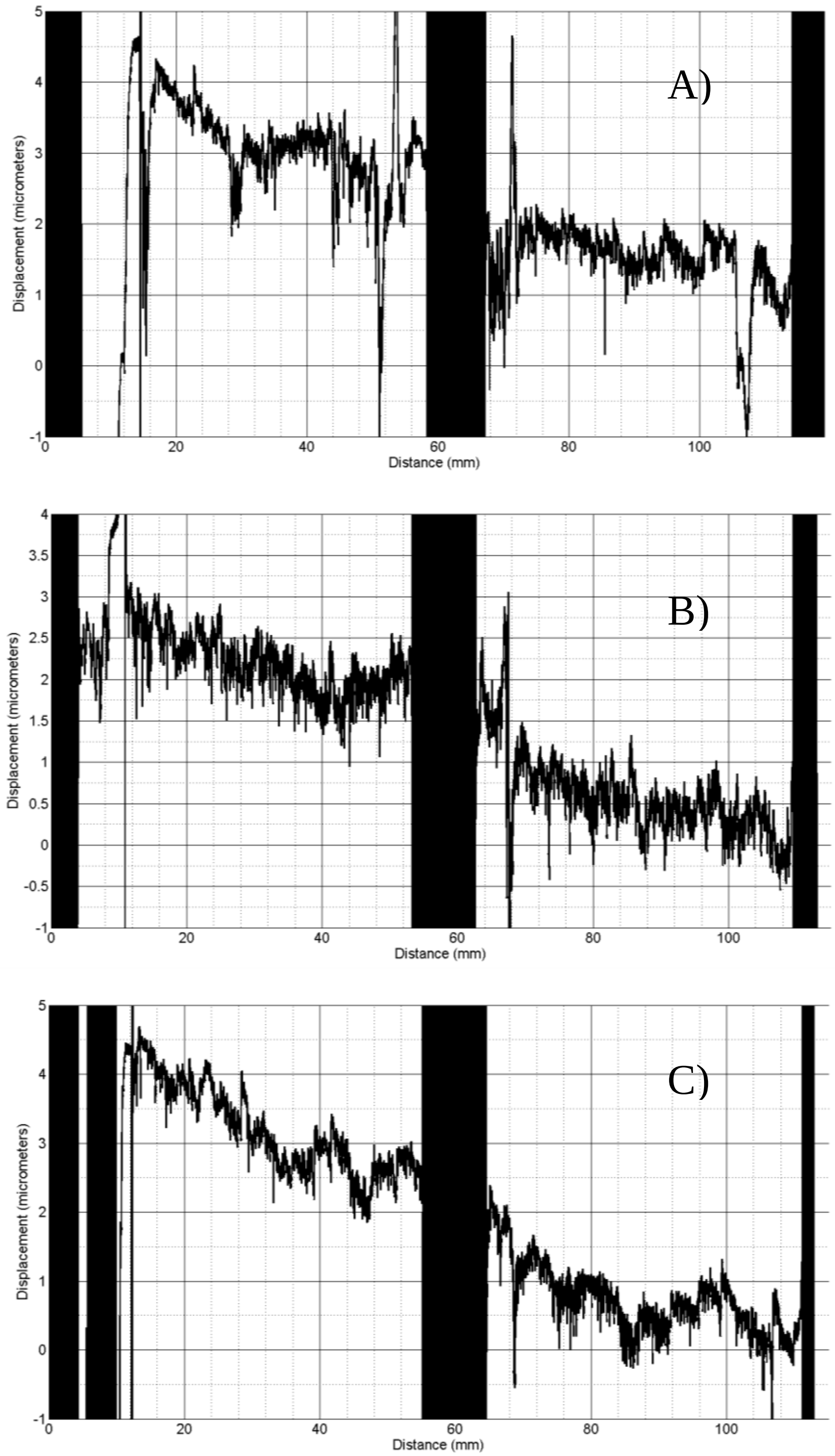

Figure 53: Indicator radial measurements. Radial lines shown are a) line 14, b) line 15, and c) line 17.

With these measurements, the measurement is a complete linear, downward sloping line from beginning to the end of the measurement. The measurements do not indicate more of the kinematic relationship between the x-axis and the spindle and less of the profile of the workpiece as seen with the previous data sets from the other measurement systems.

The tilt in the spindle measured by the indicator does support the tilt seen by the capacitance sensor. The continuous tilt across the workpiece that was not seen with the capacitance sensor may be due to the fact that the indicator's end of travel is not zeroed relative to the starting point.

This conclusion is also reinforced by the results of the circular measurements with the indicator that were taken with the spindle moving at 20 rpm and given by Figure 54. The measurement taken on the perimeter of the workpiece (Figure 54a) shows more peaks and valleys and the once per revolution vibration pattern of the spindle. The measurement taken of the workpiece near the center (Figure 54b) has less peaks and valleys and the once per revolution pattern cannot be distinguished from the noise. Once again, the electronic indicator can measure the error of the spindle as expected.

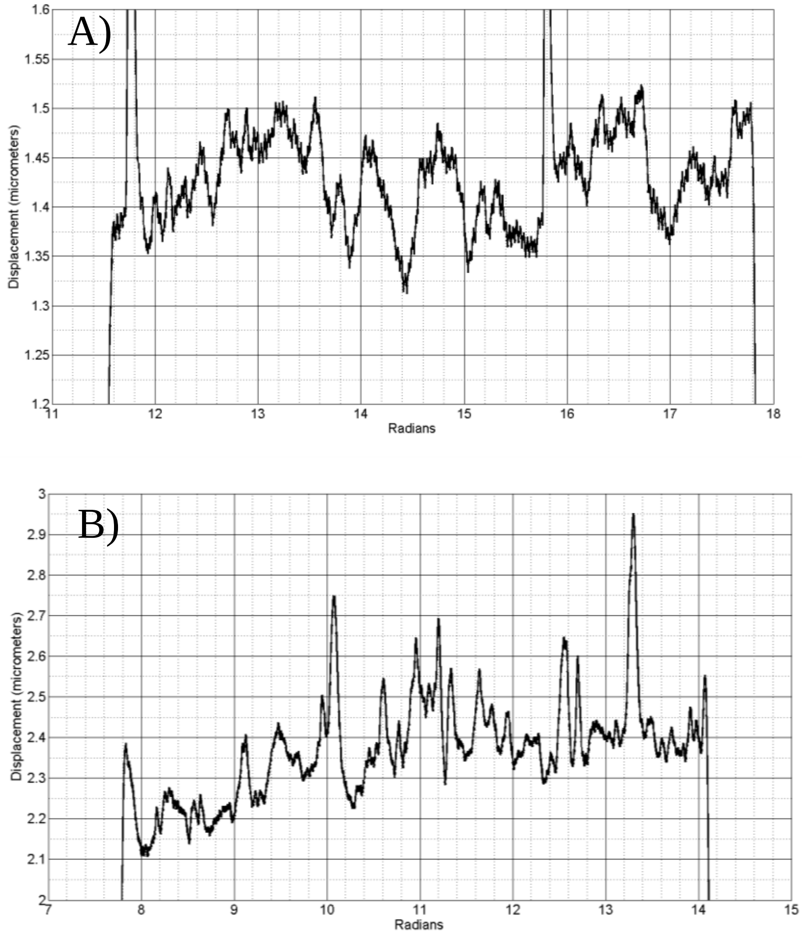

Figure 54: Electronic indicator circular measurements. A) Measurement taken at X108 or perimeter of workpiece and b) measurement taken at X147 near center of workpiece.

Figure 55 reinforces the amount of noise the indicator detects in a static position with and without oil on the surface. The amount of noise is quite large with the indicator.

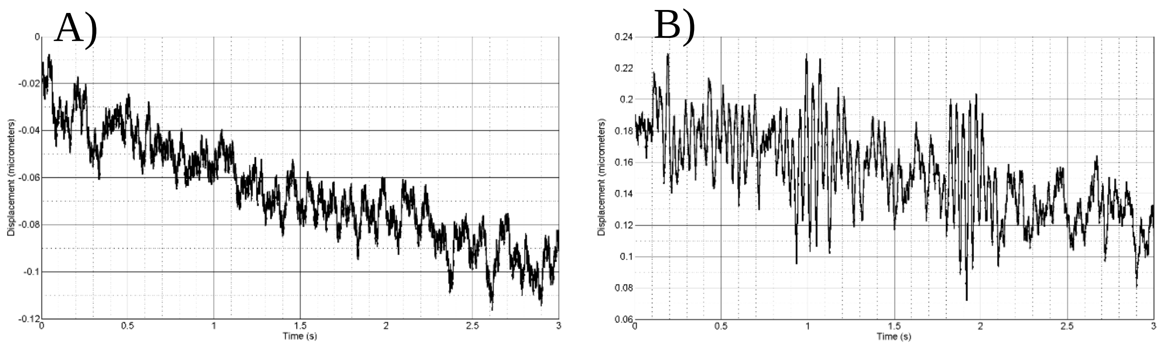

Figure 55: Noise taken by indicator on the workpiece prior to circular measurement. A) Noise with no oil added to indicator tip and b) noise with oil added to indicator tip.

The measurements with the indicator were continuously taken across the workpiece. The indicator could be set-up to take a series of point measurements across the workpiece. However, when setting up the electronic indicator in initial trials, moving the indicator to and from the surface of the workpiece had to be done at the slowest possible speed of 5 mm/min. The indicator tends to drift outside the ±5 Voltage range of the analog to digital converter very quickly. The sensor is very sensitive to the vibration of the machine and the motion of the indicator when not in a measurement position.

Chapter 5. Conclusions

The workpiece surface was measured using three different techniques. Two of those three techniques were applied while the workpiece was on the machine. The third technique, the laser interferometer is a standard offline measuring system commonly used to measure the low to mid spatial frequencies, in this case the form error of a workpiece and was the reference data against which the other two measuring techniques were compared.

The electronic indicator though of high resolution damages the surface of the workpiece and so makes the measurement technique unsuitable for in process measurement of finished parts. The electronic indicator measurements were also slow and did not capture the full profile as measured by the laser interferometer.

The capacitance sensor is a nondestructive method capable of measuring the surface profile of the workpiece on the machine with acceptable resolution for this application. The radial and circular measurements show that a strong qualitative relationship exists between the profile measured offline and the one online. The measurements from the capacitance sensor also revealed a workpiece fixture deformation issue. The other issues with the environment and the dominant vibrations emanating from the spindle dynamics must be examined and corrected to ensure a reliable, repeatable, and robust measurement system. With more in-depth research, one could determine what kind of affect the variation in the topography has on the sensor measurements and the best parameters for measuring the surface finish with a more in-depth knowledge of the machine's dynamics.

Overall, this measurement system is quite compact, easy to set-up, inexpensive when based on using a single sensor, and quick to measure and process the surface profile when compared against the machining production cycle time. Properly implemented this sensor system could not only reduce production cycle times, improve the performance of the machine, but increase the productivity and quality of the machine.

Chapter 6. Future Work and Recommendations

The next step for this research project is to incorporate the sensor system into a production environment. To do this a mounting system must be developed that includes the mechanical design of the physical automated system. Then, a data collection system with a graphical user interface that can interpret the data evaluated and present it in a user friendly manner is needed.

The current test setup should evolve into a production system setup. The current setup had drawbacks: too much time to take the linear measurements, the lack of environmental control, coolant control, air control, manual setup of measurement setup to take multiple linear surface measurements, and the manual cleaning of the finished workpiece surface followed by the manual setup of the sensor which can all be improved.

The machine's environmental controls must be improved. These controls would improve the data quality as fluctuations in temperature can affect the measurement accuracy and repeatability.

Withstanding a properly controlled machine system environment, the measurement system set-up, data collection, and processing must be refined. This requires an analysis of the machine to calibrate the measurement system. The calibration would optimize the speed, feed, and direction of the machine parameters with regards to the sensor. As well, the filtering and sampling rate would be set in a way that reflects the machine system. The calibration would include a vibration analysis to find the dominant vibration frequencies that influence the measurement and a dynamic analysis of the spindle. The tools for this analysis are established already in this thesis, but the vibration issues were deemed to be outside of the scope of this research.

Improvements in set-up and in decreasing the measurement time can be found within previous research. For set-up, the air used to remove the chips from the tool tip could be used to effectively clean the surface of the part as stated in [34] and may occur just ahead of the measurement system as the measurement is taking place. As well, to shorten the measurement cycle time, the measurements taken in this report could be combined into a spiral measurement as in [26], where the research significantly reduced the cycle time for an indicator by using this method.

Once this base system is in place, then there are other areas within the production process where this setup may be useful toward improving the production process as a whole. The following could be created from this base system.

The sensor system may be used to setup the tool in the x-axis and y-axis online with respect to the center of the workpiece. The improper setup leads to an ogive error, which may be seen with the capacitance sensor and hence be corrected in a subsequent finishing pass before the part is removed from the machine.

With spiral data, one could easily create a three-dimensional rendering of the surface using the data collected for a more visual inspection of the surface.

Quantitative analysis of the data taken to give a surface form value that compares with the laser interferometer, or provides a value that is relatable to the objective of the surface finish.

Data could be collected at various points in the cutting process to see how surface swelling and a changing environment has an effect on the surface finish qualitative data that leads to more effective ways of cutting the surface of the workpiece.

Further research needs to be done to the sensor setup to use it to measure curved, concave, and spherical type surfaces. The sensor would be able to measure the overall curvature of the surface and the sensor could follow the part using the programmed tool path to note any other discrepancies in the form error.

References

[1] M. Boltau, "Optical Components - based photonics," Photonik Forschung Deutschland, [Online]. Available: http://www.photonikforschung.de/forschungsfelder/optikkomponenten/. [Accessed 21 October 2015].

[2] "Industry Report Photonics 2013 Management Report - World," 2013.

[3] W. Zong, Z. Li, T. Sun, K. Cheng, L. D and S. Dong, "The basic issues in design and fabrication of diamond-cutting tools for ultra-precision and nanometric machining," *International Journal of Machine Tools & Manufacture,* vol. 50, pp. 411-419, 2010.

[4] A. Thornton and J. Wilks, "Clean surface reactions between diamond and steel," *Nature,* pp. 792-793, 1978.

[5] E. Paul, J. Chris Evans, A. Mangamelli, M. L. McGlauflin and R. S. Polvani, "Chemical aspects of tool wear in single point diamond turning," *Precision Engineering,* vol. 18, pp. 4-19, 1996.

[6] B. Lane, M. Shi, T. Dow and R. Scattergood, "Diamond tool wear when Al 6061 and 1215 Steel," *Wear,* vol. 268, pp. 1434-1441, 2010.

[7] M. Z. Ngoi and B.K.A, "Effect of Tool Wear and Tool Setting on Profile Accuracy of Diamond Tunred Nonferrous Components," *Materials & Manufacturing Processes,* vol. 16, no. 1, pp. 79-89, 2001.

[8] E. I. Rivin, "Vibration isolation of precision equipment," *Precision Engineering,* no. 17, pp. 41-56, 1995.

[9] zygo corporation, GPI XP, GPI XPHR, GPI HS System Manual OMP-0472G, Middlefield: zygo corporation, 2002.

[10] T. E. ToolBox, "Coefficients of Linear Thermal Expansion," [Online]. Available: http://www.engineeringtoolbox.com/linear-expansion-coefficients-d_95.html. [Accessed 10 02 2016].

[11] G. Cogburn, A. Symmons and L. Mertus, "Molding Aspheric Lenses for Low-Cost Production Versus Diamond Turned Lenses," *Proceedings of SPIE,* vol. 7660, no. XXXVI, p. 766020, 2010.

[12] Zygo Corporation, "www.zygo.com," 2016. [Online].

[13] S. H. Ali, "Advanced Nanomeasuring Techniques for Surface Characterisation," *ISRN Optics,* vol. 2012, p. 23, 2012.

[14] J. Schmit, "An Introduction to Non-contact Surface Metrology," 26 6 2013. [Online]. Available: https://www.bruker.com/fileadmin/user_upload/8-PDF-Docs/SurfaceAnalysis/3D-OpticalMicroscopy/Webinars/An_introduction_to_non-contact_surface_metrology-Jun_2013.pdf. [Accessed 18 05 2016].

[15] C. Prelle, F. Lamarque and P. Revel, "Reflective optical sensor for long-range and high-resolution displacements," *Sensors and Actuators A: Physical,* vol. 127, pp. 139-146, 2006.

[16] F. Gao, H. Muhamedsalih and X. Jiang, "In-processs fast surface measurement using wavelength scanning interferometry," in *2012 International Conference on Manufacturing and Optimization September 15-16*, Beijing, China, 2012.

[17] M. Stedman, "Limits of surface measurement by optical probes," *SPIE Surface Measurement and Characterization,* vol. 1009, 1988.

[18] A. J. Fleming, "A review of nanometer position sensors: operation and performance," *Sensors and Actuators A: Physical,* vol. 190, pp. 106-126, 2013.

[19] S. Nihtianov, "Measuring in the Subnanometer Range Capacitive and Eddy Current Nanodisplacement Sensors," *IEEE Industrial Electronics Magazine,* pp. 6-15, 19 March 2014.

[20] M. Reza Nabavi and S. N. Nihtianov, "Design Strategies for Eddy-Current Displacement Sensor Systems: Review and Recommendations," *IEEE Sensors Journal,* vol. 12, no. 12, pp. 3346-3355, 2012.

[21] H. Wang and Z. Feng, "Ultrastable and highly sensitive eddy current displacement sensor using self-temperature compensation," *Sensors and Actuators A: Physical,* vol. 203, pp. 362-368, 2013.

[22] K. Soo-Hyun and C. Dong-June, "High Sensitivity Displacement Measureing Device Using Linear Variable Differential Transformer". United States Patent US 6489760 B2, 3 December 2002.

[23] E. Peiner, M. Balke and L. Doering, "Form measurement inside fuel injector nozzle spray holes," *Microelectronic Engineering,* no. 86, pp. 984-986, 2008.

[24] E. Bos, "Aspects of tactile probing on the micro scale," *Precision Engineering,* no. 35, pp. 228-240, 2010.

[25] P. Pawlus and M. Smieszek, "The influence of stylus flight on change of surface topography parameters," *Precision Engineering,* vol. 29, pp. 272-280, 2005.

[26] M. Wieczorowski, "Spiral sampling as a fast way of data acquisition in surface topography," *International Journal of Machine Tools and Manufacture,* vol. 41, pp. 2017-2022, 2001.

[27] Lion Precision, "Capacitive Sensor Operation and Optimization (How Capacitive Sensors Work and How to Use Them Effectively)," 2012. [Online]. Available: http://www.lionprecision.com/tech-library/technotes/cap-0020-sensor-theory.html#capmeas. [Accessed 06 06 2016].

[28] H. R. Carlon, "Electrical Properties of Atmospheric Moist Air: A Systematic, Experimental Study," September 1988. [Online]. Available: http://www.dtic.mil/dtic/tr/fulltext/u2/a199599.pdf. [Accessed 09 06 2016].

[29] S. Nihtianov, "CAPACITIVE SENSOR SURFACE QUALITY CONSIDERATIONS WHEN MEASURING SUB-NANOMETER DISPLACEMENT1," in *Proceedings of Electronics,* Sozopol, Bulgaria, 2008.

[30] S. Xia, J. P. Van Schieveen, S. Nihtianov and J. W. Spronck, "Concept evaluation of a high performance self-aligning capacitive displacement sensor," in *2010 IEEE International Conference on Industrial Technology,* 2010.

[31] R. Nerino, "Capacitive Sensor Arrays in Dimensional Analysis of Surfaces," *IEEE Transactions on Instrumentation and Measurement,* vol. 44, no. 4, pp. 875-880, 1995.

[32] M. Schulz, G. Ehret and P. Kren, "High accuracy flatness metrology within the European Metrology Research Program," *Nuclear Instruments and Methods in Physics Research A,* vol. 710, pp. 37-41, 2013.

[33] A. Murugarajan and G. Samuel, "Measurement, modeling and evaluation of surface parameter using capacitive-sensor-based measurement system," *Metrology and Measurement Systems,* vol. 18, no. 3, pp. 403-418, 2011.

[34] B. Nowicki and A. Jarkiewicz, "The in-process surface roughness measurement using fringe field capacitive (FFC) method," *International Journal of Machine Tools and Manufacture,* vol. 38, no. 5, pp. 725-732, 1998.

[35] K.-W. Lee, Y.-J. Noh, W. Gao, Y. Arai, Y. Shimizu, K. Tanaka, M. Fukuta and Y. Kai, "Experimental investigation of an air-bearing displacement sensor for on-machine surface form measurement of micro-structures," *International Journal of Precision Engineering and Manufacturing,* vol. 12, no. 4, pp. 671-678, 2011.

[36] H. K. Chang, J. H. Kim, I. H. Kim, D. Y. Jang and D. C. Han, "In-process surface roughness prediction using displacement signals from spindle motion," *International Journal of Machine Tools and Manufacture,* vol. 47, no. 6, pp. 1021-1026, 2007.

[37] T. Wilkinson, Interviewee, *Applications Engineer.* [Interview]. 8 2013.

[38] National Instruments, "Operating Instructions and Specifications NI 9234," 24 09 2014. [Online]. Available: http://www.ni.com/datasheet/pdf/en/ds-316. [Accessed 27 09 2016].

[39] H. Khanfir, M. Bonis and P. Revel, "Improving waviness in ultra precision turning by optimizing the dynamic behavior of a spindle with magnetic bearings," *International Journal of machine tools and manufacture,* vol. 45, pp. 841-848, 2005.

[40] L. Baxter, "Capacitive Sensors," 20 7 2000. [Online]. Available: http://www.capsense.com/capsense-wp.pdf. [Accessed 06 11 2013].

[41] H. Golnabi, "Design of an optical fiber sensor for linear thermal expansion measurement," *Optics & Laser Technology,* vol. 34, pp. 389-394, 2002.

[42] J. Fraden, Handbook of Modern Sensors Physics, Designs, and Applications, New York: Springer, 2010.

[43] H.-S. Kim, I.-L. Kwang, K.-M. Lee and Y.-B. Bang, "Fabrication of free-form surfaces using a long-stroke fast tool servo and corrective figuring with on-machine measurement," *International Journal of Machine Tools & Manufacture,* vol. 49, pp. 991-997, 2009.

[44] Y. Tian, B. Shirinzadeh and D. Zhang, "A flexure-based mechanism and control methodology for ultra-precision turning operation," *Precision Engineering,* vol. 33, pp. 160-166, 2009.

[45] K. Prashant, M. Haydn, M. Graeme and J. Xiang, "Design and Development of a Self Calibrated Optical Chip Interferometer for High Precision On-line Surface Measurement," in *Proceedings of the Queen's Jubilee Computing and Engineering Annual Researchers' Conference 2012*, Huddersfield, 2012.

[46] N. R. Kane, J. Sihler, J. W. Roblee, M. M. Walter, B. Blair, R. J. Koning and A. H. Slocum, "Precision Product Design - From University Labs to Company Catalog," 2004.

[47] P. Chapman, "A capacitance based ultra-precision spindle error analyser," *Precision Engineering,* vol. 7, no. 3, pp. 129-137, 1985.

Appendix A-1: Radial Measurements Indicator Calibration Data

Axial Position (mm)	Measurements (V)				
-74.658	1.3	1.3	1.3	1.3	1.4
-74.659	2.7	2.8	2.5	2.8	2.8
-74.660	4.1	4.1	4.4	4.1	4.1
-74.661	5.3	5.5	5.3	5.5	5.3
-74.656	-1.3	-1.3	-1.3	-1.3	-1.3
-74.655	-2.7	-2.7	-2.7	-2.7	-2.7
-74.654	-4.1	-3.9	-4.1	-4.1	-4.1
-74.653	-5.5	-5.3	-5.5	-5.5	-5.5

Table 14: Line 14 Indicator Test Set-up Calibration Measurements

Axial Position (mm)	Measurements (V)				
-74.658	1.6	1.6	1.6	1.6	1.6
-74.659	3.1	3.1	3.1	3.0	3.1
-74.660	4.4	4.5	4.5	4.4	4.5
-74.661	5.8	6.1	5.8	5.8	5.8
-74.656	-1.4	-1.4	-1.4	-1.4	-1.2
-74.655	-2.7	-2.7	-2.7	-2.7	-2.7
-74.654	-4.1	-4.1	-4.1	-4.1	-4.1
-74.653	-5.5	-5.5	-5.5	-5.5	-5.5

Table 15: Line 15 Indicator Test Set-up Calibration Measurements

Axial Position (mm)	Measurements (V)				
-74.658	1.6	1.6	1.6	1.6	1.6
-74.659	2.8	3.1	3.0	3.1	3.0
-74.660	4.5	4.5	4.5	4.5	4.5
-74.661	5.8	6.1	5.8	5.8	5.8
-74.656	-1.4	-1.4	-1.4	-1.4	-1.2
-74.655	-2.8	-3.1	-2.8	-2.8	-2.8
-74.654	-4.4	-4.4	-4.4	-4.4	-4.4
-74.653	-5.8	-5.8	-5.8	-5.8	-5.8

Table 16: Line 16 Indicator Test Set-up Calibration Measurements

Axial Position (mm)	Measurements (V)				
-74.658	1.1	1.4	1.4	1.6	1.4
-74.659	3.1	3.1	3.1	3.1	3.1
-74.660	4.5	4.5	4.5	4.5	4.5
-74.661	5.8	5.6	5.8	5.8	5.8
-74.656	-1.4	-1.6	-1.6	-1.6	-1.6
-74.655	-2.8	-3.0	-3.0	-3.0	-3.0
-74.654	-4.4	-4.4	-4.4	-4.4	-4.4
-74.653	-5.9	-5.8	-5.8	-5.9	-6.1

Table 17: Line 18 Indicator Test Set-up Calibration Measurements

Axial Position (mm)	Measurements (V)				
-74.658	1.6	1.3	1.3	1.6	1.6
-74.659	3.1	3.1	2.8	3.0	3.0
-74.660	3.6	4.4	4.2	4.4	4.2
-74.661	5.6	5.6	5.6	5.6	5.6
-74.656	-1.6	-1.6	-1.4	-1.4	-1.4
-74.655	-2.8	-2.8	-2.8	-2.8	-2.8
-74.654	-4.2	-4.2	-4.2	-4.2	-4.2
-74.653	-5.6	-5.6	-5.6	-5.6	-5.3

Table 18: Line 19 Indicator Test Set-up Calibration Measurements

Appendix A-2: Circular Measurements Indicator Calibration Data

Axial Position (mm)	Measurements (V)		
-75.792	0.9	0.9	0.9
-75.793	1.9	1.9	1.9
-75.794	3.0	3.0	3.0
-75.790	-0.6	-0.6	-0.6
-75.789	-1.7	-1.7	-1.7
-75.788	-2.8	-2.8	-2.8

Table 19: Circular Indicator Test Set-up Calibration Measurements